JACS
JOURNAL OF THE AMERICAN CHEMICAL SOCIETY
pubs.acs.org/JACS

Article

High-Throughput Aptamer Characterization via Real-Time Nuclease Digestion

Caleb Byrd, Obtin Alkhamis, Gabriel Castro, Thinh Phuc Nguyen, Juan Canoura, and Yi Xiao*

Cite This: J. Am. Chem. Soc. 2026, 148, 10421−10436

Read Online

ACCESS | Metrics & More | Article Recommendations | Supporting Information

ABSTRACT: Aptamers, oligonucleotides that bind specific molecules with high affinity, have become popular biorecognition elements for diverse applications. While aptamer discovery via *in vitro* selection has become more straightforward, it remains challenging to accurately characterize aptamer binding in an accurate and high-throughput manner. Here, we present a next-generation version of our previously reported first-generation exonuclease digestion assays for screening aptamer-ligand interactions in a parallel and label-free manner. Our new real-time exonuclease (RT-Exo) assay delivers throughput exceeding that of the previous-generation method by orders of magnitude, with considerably less labor and resource consumption. The RT-Exo assay uses a fluorogenic aptamer as a signal reporter to monitor exonucleolytic digestion of aptamers in real time. Once samples are prepared and loaded into a microplate, a reader can autonomously monitor the digestion process, generating hundreds of data points per sample. Our fluorogenic reporter functions under many buffer and salt conditions, and we have validated the performance of RT-Exo with multiple aptamers of diverse structures binding to targets of varying physicochemical properties and divergent binding affinities. Finally, we showcase the utility of RT-Exo by screening mutants as part of structure−activity studies and its impressive throughput by profiling aptamer binding to 120 fentanyl analogs in a single run with just one experimentalist. With the greatly increased throughput, precision, and simplicity of the RT-Exo assay, the aptamer characterization process should become far more streamlined and efficient.

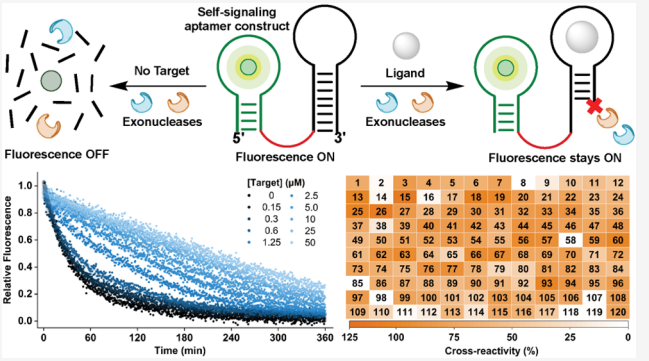

INTRODUCTION

Aptamers are oligonucleotides that bind to specific targets such as ions, small molecules, and proteins with high affinity and specificity.[1,2] They are typically used as specific recognition elements in biosensors, for the design of functional materials, and as therapeutics.[3,4] Each of these applications requires aptamers with appropriate binding affinity, specificity, and kinetics. Aptamers are discovered from randomized oligonucleotide libraries through methodologies such as systematic evolution of ligands by exponential enrichment (SELEX). Here, a starting library of 10^{12}−10^{15} unique sequences undergoes several rounds of *in vitro* selection to bind a target molecule, resulting in an enriched pool of ∼10^{2}−10^{5} aptamer candidates. The pools are then subjected to high-throughput DNA sequencing to reveal the sequence of each aptamer; the sequencing data set can be further analyzed using bioinformatic tools to identify potential candidate sequences. Even after such analysis, however, identifying the best aptamers for a given application typically requires measurement of the binding affinity and specificity of numerous candidate sequences. Conventional biophysical methods such as isothermal titration calorimetry, surface plasmon resonance, microscale thermophoresis, and biolayer interferometry can provide quantitative, robust measurements of the thermodynamics and kinetics of aptamer-ligand binding.[5−9] However, the throughput of these methods is very low. For example, determining the binding interaction of 30 aptamer candidates with 20 different ligands—a task commonly performed by our laboratory to identify suitable aptamers—can require several months of continuous labor. Simpler methods have been developed to enable higher-throughput screening, but these approaches have notable drawbacks. For instance, strand-displacement assays require fluorophore/quencher-labeled oligonucleotides, making the characterization of more than a few different aptamers prohibitively expensive.[10] Dye-displacement assays can screen aptamer binding properties without the need for aptamer labeling,[11] but these methods are not broadly generalizable because some aptamers cannot bind the dye probe and release it upon ligand binding.

Received: October 6, 2025
Revised: February 21, 2026
Accepted: February 24, 2026
Published: March 2, 2026

https://doi.org/10.1021/jacs.5c17561
J. Am. Chem. Soc. 2026, 148, 10421−10436

To address the above limitations, we recently developed a label-free exonuclease-based assay for screening aptamer-ligand binding interactions.[12,13] In this assay, aptamers are digested by exonucleases in the absence and presence of a ligand. Whereas nonbinding sequences are readily digested by the exonucleases, ligand-bound aptamers resist digestion in a manner that is correlated with their ligand-binding affinity. We and others have used this exonuclease digestion assay to characterize the binding of hundreds of aptamers with varying sequences and secondary structures to a range of small-molecule and protein ligands with diverse physicochemical properties.[14] However, this assay is labor- and resource-intensive, and the sample throughput remains limited to <10 in the hands of a novice and <30 in the case of experienced personnel.

Here, we introduce a second generation of this assay, the real-time exonuclease (RT-Exo) assay, which offers substantially improved accuracy, efficiency, precision, speed, and sample throughput. Our RT-Exo assay couples the aptamer of interest to a fluorescent light-up DNA aptamer, which serves as a sensitive reporter for continuously monitoring the aptamer digestion process with high temporal resolution, precision, and accuracy. Upon treatment with exonuclease, ligand-bound aptamers resist digestion, which leaves the fluorescent reporter intact and active, whereas unbound aptamers—and the associated fluorescent probe—are completely digested, thus turning off fluorescence. The RT-Exo assay exhibits greater throughput than the first-generation assay, and is straightforward to perform, requiring only reagent mixing and subsequent reading with a microplate reader. As an initial demonstration of the versatility of the RT-Exo method, we analyzed the binding of eight different aptamers to several dozen ligands. To demonstrate how RT-Exo can push the throughput limits of aptamer characterization, we next characterized the binding of a fentanyl-binding aptamer versus 120 fentanyl analogs in a single experiment. Finally, we demonstrate that the RT-Exo assay can be used to conduct mutagenesis studies with aptamers to determine structure−activity relationships and identify variants with differing binding properties. Our findings indicate that RT-Exo is a generalizable and powerful tool for sensitively and efficiently identifying aptamers suitable for a variety of applications.

MATERIALS AND METHODS

Reagents

All oligonucleotides were purchased from Integrated DNA Technologies with standard desalting purification. The sequences used in this work are listed in Supporting Information (SI), Table S1. Exonuclease I (*E. coli*) (Exo I) (20 U/μL) and exonuclease III (*E. coli*) (Exo III) (100 U/μL) were purchased from New England Biolabs. 10X phosphate-buffered saline (PBS) and molecular biology-grade water were purchased from Corning. Trizma preset crystals (pH 7.4), HEPES, bovine serum albumin (BSA), DFHBI-1T, 5 M sodium chloride solution, 1 M magnesium chloride solution, potassium chloride, sodium dodecyl sulfate, 3,3′-diethylthiatricarbocyanine iodide, adenosine, adenosine 5′-monophosphate (AMP) sodium salt, adenosine 5′-diphosphate (ADP) sodium salt, caffeine, (1S, 2S)-(+)-pseudoephedrine, dopamine HCl, ibuprofen sodium salt, procaine HCl, benzocaine, quinine hemisulfate salt monohydrate, diphenhydramine HCl, acetaminophen, serotonin HCl, D-lactose monohydrate, D-mannitol, naloxone HCl dihydrate, and naltrexone HCl were purchased from Sigma-Aldrich. Dimethyl sulfoxide (DMSO), formamide, 0.5 M EDTA, SYBR Gold, adenosine 5′-triphosphate (ATP) disodium salt trihydrate, inosine 5′-triphosphate (ITP) trisodium salt hydrate, beta-nicotinamide adenine dinucleotide, guanosine 5′-triphosphate (GTP), cytidine 5′-triphosphate (CTP), uridine 5′-triphosphate (UTP), and dATP were purchased from Thermo Fisher Scientific. Cocaine HCl, benzoylecgonine, mephedrone HCl, heroin HCl, oxycodone HCl, (+)-methamphetamine HCl, (±)-amphetamine HCl, (±)-3,4-methylenedioxypyrovalerone (MDPV) HCl, 3,4-MDMA HCl, (±)-methadone HCl, (±)-threo-methylphenidate HCl, fentanyl HCl, methcathinone HCl, α-pyrrolidinopentiophenone (α-PVP) HCl, pentylone HCl, ethylone HCl polymorph B, cis-tramadol HCl, (−)-nicotine, morphine sulfate hydrate, codeine phosphate hydrate, Δ^9-tetrahydrocannabinol (THC), (±)-11-nor-9-carboxy-Δ^9-THC (THC−COOH), Δ^9-THC carboxylic acid A (THCA), tetrahydrocannabivarin (THCV), cannabinol (CBN), cannabidiol (CBD), cannabidiolic acid (CBDA), cannabigerolic acid (CBGA), UR-144, XLR-11, AB-FUBINACA, alprazolam, diazepam, clonazepam, and the Fentanyl Analog Screening Kit were purchased from Cayman Chemical Company. Scopolamine hydrobromide trihydrate and papaverine HCl were purchased from Acros Organics. Lidocaine HCl monohydrate and clomipramine were purchased from Alfa Aesar. Levamisole HCl was purchased from MP Biomedicals. Fluoxetine HCl, noscapine HCl hydrate, and amoxapine were purchased from TCI America. Deionized (DI) water was obtained from a Milli-Q EQ 7000 ultrapure water purification system with a conductivity of 18.2 MΩ×cm.

Determining Fluorescence of Fluorogenic Aptamers under Varying Buffer Conditions

The ability of the fluorogenic aptamers Lettuce-4bp, Lettuce-mini, R91, and R91−4bp to activate DFHBI-1T fluorescence was determined by recording the fluorescence of solutions containing 5 μM DFHBI-1T alone or with 1 μM of each aptamer. For all experiments, 2× aptamer solution was prepared in buffer without salt, heated at 90 °C for 10 min, and then immediately cooled on ice. Salts and BSA were subsequently added to the aptamer solution. 2× DFHBI-1T was prepared by diluting the stock solution (in DMSO) with 1× buffer. Finally, the aptamer and dye were mixed at a 1:1 ratio, and 75 μL of this solution was added to the wells of a 384-well flat-bottom black microplate (Nunc). All fluorescence measurements were performed using a Tecan Spark microplate reader with excitation at 460 nm and emission at 505 nm with a step size of 5 nm. The buffers used for each experiment are listed in SI, Table S2.

DFHBI-1T Cross-Reactivity Test

A panel of 19 small-molecule binding aptamers (final concentration: 1 μM) was challenged with DFHBI-1T (final concentration: 5 μM) in buffer to determine their ability to activate DFHBI-1T fluorescence. Buffer conditions for each aptamer are shown in SI, Table S3. All aptamers were initially prepared at a 2× concentration by first dissolving each aptamer in their respective binding buffer without salt, heating at 90 °C for 10 min, and then immediately cooling on ice. Salts and BSA were subsequently added to the aptamer solutions. Then, the aptamer was mixed in a 1:1 ratio with 2× DFHBI-1T diluted in 1× buffer, and 75 μL of each sample was loaded in the wells of a 384-well microplate. Fluorescence measurements were recorded as described above.

Fluorescence Affinity Assay

Fluorescence assays were performed to determine the binding affinity of R91−4bp and related conjugates to DFHBI-1T. Aptamers at a concentration of 1.01× were first prepared in buffer as described above (conditions are provided in SI, Table S4). Then, 99 μL of the aptamer was mixed with 1 μL of 100× DFHBI-1T dissolved in pure DMSO, (final concentrations: 1 μM aptamer and 0−50 μM DFHBI-1T). 75 μL of each sample was loaded into the wells of a microplate, and fluorescence was recorded as described above. The background fluorescence of control samples with DFHBI-1T alone was subtracted from the fluorescence of samples containing both aptamer and dye at each respective concentration. The dissociation constant (K_D) of the dye-aptamer complex was determined by plotting fluorescence intensity versus dye concentration and fitting the data set with the Hill equation using the 2025 Origin PRO software. For aptamer

https://doi.org/10.1021/jacs.5c17561
J. Am. Chem. Soc. 2026, 148, 10421−10436

constructs conjugated to R91−4bp, binding affinity to DFHBI-1T was determined in a similar manner, except that dye affinity was determined both in the absence and presence of each aptamer's respective target. In the latter case, prior to mixing the conjugate with DFHBI-1T, the conjugate was first incubated with its respective target for 5 min.

Isothermal Titration Calorimetry (ITC)

All ITC experiments were performed on a MicroCal PEAQ-ITC instrument at 23 °C in the respective buffer of each aptamer. For each experiment, the parent aptamer or aptamer-R91−4bp construct was first prepared in buffer without salt, heated for 10 min at 90 °C, and then rapidly cooled to room temperature; salts were subsequently added to the solution. The aptamer was loaded into the cell and ligand was loaded in the syringe. Specific run parameters are reported in SI, Table S5. In general, each run consisted of a single 0.4 μL purge injection followed by 19 successive 2-μL injections. For some constructs, a double titration was required, which was performed by reloading the injection syringe after an initial titration without emptying the sample cell and starting another titration with the same parameters. All data were analyzed using MicroCal PEAQ-ITC Analysis Software (data summarized in SI, Table S6).

Traditional Exonuclease Digestion Assay for R91−4bp

R91−4bp (final concentration 0.5 μM) was prepared in buffer without salts, heated at 90 °C for 10 min, then immediately cooled on ice; salts and BSA were added after cooling. DFHBI-1T (final concentration: 0−25 μM, 1% v/v of reaction mixture) was then prepared in 1× buffer and added to the reaction mixture. Twenty-five μL of this solution was incubated at 25 °C in a dry bath incubator for 30 min. Afterward, 25 μL of exonuclease mixture (final concentration: 0.05 U/μL Exo I and 0.025 U/μL Exo III) was added to the aptamer solution to initiate digestion. To monitor the progress of digestion, 5 μL aliquots of the reaction mixture were collected at predefined time-points and mixed with 30 μL of quenching solution (final concentration: 12.5% formamide, 21.4 mM EDTA, 1× SYBR Gold buffered to pH 7.4 with either Tris, phosphate buffered saline, or HEPES) in a 384-well plate. Fluorescence measurements were performed using a Tecan M1000 PRO microplate reader with excitation at 495 nm and emission at 537 nm. Time-course plots of the digestion were constructed using the fluorescence of each time-point normalized to its starting value, and the area under the curve (AUC) for each sample was determined.[13] The resistance value of R91−4bp was calculated using the equation $(AUC_T - AUC_0)/(AUC_0)$ where AUC_T and AUC_0 are the AUC with and without DFHBI-1T, respectively.

Traditional Exonuclease Digestion Assay with SYBR Gold

A schematic of the experimental procedure for the first-generation exonuclease assay is provided in SI, Figure S1. The aptamer (final concentration: 200 nM) was dissolved in buffer without salt, heated at 90 °C for 10 min, and then immediately cooled on ice; salts and BSA were added thereafter. Then, target prepared in 1× buffer was mixed with the aptamer. Subsequently, SYBR Gold in 1× buffer (final concentration 1×) was added to the aptamer solution. A series of control samples without SYBR Gold were created in similar fashion. Thirty μL of this reaction mixture was added to the wells of a 384-well microplate and incubated at 22 °C for 30 min. Afterward, 30 μL of exonuclease mixture (final concentration: 0.05 U/μL Exo I and 0.025 U/μL Exo III) was added to the reaction mixture to initiate digestion. At predefined time-points, 14 μL of quenching solution (final concentration: 14.5% formamide and 25 mM EDTA) was added to the wells to stop digestion. At the end of the digestion period, 1.5 μL of SYBR Gold was added to each sample to a final concentration of 1×. Fluorescence measurements and digestion resistance were collected and calculated as described above.

Real-Time Exonuclease (RT-Exo) Digestion Assay

A schematic of the experimental setup for the RT-Exo assay is provided in SI, Figure S2. The aptamer construct was prepared in its respective buffer (final concentration 1 μM) without salt, heated for 10 min at 95 °C, and then cooled on ice, after which salts and BSA were added. Various concentrations of ligand were then added to the aptamer-ligand mixture as well as DFHBI-1T (final concentration: 5 μM). A control solution was also prepared containing ligand and dye, but no aptamer. For each aptamer, four samples were prepared: (1) dye alone, (2) dye with enzyme, (3) aptamer and dye without enzyme, (4) aptamer and dye with enzyme (see SI, Figure S3 for sample composition and setup). Specifically, 37.5 μL of the dye-ligand control sample (for samples 1 and 2) and aptamer-dye-ligand mixture (for samples 3 and 4) were each loaded twice into the wells of a 384-well microplate. These samples were incubated at 22 °C for 30 min, during which 2× exonuclease mixture was prepared in 1× buffer. Afterward, 37.5 μL of 1× buffer was added to the wells comprising samples 1 and 3, and 37.5 μL exonuclease mixture was added to the wells comprising samples 2 and 4. After centrifuging the microplate for 120 s (at 1,200 rcf), the microplate was scanned using a Tecan Spark microplate reader with a TECool module that maintained the instrument at 22 °C. The fluorescence of the solutions was measured with excitation at 460 nm (bandwidth: 5 nm) and emission at 505 nm (bandwidth: 20 nm) every 20−150 s (depending on the number of samples) for 6 h. Final enzyme concentrations were 0.1 U/μL Exo I and 0.025 U/μL Exo III, with two exceptions; for the PHEapt1 construct, enzyme concentrations were reduced by 75%, and for the MNS4.1 construct, the concentration of both enzymes was increased by 3-fold. Data analysis was carried out as follows (refer to SI, Figure S4 for details). First, we subtracted the fluorescence values of sample 1 and 2 (no aptamer controls) from the fluorescence values of samples 3 and 4 (aptamer-containing samples), respectively. These fluorescence values were then normalized by dividing each fluorescence value at every time point by the initial fluorescence at the beginning of the experiment. Next, the fluorescence values in sample 4 were normalized based on the fluorescence values in sample 3 to account for the drift in DFHBI-1T fluorescence over the course of the experiment. After this normalization, resistance value was calculated using the AUC as described previously. Since the results of the RT-Exo assay depend not only on aptamer-ligand binding but also exonuclease activity, probe stability, and fluorophore behavior, resistance values should only be compared between the same aptamer. For each experiment, E1-R91−4bp was included as control sample to assess variation in factors such as enzyme concentration between differing trials.

RESULTS

Working Principle of the Exonuclease Digestion Assay

The exonuclease digestion assay enables the measurement of an aptamer's relative affinity and specificity in a label-free and parallelizable manner.[15] Here, aptamers are digested without and with a ligand using a mixture of Exonuclease I (Exo I) and Exonuclease III (Exo III), which respectively digest single-stranded and double-stranded DNA. The digestion of ligand-free aptamers occurs relatively unimpeded (SI, Figure S5A), however, digestion of ligand-bound aptamers is greatly impaired (SI, Figure S5B) because these enzymes are unable to bind and digest the aptamer in its ligand-bound form. To date, we have monitored the digestion process by measuring the concentration of aptamer in aliquots of the reaction mixture taken at different time-points in the digestion process using the nucleic-acid staining dye SYBR Gold. The strength of aptamer-ligand binding has been measured through different metrics, such as differences in reaction half-life without versus with ligand,[16] or differences in cumulative resistance to digestion over the entire experiment.[13] The generalizability of the exonuclease assay is quite broad. We and others have used this assay to characterize the binding of hundreds of DNA aptamers with different structures to both protein and small-

https://doi.org/10.1021/jacs.5c17561
J. Am. Chem. Soc. 2026, 148, 10421−10436

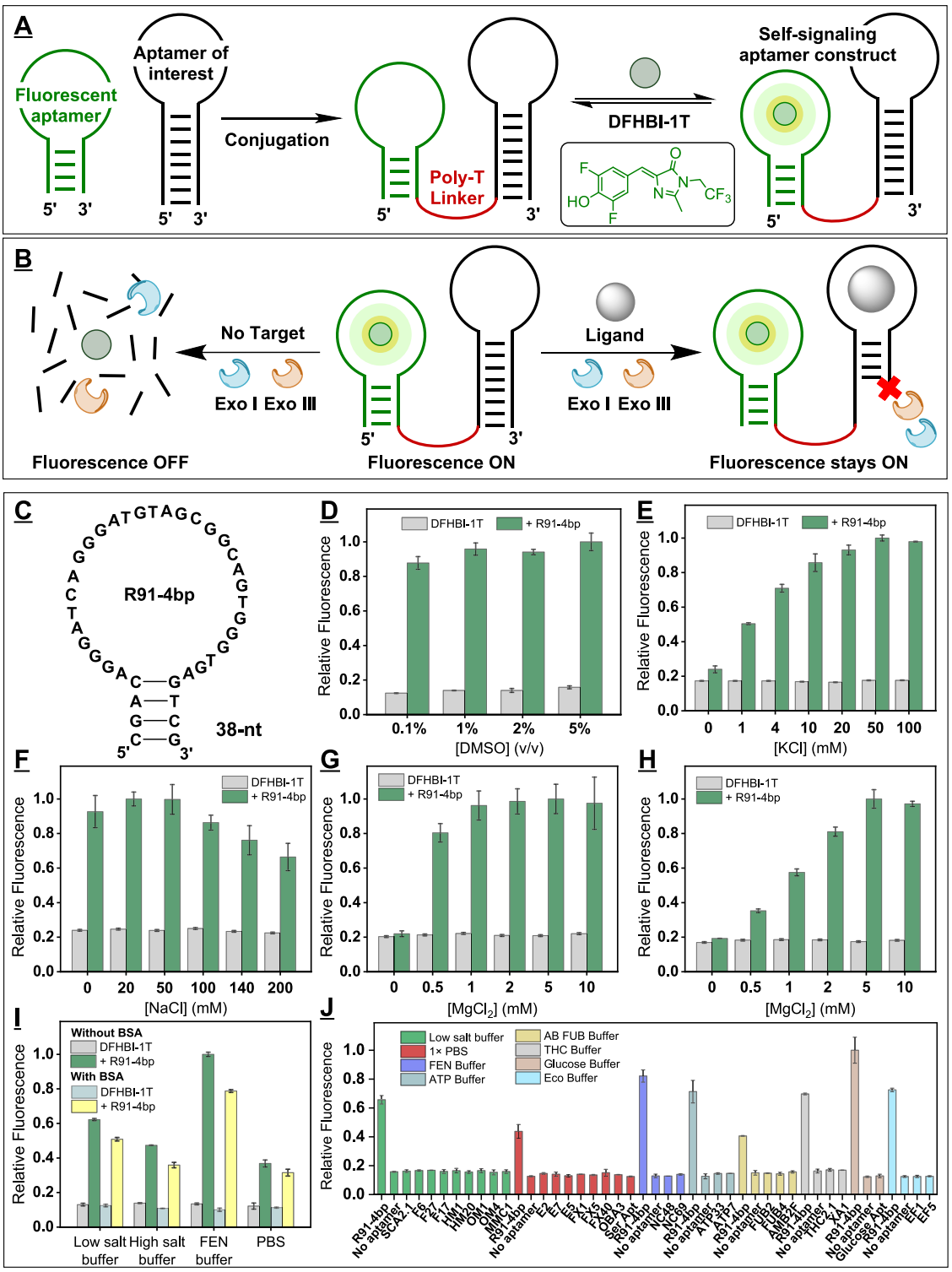

Figure 1. Utilizing the fluorogenic aptamer R91−4bp as a general signal reporter for real-time exonuclease digestion assays. (A) Engineering of self-signaling aptamer constructs, wherein R91−4bp is conjugated to an arbitrary aptamer via a polythymidine linker. (B) Working principle of the RT-Exo assay. (C) Secondary structure of R91−4bp. Examining the fluorogenic properties of R91−4bp in aqueous buffer with varying concentrations of (D) DMSO, (E) KCl, (F) NaCl, (G) $MgCl_2$ (in low-salt buffer), and (H) $MgCl_2$ (in 1X PBS). (I) Effect of BSA on R91−4bp fluorescence activation. (J) Fluorogenic function of R91−4bp and a variety of other DNA aptamers in the presence of DFHBI-1T under different buffer conditions.

molecule ligands of diverse chemistries in reaction conditions with varying ionic strength and temperature.[14]

The advantages of exonuclease assays notwithstanding, they have several shortcomings that limit their broader accessibility and throughput. First, the assay is cumbersome, labor-intensive, and prone to error. These issues stem from the way in which aptamer concentration must be frequently monitored during the digestion process. This entails with-

https://doi.org/10.1021/jacs.5c17561
J. Am. Chem. Soc. 2026, 148, 10421−10436

drawing multiple aliquots of the reaction mixture at predefined time points, quenching the enzymatic reaction, staining the remaining aptamer with SYBR Gold , and finally quantifying the fluorescence of the solution. Errors in each of these steps can accumulate, which reduces the accuracy and precision of the collected data. Furthermore, the throughput of the assay is limited because each aptamer requires at least two samples—a solution without and with ligand—and at least 8−10 time-points collected to robustly analyze the entire digestion process. While characterizing one aptamer-ligand pair is straightforward, using such an assay to screen multiple pairs simultaneously is both technically challenging and resource-intensive. For example, screening six aptamers against one ligand requires a 12-channel micropipette and an entire 96-well microplate. However, our aptamer screens following *in vitro* selections, which typically identify hundreds of aptamer candidates, are often much more comprehensive than this, involving up to 40−50 aptamers and 30−40 different ligands. As such, streamlining this exonuclease characterization method could greatly reduce assay labor and resource requirements and increase accuracy, reproducibility, and throughput.

Determining the Feasibility of Continuous Monitoring of Exonuclease Digestion

We reasoned that enabling continuous, real-time monitoring of aptamer degradation during the exonuclease digestion process could obviate several of the aforementioned challenges. To achieve this, we first assessed whether SYBR Gold could be directly incorporated into the reaction mixture and serve as a signal reporter to continuously monitor aptamer concentration during the digestion process. As a test, we used the DNA aptamer E1, which binds to fentanyl with a dissociation constant (K_D) of 80 nM.[17] We first performed the exonuclease digestion assay in a traditional manner by digesting the aptamer in the absence or presence of 100 μM fentanyl, taking aliquots at predefined time points, and staining the aliquots with SYBR Gold. In the absence of fentanyl, the aptamer was mostly (∼90%) digested within 1 h, whereas aptamer digestion was greatly inhibited in the presence of fentanyl, even after 3 h (SI, Figure S6A). We next performed the same assay with SYBR Gold in the reaction mixture, and observed that E1 digestion was strongly inhibited both in the absence and presence of fentanyl, with minimal difference in the extent of aptamer digestion even after 3 h (SI, Figure S6B). This is most likely because SYBR Gold itself binds to DNA, which may impede aptamer digestion independent of whether E1 is bound to its target. We also performed the same experiments with the DNA aptamer A23T, which binds to adenosine with a K_D of 18 μM.[16] As with E1, we observed clear differences in the extent of aptamer digestion without versus with target with the traditional assay (SI, Figure S6C), but again observed target-independent resistance to digestion when SYBR Gold was included in the exonuclease reaction mixture (SI, Figure S6D). These results demonstrate that SYBR Gold is unsuitable for continuously monitoring the progress of the exonuclease digestion assay.

Implementation of Fluorogenic Aptamers as Signal Reporters for the RT-Exo Assay

An ideal probe for continuous real-time monitoring of aptamer digestion must be able to report whether the aptamer is intact or degraded during the digestion process, and should not meaningfully perturb the functionality/structure of the aptamer, alter activity of the exonucleases, or interact with ligands. We hypothesized that the fluorogenic DNA aptamer Lettuce, which binds to the organic small-molecule dye DFHBI-1T,[18] could be suitable for this purpose. DFHBI-1T alone weakly fluoresces, but upon binding Lettuce, the fluorescence of the dye increases greatly due to restriction of dye intramolecular rotation. We developed a design in which the 5′ terminus of an aptamer of interest is connected with the 3′ terminus of the Lettuce aptamer via a poly (T) linker, forming a self-signaling aptamer construct whose integrity could be monitored in real time during exonuclease digestion (Figure 1A). Initially, the aptamer-Lettuce conjugate is complexed with DFHBI-1T, resulting in high fluorescence (Figure 1B, middle). Upon exonuclease addition, in the absence of ligand, the entire construct is fully digested; the gradual depletion of Lettuce results in increased levels of unbound DFHBI-1T, such that the fluorescence of the solution decreases as aptamer digestion progresses (Figure 1B, left). In the presence of target, however, aptamer-ligand binding prevents aptamer digestion, preserving the Lettuce aptamer and resulting in persistently high fluorescence (Figure 1B, right).

One major drawback of Lettuce is that the aptamer is 99 nucleotides (nt) in length (SI, Figure S7A), which makes it technically challenging to produce aptamer-Lettuce conjugates (>130 nt for a typical aptamer of 46−52 nt) given the low synthetic yields of such long oligonucleotides. We therefore assessed whether Lettuce could be truncated to reduce its size without compromising its functionality. We engineered two constructs, one in which the initial stem of Lettuce is reduced to 4 base pairs (Lettuce-4bp, 58 nt) (SI, Figure S7B) and another in which an internal stem located in the middle of the aptamer is truncated (Lettuce-mini, 45 nt) (SI, Figure S7C). We tested the ability of both Lettuce variants to bind and activate DFHBI-1T in their selection buffer[18] and observed that Lettuce-4bp increased dye fluorescence by only 2.9-fold after 4 h. In contrast, Lettuce-mini increased dye fluorescence by 9-fold, although binding of this aptamer to the dye was relatively slow, taking 4 h to complete (SI, Figure S8). We also examined the suitability of another fluorescent aptamer reported by the same group that discovered Lettuce, termed R-9-1 (henceforth referred to as R91).[18] Since R91 is 71 nt in length (SI, Figure S7D), we truncated it by reducing its initial stem to 4 base pairs (R91−4bp, 38 nt) (Figure 1C). We further assessed the ability of R91 and R91−4bp to bind and activate DFHBI-1T fluorescence and observed that both aptamers immediately increased fluorescence by 8-fold relative to dye alone (SI, Figure S8). Given its short length and the extent to which it rapidly activates DFHBI-1T fluorescence with a high signal-to-noise ratio, we selected R91−4bp as a probe for subsequent aptamer characterization experiments.

Assessing the Functionality of R91−4bp under Different Experimental Conditions

We next examined how well R91−4bp functions under various buffer conditions and ionic strengths in order to ensure that it could be used to characterize a wide range of aptamers. As a starting point, we began with the buffer conditions under which R91 was discovered: 40 mM HEPES buffered to pH 7.4 (with approximately 20 mM Na^+ originating from NaOH used to adjust pH), 100 mM KCl, 1 mM $MgCl_2$, and 0.1% (v/v) DMSO. Given that some hydrophobic molecules require a greater proportion of organic cosolvent, we began by examining the effect of different concentrations of DMSO on

https://doi.org/10.1021/jacs.5c17561
J. Am. Chem. Soc. 2026, 148, 10421−10436

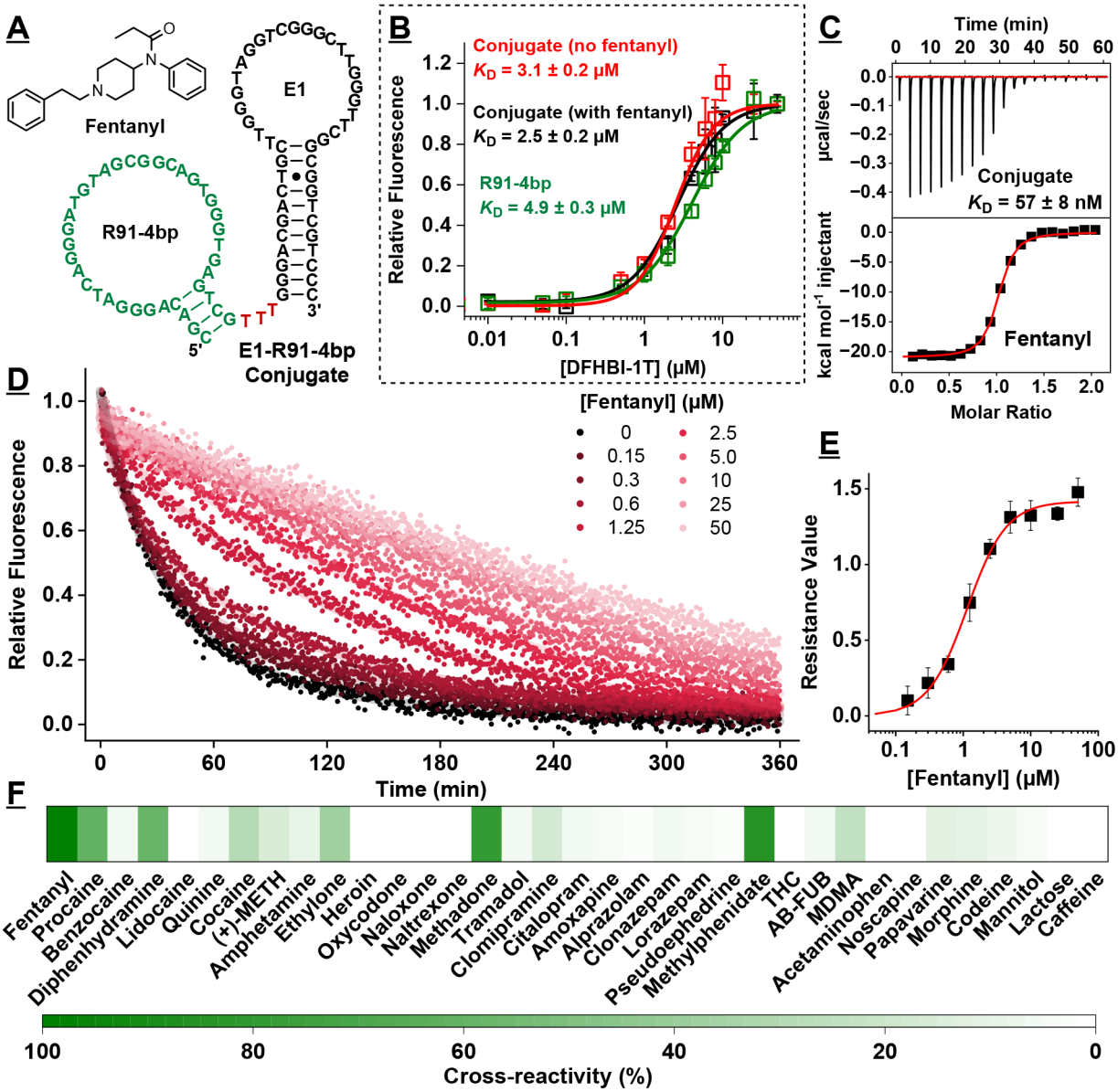

Figure 2. Demonstrating the RT-Exo assay with the fentanyl-binding aptamer E1. (A) Secondary structure of the E1-R91−4bp conjugate. (B) Binding affinity of DFHBI-1T for R91−4bp (green) and the conjugate in the absence (red) and presence (black) of fentanyl. (C) Binding affinity of the conjugate to fentanyl as determined using ITC. (D) RT-Exo assay data showing the fluorescence of the conjugate challenged with varying concentrations of fentanyl over time. (E) Resistance of E1-R91−4bp to exonuclease digestion (resistance value) plotted as a function of fentanyl concentration. (F) Specificity of E1-R91−4bp as determined using the RT-Exo assay. (+)-METH: methamphetamine, THC: Δ9-tetrahydrocannabinol, AB-FUB: AB-FUBINACA, and MDMA: methylenedioxymethamphetamine.

R91−4bp performance. As the concentration of DMSO rose from 0.1% to 5.0% (v/v), the fluorescence of R91−4bp-bound dye increased by up to 15%, while the fluorescence of DFHBI-1T alone did not meaningfully change (Figure 1D; SI, Figure S9). These results indicate that R91−4bp is compatible with DMSO at concentrations of 0.1−5.0%, which is suitable for characterizing even the most hydrophobic ligands. We also observed that R91−4bp retains its function when the buffering agent HEPES was replaced with Tris (SI, Figure S10).

We subsequently examined the effect of different cation concentrations on R91−4bp functionality. We first tested selection buffer containing various concentrations of KCl (0−100 mM), and observed that the aptamer minimally enhanced DFHBI-1T fluorescence in the absence of K^+, confirming that this ion is necessary for its function (Figure 1E). As the KCl concentration increased, the fluorescence-activating capability of R91−4bp increased monotonically, achieving saturated fluorescence at ≥20 mM KCl. R91 exhibits 73% sequence homology with Lettuce, which implies that the two aptamers may have a similar structure. A recently generated high-resolution crystal structure of Lettuce revealed that the aptamer binds two K^+ ions to form a two-layered G-quadruplex,[19] which may also explain the importance of this cation for R91 function. In subsequent experiments, we used 4 mM KCl to ensure that R91−4bp retained fluorescence function. In contrast, Na^+ is absent both in the selection buffer and in the crystal structure of Lettuce,[18,19] and we hypothesized that this cation was likewise not essential for R91−4bp function. Thus, we next examined the effect of varying NaCl concentrations on R91−4bp functionality.

https://doi.org/10.1021/jacs.5c17561
J. Am. Chem. Soc. 2026, 148, 10421−10436

Although the aptamer can function without Na^+, it achieves slightly better function in the presence of ∼50 mM NaCl (Figure 1F). However, as NaCl concentrations increased to 200 mM, we observed a linear reduction in fluorescence to 50% of its maximum value. This might be due to the increased flexibility of the aptamer under higher ionic strength,[20] which somehow weakens its interaction with DFHBI-1T. The crystal structure of Lettuce indicates that it is bound to at least three Mg^{2+} ions at its phosphodiester backbone in a fashion that allows the aptamer to achieve a relatively compact structure.[19] This suggests that Mg^{2+} may also be critical for R91−4bp to function. We therefore assessed the effect of Mg^{2+} in the range of 0−10 mM at low (20 mM) and high NaCl concentrations (140 mM). In both cases, R91−4bp was nonfunctional in the absence of Mg^{2+} (Figure 1G,H). At low NaCl conditions, R91−4bp achieved near-maximum fluorescence (80%), even at low (0.5 mM) concentrations of $MgCl_2$ (Figure 1G). In contrast, at high NaCl, the aptamer displayed a greater need for $MgCl_2$, with fluorescence rising steadily between 0−2 mM Mg^{2+} and saturating at 5 mM (Figure 1H). Therefore, in subsequent experiments involving low NaCl, we used 0.5 mM $MgCl_2$, whereas we used 1 mM $MgCl_2$ for high NaCl conditions. Overall, these experiments indicate that R91−4bp is capable of functioning under various buffer compositions and ionic strengths, with a low concentration of K^+ and Mg^{2+} necessary for function.

Finally, we assessed whether R91−4bp could function in the presence of BSA, a blocking agent typically used in exonuclease digestion assays to preclude the binding of biomolecules to plasticware and keep the exonucleases active. We measured the fluorescence produced by R91−4bp in four different buffers containing 1.5 μM BSA (see SI, Table S2 for composition). In general, we observed that the inclusion of BSA reduced the fluorescence of DFHBI-1T in the presence of R91−4bp by 10%, possibly because BSA sequestered and inactivated a portion of the dye molecules (Figure 1I).

Evaluating the Suitability of R91−4bp as a Probe for the RT-Exo Assay

We next performed a series of experiments to determine whether R91−4bp could serve as a viable probe for continuous monitoring of exonuclease digestion assays. First, we assessed whether DFHBI-1T could interact with aptamers other than R91−4bp. We determined the fluorescence of 5 μM dye with or without 1 μM of 29 different DNA aptamers previously reported to bind a variety of small molecule ligands in differing buffer conditions. The secondary structure and nucleotide composition of these aptamers vary greatly, with G-content ranging from 46 to 70% (SI, Figure S11, Table S1). None of the aptamers increased DFHBI-1T fluorescence relative to dye fluorescence alone, indicating that they do not activate the dye (Figure 1J). In contrast, we found significantly increased fluorescence from DFHBI-1T with R91−4bp in seven different buffers (see SI, Table S3 for composition), ranging from a minimum 3-fold to a maximum 8-fold fluorescence increase relative to background levels (Figure 1J). These results indicate that only the binding of DFHBI-1T to R91−4bp will activate dye fluorescence.

We then examined the correlation between the fluorescence signal of DFHBI-1T and the concentration of R91−4bp. To assess this, we determined the fluorescence intensity of 1, 2, or 5 μM DFHBI-1T at different concentrations of R91−4bp spanning from 0 to 1 μM. Regardless of dye concentration, the relationship between aptamer concentration and fluorescence was linear (SI, Figure S12), which indicates that the fluorescence of the solution is a direct measure of the concentration of intact R91−4bp. We next set out to identify the optimal concentration of DFHBI-1T, at which dye fluorescence is sufficient to provide a high signal-to-noise ratio and R91−4bp can be digested by the exonucleases without meaningful inhibition, enabling continuous monitoring of exonuclease digestion with minimal background. We digested 1 μM R91−4bp with a mixture of Exo I and Exo III in the absence or presence of various concentrations of DFHBI-1T in two different buffer conditions. In all cases, R91−4bp was completely digested in the absence of dye within 20 min. At concentrations of up to 5 μM DFHBI-1T, we observed minimal inhibition of R91−4bp digestion, although notable inhibition occurred at ≥10 μM dye (SI, Figure S13). These results indicate that continuous monitoring of exonuclease digestion is feasible using 5 μM DFHBI-1T and 1 μM R91−4bp.

Demonstrating Proof-of-Principle for the RT-Exo Digestion Assay

Having established the potential of R91−4bp and DFHBI-1T to serve as a signaling probe for exonuclease digestion assay, we determined whether the assay could be monitored in real time with the probe. As a demonstration, we conjugated the fentanyl aptamer E1[17] to R91−4bp at its 5′ end with a $(T)_3$ linker (Figure 2A) and performed a series of experiments to evaluate whether the conjugation of E1 to R91−4bp impacted binding to either fentanyl or DFHBI-1T, respectively. We found that R91−4bp and the conjugate (E1-R91−4bp) had similar affinity to DFHBI-1T (K_D = 4.9 ± 0.3 μM and 3.1 ± 0.2 μM, respectively), and also determined that the affinity of E1-R91−4bp for the dye remains essentially unchanged whether fentanyl was absent (K_D = 3.1 ± 0.2 μM) or present (K_D = 2.5 ± 0.2 μM) (Figure 2B). These results indicate that the binding of dye to the conjugate is unaffected by E1-fentanyl binding. Next, we used isothermal titration calorimetry (ITC) to determine the affinity of E1-R91−4bp and E1 for fentanyl, and again observed no meaningful difference between the two, with a K_D of 57 ± 8 nM (Figure 2C) and 79 ± 7 nM,[17] respectively. These data indicate that the conjugation of E1 to R91−4bp does not affect the binding properties of either aptamer.

We then demonstrated the performance of the RT-Exo digestion assay. We loaded 1 μM of E1-R91−4bp in buffer (1X PBS, 1 mM $MgCl_2$, 1% DMSO) with 5 μM DFHBI-1T and varying concentrations of fentanyl into the wells of a 384-well microplate. After allowing the conjugate and target to bind over 30 min, we recorded the fluorescence of the samples to obtain a steady baseline reading with a microplate reader. To initiate the reaction, we next added a mixture of exonuclease III and exonuclease I to the samples and performed fluorescence readings every ∼30 s for the next 6 h to monitor the entire course of digestion. This resulted in a total of 720 readings for each sample, which would be impossible with the conventional exonuclease assay. We observed that in the absence of fentanyl, fluorescence rapidly decreased and reached a minimum after 4 h, indicating that the conjugate was completely digested (Figure 2D). However, in the presence of fentanyl, the digestion of the conjugate was significantly slower and inhibited in a manner proportional to fentanyl concentration up to 50 μM. Notably, even at a

https://doi.org/10.1021/jacs.5c17561
J. Am. Chem. Soc. 2026, 148, 10421−10436

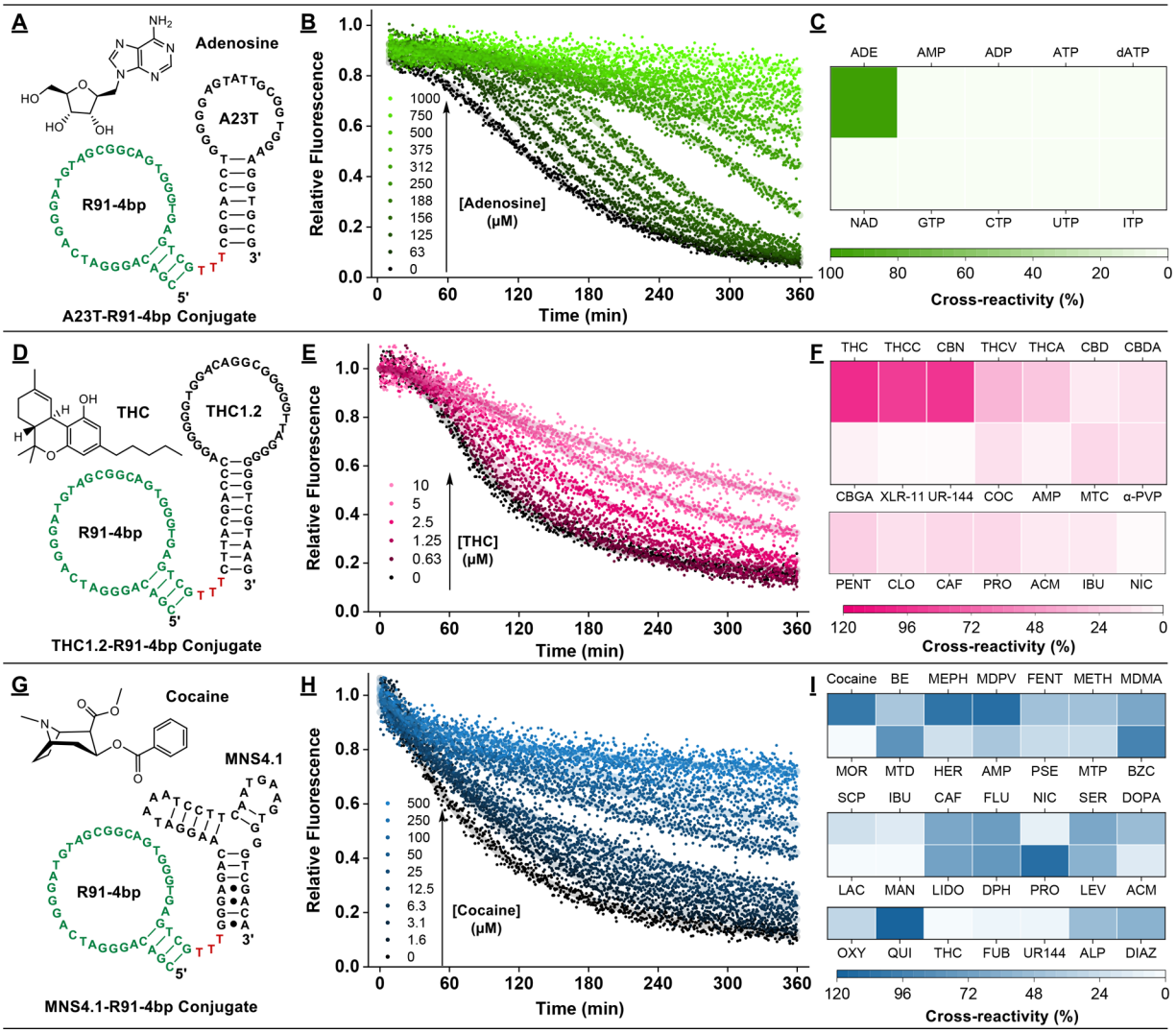

Figure 3. Demonstrating the generalizability of RT-Exo to characterize aptamers with distinct structures binding various targets. (A) Structure of the adenosine aptamer conjugate A23T-R91−4bp. (B) RT-Exo assay data showing fluorescence over time at different concentrations of adenosine, and (C) specificity of A23T-R91−4bp as determined using the RT-Exo assay. (D) Structure of the THC aptamer conjugate THC1.2-R91−4bp. (E, F) RT-Exo assay data for THC1.2-R91−4bp (E) binding to THC and (F) specificity. (G) Structure of the cocaine aptamer conjugate MNS4.1-R91−4bp. (H, I) RT-Exo assay data for MNS4.1-R91−4bp (H) binding to cocaine and (I) specificity. THCC: (±)-11-nor-9-carboxy-Δ^9-THC, CBN: cannabinol, THCV: tetrahydrocannabivarin, THCA: THC carboxylic acid A, CBD: cannabidiol, CBDA: cannabidiolic acid, CBGA: cannabigerolic acid, COC: cocaine, AMP: amphetamine, MTC: methcathinone, PENT: pentylone, CLO: clonazepam, CAF: caffeine, PRO: procaine, ACM: acetaminophen, IBU: ibuprofen, NIC: nicotine, BE: benzoylecgonine, MEPH: mephedrone, MDPV: methylenedioxypyrovalerone, FENT: fentanyl, METH: (+)-methamphetamine, MOR: morphine, MTP: methylphenidate, HER: heroin, PSE: pseudoephedrine, MTD: methadone, BZC: benzocaine, SCP: scopolamine, FLU: fluoxetine, SER: serotonin, DOPA: dopamine, LAC: lactose, MAN: mannitol, LIDO: lidocaine, DPH: diphenhydramine, LEV: levamisole, OXY: oxycodone, QUI: quinine, FUB: AB-FUBINACA, ALP: alprazolam, DIAZ: diazepam.

concentration of 150 nM fentanyl, we could distinguish the positive signal relative to the background from the blank. This increased sensitivity is made possible by the higher number of data points and hence greater time resolution that RT-Exo assay provides. In contrast, if the assay were performed in a traditional manner, we would not be able to discern such signal due to the limited number of samples that could be procured in a short duration of time, as well as the imprecision associated with the multiple-step procedure. To quantify target-induced inhibition of aptamer digestion, we used the resistance value metric, which is defined as the difference in the area under the curve of the fluorescence time-course in the presence versus the absence of target. Plotting resistance value as a function of fentanyl concentration, we observed that resistance value positively correlated with the concentration of employed target, which likely reflects that the aptamer is more extensively bound with fentanyl at higher target concentrations, resulting in increased aptamer-target-binding induced inhibition of digestion.

We also demonstrated that we could use the same assay to characterize the specificity of E1-R91−4bp against a panel of 34 different interferent molecules, including other drugs of abuse, cutting agents, and pharmaceuticals. For comparison, we evaluated our results relative to the results of an exonuclease digestion assay that we performed previously using the conventional protocol with the E1 aptamer under identical conditions.[17] As expected, the results of both assays were very similar, indicating that E1 cross-reacts moderately

https://doi.org/10.1021/jacs.5c17561
J. Am. Chem. Soc. 2026, 148, 10421−10436

(>25% cross-reactivity relative to fentanyl) to procaine, diphenhydramine, cocaine, methadone, ethylone, methylphenidate, and methylenedioxymethamphetamine, with weaker (10−25%) cross-reactivity to methamphetamine, clomipramine, papaverine, and morphine (Figure 2F ; SI, Figures S14−16). These results demonstrate that the RT-Exo digestion assay delivers accurate results for the analysis of both aptamer target affinity and specificity, and is also significantly simpler and more robust with high sample throughput and a degree of temporal resolution that would be unattainable with the existing exonuclease assay.

Having successfully demonstrated the RT-Exo assay using E1-R91−4bp, we next determined the effect of altering the length of the linker between E1 and R91−4bp on assay performance. To assess this, we designed new constructs containing E1 conjugated to R91−4bp with a $(T)_1$ or $(T)_6$ linker. We first confirmed that these constructs had similar affinity for fentanyl (SI, Figure S17) and DFHBI-1T (SI, Figure S18) as the $(T)_3$ linker-containing conjugate and the parent aptamers. We next performed the RT-Exo assay with these conjugates in the absence and presence of 50 μM fentanyl (SI, Figure S19). All constructs were digested at similar rates in the absence of fentanyl. However, while the $(T)_3$ and $(T)_6$ linker-containing constructs displayed similar levels of resistance to digestion in the presence of fentanyl, the $(T)_1$ linker-containing construct exhibited much lower resistance to digestion. This suggested that the target-binding affinity of the major digestion products of this particular conjugate may have inferior fentanyl-binding affinity. These results therefore indicate that a linker length of at least 3 nucleotides is preferable in the design of such conjugates.

Assessing the Generalizability of the RT-Exo Assay

We next set out to demonstrate that our RT-Exo digestion assay with continuous monitoring can be applied to other aptamers, starting with A23T,[16] an engineered variant of an adenosine-binding DNA aptamer initially reported by the Szostak group. A23T binds two molecules of adenosine with micromolar affinity but has considerably less affinity for adenosine triphosphate (ATP), adenosine diphosphate (ADP), and adenosine monophosphate (AMP). We synthesized A23T with R91−4bp conjugated at its 5′ terminus via a $(T)_3$ linker (Figure 3A), and observed that this A23T-R91−4bp conjugate had similar affinity to DFHBI-1T (K_D = 0.9 ± 0.1 μM) (SI, Figure S20A) as R91−4bp (K_D = 1.4 ± 0.2 μM) under the same buffer conditions (10 mM Tris, 20 mM NaCl, 1.5 mM $MgCl_2$, 4 mM KCl, 1% DMSO) (SI, Figure S20B). Additionally, the affinity of this conjugate for the dye was unaffected by the absence (K_D = 0.9 ± 0.1 μM) or presence (K_D = 1.1 ± 0.2 μM) of adenosine (SI, Figure S20C), demonstrating that both aptamer modules function independently. Lastly, we confirmed that the A23T-R91−4bp conjugate has similar binding affinity to adenosine (K_{D1} = 14.9 ± 0.9 μM, K_{D2} = 26.1 ± 0.4 μM) (SI, Figure S21A) relative to the A23T parent aptamer (K_{D1} = 14.8 ± 1.1 μM, K_{D2} = 28.6 ± 0.5 μM) (SI, Figure S21B). Thus, conjugation of R91−4bp with A23T does not perturb either aptamer's binding affinity to its respective ligand. The fact that this construct does not seem to misfold is interesting, given that both A23T and R91−4bp are G-rich and that R91−4bp may contain a G-quadruplex. We subsequently performed the RT-Exo digestion assay in the presence of varying concentrations of adenosine. In the absence of target, A23T-R91−4bp was completely digested after 6 h, but the presence of adenosine inhibited digestion in a concentration-dependent manner (Figure 3B; SI, Figure S22). As with the E1 assay above, we were able to obtain 720 data points for each sample over the course of the entire digestion—nearly 100-fold more data-points than would be possible with the conventional assay, without any additional intervention by the experimenter. Finally, we assessed the specificity of A23T using the RT-Exo assay and determined that A23T-R91−4bp only responded to adenosine, but not ATP, ADP, AMP, inosine triphosphate (ITP), nicotinamide adenine dinucleotide (NAD), guanosine triphosphate (GTP), cytosine triphosphate (CTP), uridine triphosphate (UTP), or deoxyadenosine triphosphate (dATP) (Figure 3C ; SI, Figure S23). These results are in line with the specificity data from previous reports for the same aptamer.[16]

To determine if the RT-Exo assay is compatible with hydrophobic ligands, we next assessed the binding properties of our DNA aptamer THC1.2, which binds the highly hydrophobic molecule tetrahydrocannabinol (THC) with a K_D of 50 nM.[21] This aptamer proved particularly challenging because it was among the most G-rich aptamers in our study (68% G in the putative binding domain), which made the likelihood of the construct misfolding higher. After synthesizing the THC1.2-R91−4bp conjugate (Figure 3D), we confirmed that it bound to DFHBI-1T with similar affinity in the absence and presence of target (K_D = 2.4 ± 0.3 μM and 2.0 ± 0.3 μM) (SI, Figure S24A,B) relative to R91−4bp (K_D = 2.3 ± 0.2 μM) (SI, Figure S24C). We then performed the RT-Exo digestion assay to assess the relative binding affinity of the conjugate to THC. As with the other aptamers, the conjugate was eventually digested after 6 h in the absence of THC, whereas the presence of THC inhibited the digestion of the conjugate in a manner proportional to THC concentration (Figure 3E; SI, Figure S25). We also determined the specificity of the THC1.2 construct versus 20 different drugs of abuse and pharmaceuticals using the RT-Exo digestion assay, and found that they were consistent with previously reported specificity data for THC1.2[21] (Figure 3F; SI, Figures S26, 27), confirming the validity of our assay results. Thus, RT-Exo seems to be compatible with a broad range of aptamers and ligands.

We next determined whether the assay could be used to study the binding properties of aptamers reported by others. We first applied our assay to the cocaine-binding DNA aptamer MNS4.1,[22] conjugating this aptamer to R91−4bp at its 5′ end via a $(T)_3$ linker (Figure 3G). We confirmed that the affinity of MNS4.1-R91−4bp conjugate for DFHBI-1T without or with cocaine target (K_D = 4.4 ± 0.3 μM and 4.0 ± 0.4 μM, respectively) was essentially unchanged relative to R91−4bp (K_D = 4.9 ± 0.3 μM) (SI, Figure S28), and its affinity for cocaine (K_D = 10.7 ± 0.6 μM) was similar to that of the parent aptamer (K_D = 8.9 ± 0.8 μM) (SI, Figure S29). We then performed the RT-Exo assay to characterize the relative binding affinity of the construct for cocaine and observed concentration-dependent inhibition of aptamer digestion, with highly resolved and well-defined digestion curves (Figure 3H; SI, Figure S30). We also assessed the binding specificity of MNS4.1 to 34 different ligands using our RT-Exo assay, and determined that it cross-reacts with several including methylenedioxypyrovalerone (MDPV), methadone, benzocaine, procaine, and quinine (Figure 3I; SI, Figures S31−33), which accurately reflected the previously reported binding profile of MNS4.1.[23]

https://doi.org/10.1021/jacs.5c17561
J. Am. Chem. Soc. 2026, 148, 10421−10436

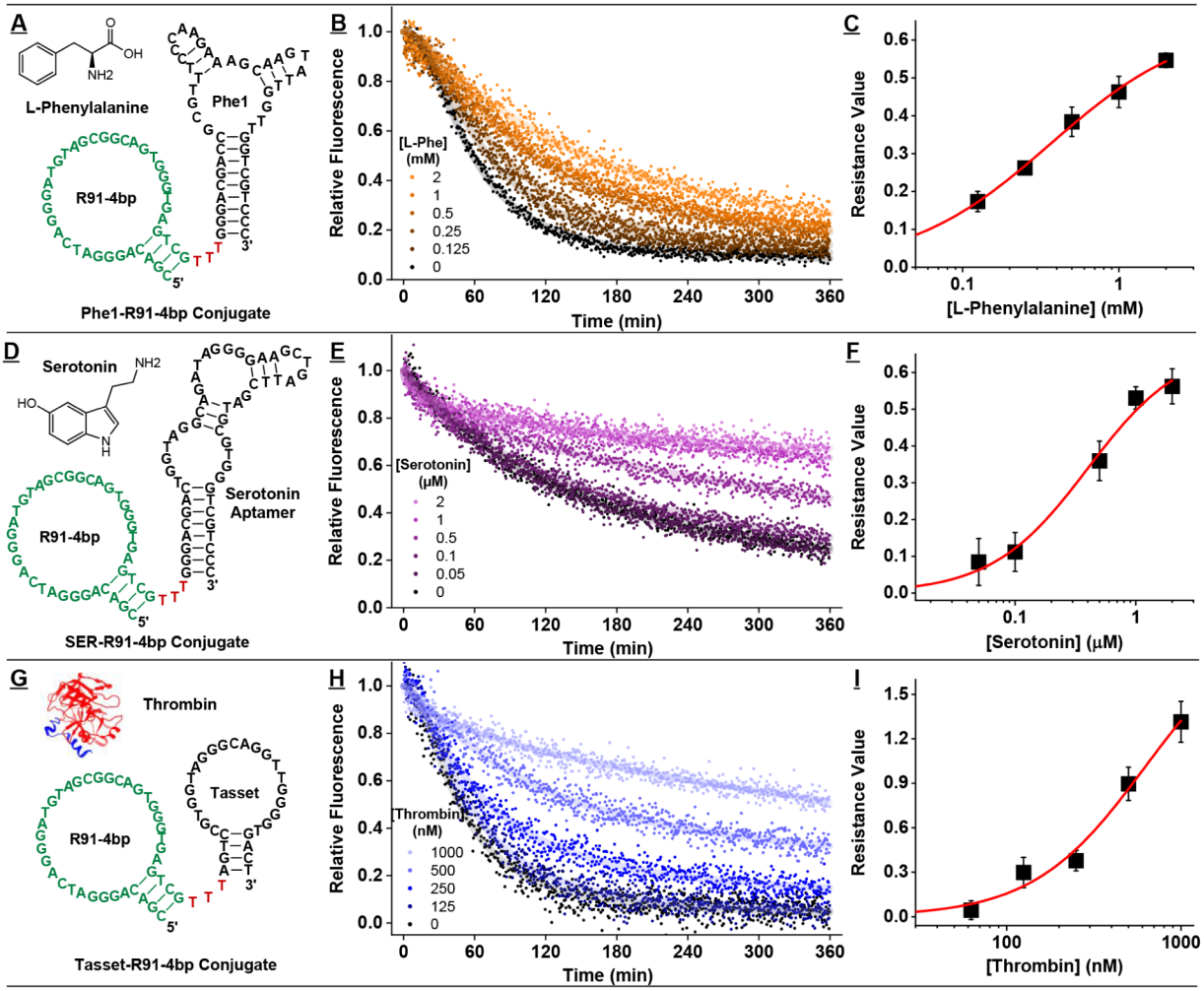

Figure 4. RT-Exo assay is applicable to both small-molecule and protein-binding aptamers. (A) Structure of the phenylalanine aptamer conjugate Phe1-R91−4bp. (B) RT-Exo assay data showing fluorescence over time at different concentrations of phenylalanine, and (C) resistance to exonuclease digestion as a function of phenylalanine concentration. (D) Structure of the serotonin aptamer conjugate SER-R91−4bp. (E) RT-Exo assay data showing fluorescence over time at different concentrations of serotonin, and (F) resistance to exonuclease digestion as a function of serotonin concentration. (G) Structure of the thrombin aptamer conjugate Tasset-R91−4bp. (H) RT-Exo assay data showing fluorescence over time at different concentrations of thrombin, and (I) resistance to exonuclease digestion as a function of thrombin concentration.

As a further demonstration of the method's generalizability, we performed RT-Exo assays with serotonin and phenylalanine DNA aptamers, which bind their respective targets with a K_D of 30 nM and 10 μM.[24,25] We coupled each aptamer to R91−4bp at its 5′ end via a $(T)_3$ linker (Figure 4A,D), and confirmed that each construct's affinity for DFHBI-1T (K_D = 2.2 ± 0.2 μM and 1.7 ± 0.4 μM for the serotonin and phenylalanine conjugates, respectively) was not meaningfully different from that of R91−4bp (K_D = 2.2 ± 0.2 μM under the same binding buffer conditions, 1X PBS, 2 mM $MgCl_2$, 1% DMSO) (SI, Figure S34). Similarly, the affinity of each construct for its target (K_D = 28 ± 5 nM, and 8.8 ± 0.3 μM for serotonin and phenylalanine, respectively) was essentially the same as that of their parent aptamers[24,25] (K_D = 49 ± 5 nM and 8.2 ± 0.3 μM, respectively) (SI, Figure S35). When we employed these constructs in the RT-Exo digestion assay, they both displayed target concentration-dependent inhibition of aptamer digestion, with highly resolved and well-defined digestion curves (Figure 4B, C, E and F). These results offer further proof that the RT-Exo assay is compatible with a diverse array of small-molecule-binding aptamers.

Finally, we assessed whether our RT-Exo assay could be applied to protein-binding aptamers. As a model system, we used the thrombin-binding DNA aptamer reported by Tasset et al.,[26] which has a K_D of 500 pM. We conjugated this aptamer to R91−4bp at its 5′ end via a $(T)_3$ linker (Figure 4G). Interestingly, we observed a 2-fold poorer affinity for DFHBI-1T in the absence of thrombin (K_D = 8.1 ± 0.7 μM) versus in the presence of thrombin (K_D = 3.5 ± 0.2 μM) (SI, Figure S36A,B). The K_D of R91−4bp itself to DFHBI-1T under these same conditions is 4.9 μM (SI, Figure S36C). This indicates that the conjugation of the Tasset aptamer to R91−4bp negatively impacts the affinity of the fluorophore-binding domain (in the absence of thrombin), perhaps through nonspecific interactions between R91−4bp and Tasset that cause R91−4bp to misfold. We hypothesize that the improved affinity of the conjugate for DFHBI-1T when thrombin is bound to Tasset is likely because R91−4bp can no longer engage in this unfavorable interaction with Tasset in the presence of thrombin. Using biolayer interferometry, we found that the thrombin-binding affinity of the Tasset-R91−4bp construct (K_D = 1,770 ± 490 pM) is reduced relative to that of

https://doi.org/10.1021/jacs.5c17561
J. Am. Chem. Soc. 2026, 148, 10421−10436

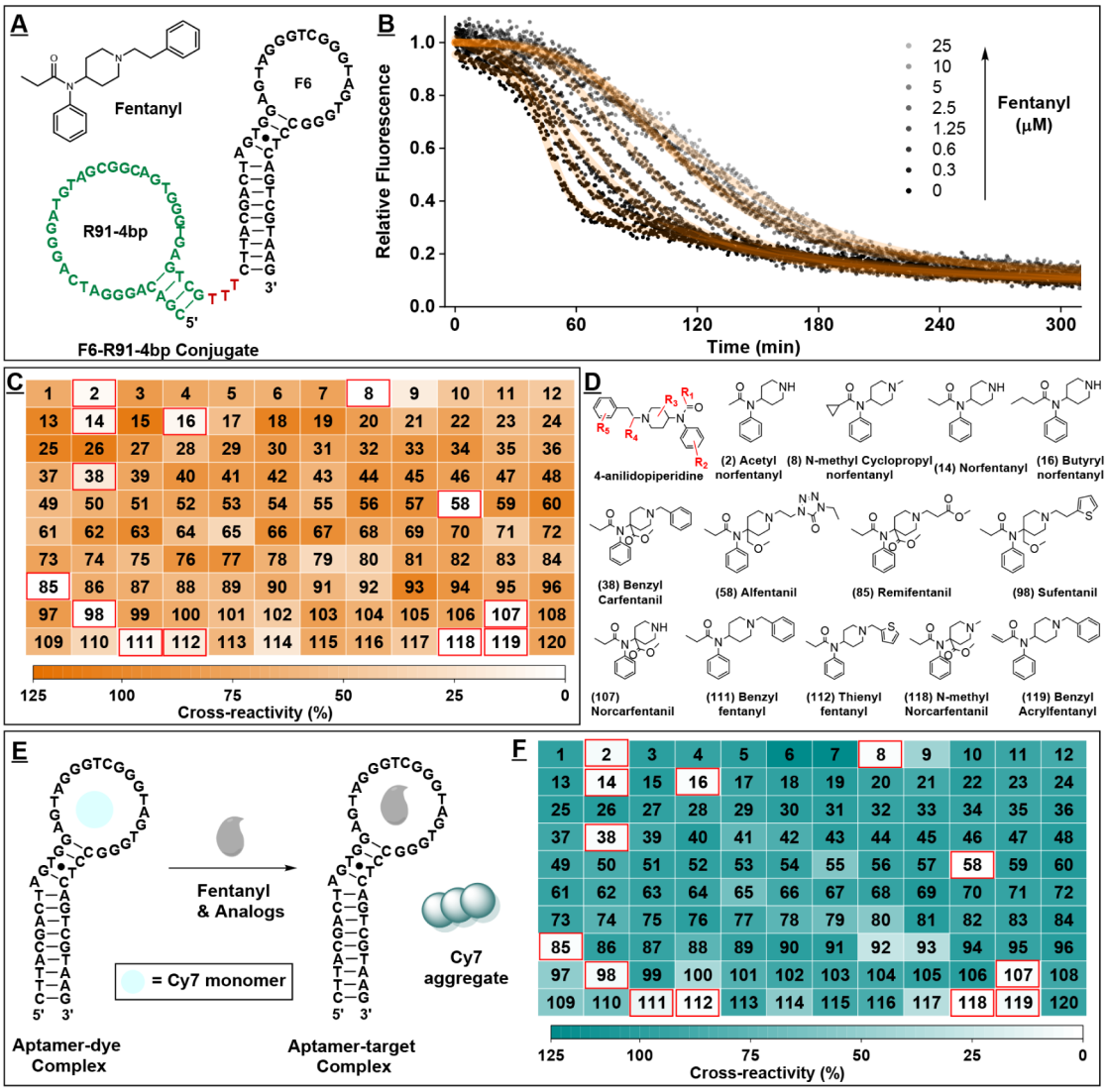

Figure 5. Demonstrating the high-throughput capabilities of the RT-Exo assay by examining the binding profile of fentanyl-binding aptamer F6. (A) Secondary structure of the F6-R91−4bp conjugate. (B) RT-Exo assay data showing fluorescence over time at different concentrations of fentanyl. (C) Cross-reactivity of F6 to 120 different fentanyl analogs as determined using the RT-Exo assay. (D) Structures of fentanyl analogs to which F6 does not cross-react. (E) Design of the dye displacement assay used to validate the results obtained with RT-Exo and (F) a heatmap of the cross-reactivity measurements from that assay.

the parent aptamer (K_D = 467 ± 37 pM) (SI, Figure S37). Finally, we performed the RT-Exo assay with varying concentrations of thrombin. As the concentration of thrombin increased, the inhibition of conjugate digestion by the exonucleases increased proportionally (Figure 4H,I), confirming that our assay is also compatible with protein-binding aptamers.

High-Throughput Characterization of a Cross-Reactive Aptamer

We next sought to demonstrate the greatly improved sample throughput that the RT-Exo assay enables with F6, a recently discovered aptamer that binds to fentanyl analogs.[15] Our goal was to simultaneously assess the cross-reactivity of F6 to 120 different fentanyl analogs in a single experiment. With the conventional exonuclease assay approach, this would require collection of ∼1,200 time-point samples via 100 precisely timed pipetting steps and the use of thousands of pipet tips and at least three 384-well microplates. With the RT-Exo assay, such experiments are much more feasible and economical, requiring just mixing the aptamer, target, and exonucleases, and recording the results with a microplate reader.

To carry out this experiment, we coupled F6 to R91−4bp via a $(T)_3$ linker (Figure 5A), and then confirmed that the affinity of this conjugate for DFHBI-1T in both the absence (K_D = 1.5 ± 0.1 μM) and presence of fentanyl (K_D = 1.4 ± 0.4 μM) is similar to that of R91−4bp (K_D = 2.3 ± 0.2 μM) (SI, Figure S38). We also determined that the F6-R91−4bp conjugate binds fentanyl with similar affinity (K_D = 76 ± 9 nM) as the parent aptamer (K_D = 69 ± 8 nM) (SI, Figure S39). As with the other aptamers we tested with RT-Exo, we were able to monitor the digestion of F6-R91−4bp in real time with high resolution in the absence and presence of fentanyl (Figure 5B). We next performed the RT-Exo assay with F6-R91−4bp against the 120 different fentanyl analogs present in the Fentanyl Analog Screening Kit distributed by the Centers for Disease Control and Prevention (SI, Figures S40−S43). The results showed that F6 could recognize 107 different analogs containing a diverse set of functional group

https://doi.org/10.1021/jacs.5c17561
J. Am. Chem. Soc. 2026, 148, 10421−10436

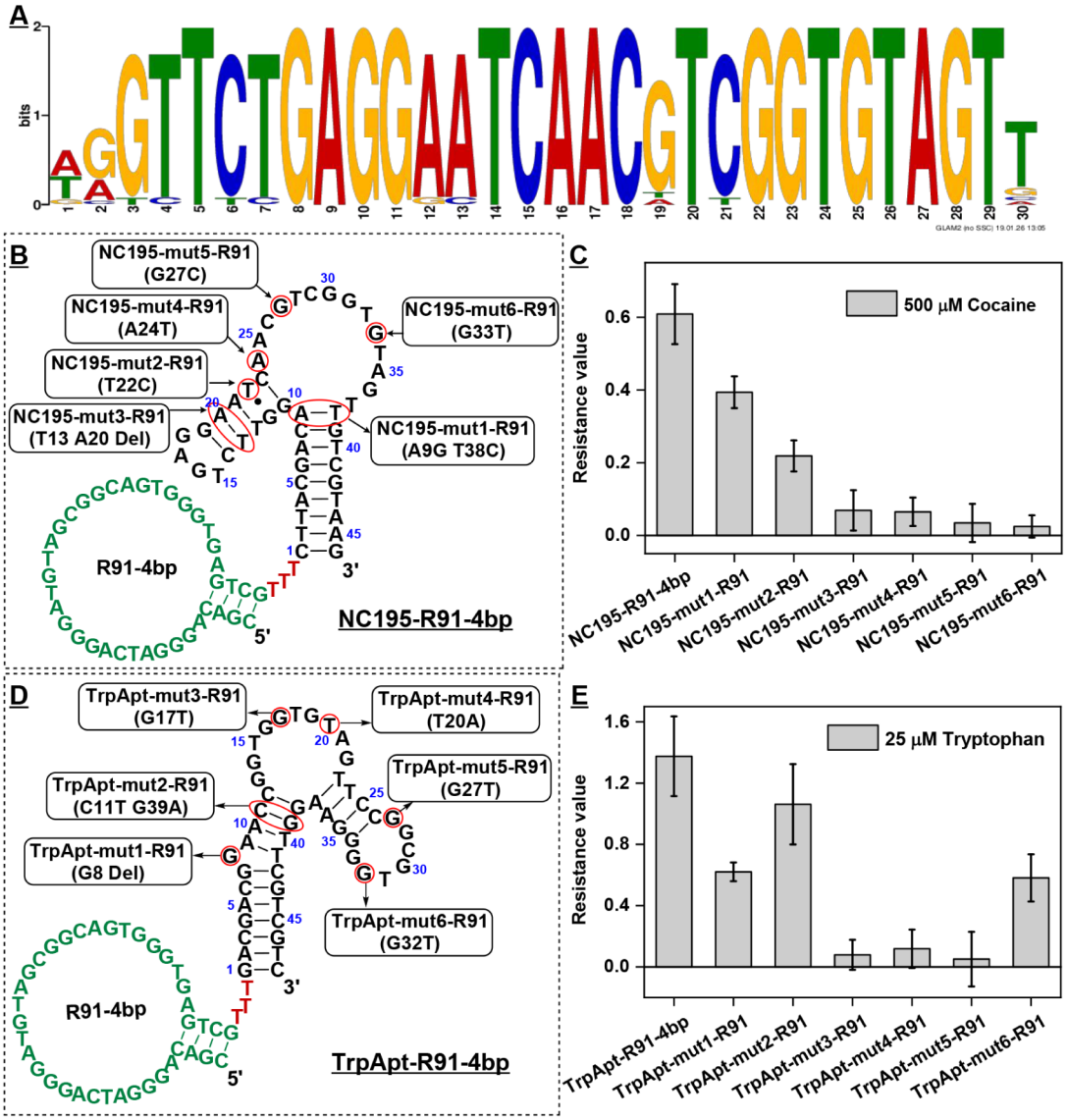

Figure 6. Using the RT-Exo assay to screen aptamers in mutagenesis studies. (A) Sequence logo representing a cluster of sequences related to NC195 discovered from an enriched SELEX pool. (B) Predicted secondary structure of NC195-R91−4bp; mutations tested in subsequent experiments are circled and labeled. (C) Results from the RT-Exo assay to measure relative binding of NC195-R91−4bp and mutants to cocaine. (D) Predicted secondary structure of TrpApt-R91−4bp, with mutations tested in these experiments circled and labeled. (E) Results from the RT-Exo assay to measure relative binding of TrpApt and mutants to tryptophan.

substituents with a cross-reactivity of 20% relative to fentanyl (Figure 5C; SI, Figures S44−53). We observed that the aptamer is mostly tolerant to substituents at the amido (R_1) and phenyl groups (R_2 & R_5) and partially tolerates variation at the piperidine ring (R_3) (Figure 5D). However, F6 could not recognize 13 analogs, including analogs that are one carbon shorter at the *N*-alkyl chain (R_4) (i.e., benzyl alfentanil, benzyl fentanyl, benzyl acryl fentanyl, and thienyl fentanyl) as well as those that have an additional non-hydrogen substituent at position 4 of the piperidine ring (i.e., alfentanil, remifentanil, and sufentanil). The aptamer also did not respond to any human metabolites of fentanyl analogs, all of which lack the *N*-phenethyl moiety, including norfentanyl, acetyl norfentanyl, *N*-methyl cyclopropyl norfentanyl, butyryl norfentanyl, norcarfentanil, and *N*-methyl norcarfentanil. We thus conclude that the aptamer most likely recognizes the analogs via structural features that are common among them, such as the piperidine ring, aniline ring, amido group, and phenylethyl group. These results highlight the plethora of information that a single RT-Exo assay can provide on aptamer binding properties with impressively high throughput.

Finally, to verify the results of the RT-Exo assay, we performed a well-established dye-displacement assay[27,28] with F6 and the cyanine dye diethylthiotricarbocyanine (Cy7) against the 120 fentanyl analogs. In this assay, Cy7 initially forms a noncovalent complex with F6 as a monomer, in which state it absorbs maximally at 770 nm. Target binding to F6 displaces Cy7 into solution, causing the dye to form H-aggregates that instead absorb at 595 nm (Figure 5E). The results of the Cy7 displacement assay corroborated well with those of the RT-Exo assay. The same 107 analogs that showed ≥20% cross-reactivity in the RT-Exo assay also cross-reacted in the dye-displacement assay, and the F6 aptamer again failed to bind to the same 13 analogs (Figure 5D; SI, Figures S54−63). To verify some of these results, we used ITC. Specifically, we characterized the binding of F6 to analogs for which both

https://doi.org/10.1021/jacs.5c17561
J. Am. Chem. Soc. 2026, 148, 10421−10436

assays indicated relatively strong binding (i.e., fentanyl, analog 13, and cyclopropyl fentanyl, analog 15) or relatively weak binding (i.e., cis-3-methyl thiofentanyl, analog 80), as well as an analog where the two assays were divergent in cross-reactivity (i.e., ortho-methyl phenyl fentanyl, analog 93) (SI, Figure S64). ITC confirmed that F6 binds with high affinity to fentanyl (K_D = 33 ± 5 nM) (SI, Figure S64A) and cyclopropyl fentanyl (K_D = 29 ± 2 nM) (SI, Figure S64B) and has lower affinity for cis-3-methyl thiofentanyl (K_D = 3.0 ± 0.2 μM) (SI, Figure S64C). Thus, ITC corroborated the results of both the RT-Exo and Cy7-displacement assay for these analogs. For ortho-methyl phenyl fentanyl, ITC indicated moderate affinity (K_D = 452 ± 46 nM) (SI, Figure S64D). Accordingly, we expected that the RT-Exo and Cy7-displacement assay should both yield cross-reactivity values of ∼100% because 100 μM ligand was used and thus >99% of the aptamer should be bound to the ligand. However, while the RT-Exo assay yielded the expected cross-reactivity value (102% cross-reactivity relative to fentanyl), the Cy7-displacement assay did not (33% cross-reactivity relative to fentanyl). We hypothesized that the Cy7-displacement assay was inaccurate due to nonspecific interaction of the dye itself with the analog, which we have observed previously for hydrophobic analytes.[28] Closer examination of the UV−vis absorbance spectrum for ortho-methyl phenyl fentanyl revealed, aside from the typically observed peaks at 595 and 770 nm respectively corresponding to Cy7 H-aggregate and monomer, an extraneous peak at λ = 680 nm (SI, Figure S61I), which may correspond to the formation of a dimer between Cy7 and ortho-methyl phenyl fentanyl. Thus, in this particular case, the Cy7-displacement assay results are less reliable than those of the RT-Exo assay.

Using the RT-Exo Assay to Perform Aptamer Structure−Activity Relationship Studies

Another practical application of the RT-Exo assay is the capability to assess the impact of mutations on aptamer binding performance. To demonstrate this, we generated a panel of six mutants of NC195 (SI, Figure S65A), a 46-nt DNA aptamer that binds cocaine with nanomolar affinity,[29] based on the consensus sequence of the NC195 family (Figure 6A), which was obtained by clustering sequences from the SELEX pool where the aptamer was discovered, as well as the predicted secondary structure of NC195 using NUPACK.[30] We initially performed the first-generation exonuclease assay (SI, Figure S65B) and confirmed the results by determining the binding affinity of the mutants using ITC (SI, Figure S66). We then conjugated R91−4bp to these mutants at their 5′ terminus (Figure 6B) and performed the RT-Exo assay (Figure 6C; SI, Figure S67). We first mutated A9 and T38 to G and C respectively (NC195-mut1) to determine whether strengthening the terminus of the stem would improve cocaine-binding affinity. Both digestion assays revealed slightly weaker binding than NC195, and ITC likewise indicated a 2-fold reduction in cocaine affinity for the mutant (NC195-mut1; K_D = 82 ± 9 nM) relative to the parent aptamer (K_D = 39 ± 8 nM). These results therefore refuted our hypothesis. We next mutated T22—which may form a wobble base-pair with G11—to C to create a complementary GC pair in the internal hairpin (NC195-mut2), with the assumption that affinity would improve. Both digestion assays again showed the opposite, with lower resistance values indicating that cocaine affinity was significantly weaker. ITC confirmed ∼ 200-fold poorer affinity for this mutant (K_D = 8.6 ± 0.5 μM) relative to NC195. Thus, perfect base-pairing at this position is deleterious for cocaine binding. Next, to investigate the effect of shortening the stem length of the internal hairpin, we removed the T13-A20 base pair (NC195-mut3). Both digestion assays indicated that this mutant had minimal affinity for cocaine, which was again corroborated by ITC (K_D = 79 ± 1 μM), confirming that stability in this hairpin is necessary for binding. Finally, based on their high degree of conservation in the NC195 family, we mutated A24 to T (NC195-mut4), G27 to C (NC195-mut5), and G33 to T (NC195-mut6). In all three cases, cocaine affinity was completely abolished according to both digestion assays and ITC, confirming that these nucleotides are critical for binding.

To further demonstrate generality, we applied the RT-Exo assay to a 48-nt DNA aptamer reported by the Stojanovic group termed TrpApt that binds L-tryptophan with sub-micromolar affinity.[11] To perform structure−activity studies, we generated six mutants of TrpApt based on its structure (SI, Figure S68A), of which NUPACK predicts that the aptamer contains a 7-bp stem connected to a 4-bp stem via a single-nucleotide bulge, followed by a 10-nt bulge, and finally an internal 4-bp hairpin with a 7-nt loop. We initially performed the first-generation exonuclease assay (SI, Figure S68B) and confirmed these results by determining their target binding affinity using ITC (SI, Figure S69). We next conjugated R91−4bp to these mutants at their 5′ terminus (Figure 6D) and performed the RT-Exo assay (Figure 6E; SI, Figure S70). We first determined whether the single nucleotide-bulge in the stem of the aptamer was necessary for binding by deleting G8 (TrpApt-mut1). Both digestion assays yielded a lower resistance value for this mutant relative to TrpApt, implying weaker affinity for tryptophan. However, ITC indicated that TrpApt-mut1 (K_D = 282 ± 28 nM) had similar affinity as TrpApt (K_D = 387 ± 15 nM). Since exonuclease assay resistance values generally correlate more closely with the K_D of the major digestion product of the aptamer being tested,[15] the lower resistance values for this mutant suggests that its truncation product has lower target affinity than the parent aptamer. We next examined the effect of weakening the C11-G39 base-pair by mutating these bases to T and A, respectively (TrpApt-mut2). Both exonuclease-based assays and ITC showed no significant difference in affinity for this mutant (K_D = 210 ± 24 nM) relative to TrpApt. Finally, we created point mutants G17T (TrpApt-mut3), T20A (TrpApt-mut4), G27T (TrpApt-mut5), and G32T (TrpApt-mut6). None of these mutants bound tryptophan except for TrpApt-mut6, which showed significantly reduced tryptophan binding in both exonuclease-based assays and also exhibited 6-fold weaker affinity per ITC (K_D = 2.3 ± 0.2 μM). These results together indicate that RT-Exo provides a generalizable approach to accurately and conveniently screen the binding properties of aptamers in structure−activity relationship studies.

DISCUSSION

Here, we present RT-Exo, a new method that enables label-free, high-throughput, real-time characterization of aptamer binding properties via exonuclease digestion assays. This approach simply entails connecting a given aptamer of interest to the fluorogenic aptamer R91−4bp, digesting the resulting construct with exonucleases, and monitoring the fluorescence change during the digestion process using a microplate reader. We have demonstrated that RT-Exo is applicable to a broad range of aptamers with diverse sequences and structural

https://doi.org/10.1021/jacs.5c17561
J. Am. Chem. Soc. 2026, 148, 10421−10436

features (*e.g.,* stem-loops, three-way junctions, G-quadruplexes), differing target affinities (*e.g.,* picomolar to micromolar K_D), and ligands of varying charge and hydrophobicity. Much like with conventional exonuclease digestion assays, RT-Exo screens aptamers for their capability to bind ligands and reports on the relative binding strengths of these interactions. However, RT-Exo represents a substantial overhaul of the first-generation assay in that aptamer digestion is monitored continuously in real time with high resolution, eliminating the need to collect numerous aliquots of the sample at precisely defined time-points. This leads to several improvements in terms of assay convenience, accuracy, precision, and throughput. First, RT-Exo is significantly simpler and more efficient, because it only requires mixing of reagents (i.e., aptamer, ligands, and exonucleases) followed by autonomous recording of the reaction progress by a microplate reader, rather than demanding the constant attention and intervention by the experimenter. For the RT-Exo assay, this also translates into greater accuracy in fluorescence measurements compared to the first-generation assay because the fluorescence of samples in the former is directly measured in the well, whereas inaccuracies can arise from the additional sampling, transferring, and mixing steps performed in the first-generation assay. Second, because the digestion reaction in the RT-Exo assay is monitored continuously with high frequency (~30 s), hundreds or even thousands of data points can be collected, orders of magnitude greater than the typical number of data points obtained in the first-generation assay (≤10). In terms of intra-assay error, uncertainties in the fit of the time-course of the fluorescence measurements are notably lower for the RT-Exo assay than for the first-generation assay due to this higher data density, leading to improved accuracy in modeling the digestion reaction—and hence improved accuracy in the resulting resistance values. Although we have not taken advantage of this here, the high temporal resolution offered by this method could provide new insights into the kinetics of aptamer-ligand binding and digestion, which is impossible with the traditional assay given its poor temporal resolution. Third, the throughput of the RT-Exo assay is notably greater than the conventional assay, enabling characterization of at least 120 aptamer-ligand pairs simultaneously in a single experiment. Due to the number of pipetting steps involved and the sheer number of samples, this cannot be done with the traditional assay. Finally, the resource consumption of the RT-Exo assay is much lower than that of the traditional assay, utilizing at least 10-fold fewer pipet tips and fewer microplates as well.

For the RT-Exo assay to be useful, it should be applicable to a wide range of aptamers of differing sequence, structures, target-binding affinities, and buffer composition. An important factor to consider regarding generality is the reaction conditions. Here, for 20 out of 22 aptamers, we were able to employ the same concentration of exonucleases and obtain adequate results. This indicates that RT-Exo should be sufficiently generalizable to enable the large-scale screening of multiple aptamers in parallel without intensive optimization of individual assay conditions. However, it is possible that, under our default enzyme concentrations (1× = 0.025 U/μL Exo III and 0.1 U/μL Exo I), some aptamers will also be digested too rapidly or slowly. Aptamers that do not undergo digestion at an ideal rate in these default conditions can be retested in separate batches (e.g., slow, medium, and fast digestors) with differing enzyme concentrations (i.e., 3×, 1×, and 0.25× relative to our default enzyme concentrations, respectively). Regarding assay generality in terms of aptamer sequence and structure, although R91−4bp is likely to form a G-quadruplex, we have shown that it is compatible even with aptamers that are very G-rich (G-content from 30−51%). However, in just one case (Tasset-R91−4bp) did we observe slight perturbations in target and DFHBI-1T affinity for the conjugate relative to the parent aptamer and R91−4bp alone. We hypothesize that misfolding or aggregation of such constructs did not frequently occur in our studies because the R91−4bp moiety within the construct is always bound to DFHBI-1T, which is present in excess relative to the conjugate. Dye binding is likely to promote folding of R91−4bp, and this may preclude interaction of R91−4bp with the adjacent aptamer domain and hence prevent misfolding. Nevertheless, it is possible that misfolding or aggregation could occur with other constructs. As it is not possible to predict which aptamers R91−4bp would be incompatible with based on sequence alone, we recommend the empirical testing of constructs. In terms of ligands, the RT-Exo assay was compatible with a wide range of small molecules with different polarities (e.g., ranging from highly hydrophobic THC to highly hydrophilic phenylalanine) as well as a protein target. We predict that RT-Exo should be generalizable to other targets as long as the target in question does not affect the digestive activity of the exonucleases themselves—for instance, by competitively binding or sequestering enzyme cofactors like Mg^{2+}, denaturing the exonucleases, or affecting the binding of R91−4bp to DFHBI-1T.

Automating the RT-Exo assay could further improve the throughput by orders of magnitude. For example, conjugates synthesized in microplates—something that is now regularly offered by companies that synthesize oligonucleotides—could be first reconstituted with reaction buffer using a liquid-handling system and then incubated with DFHBI-1T and ligands. The exonuclease mixture could then be automatically dispensed to each sample to initiate the reaction, with the microplate immediately transferred to a plate reader for continuous assay monitoring. Data processing can likewise be automated with the use of macros in spreadsheet software, making the entire aptamer screening process virtually effortless. As the liquid handling system can prepare multiple microplates ahead of time, the only limiting factor would be the availability of microplate readers to monitor the digestion progress. There are several other strategies by which the assay could be further modified to either improve its performance or obtain new insights into aptamer-ligand interactions. First, other exonucleases, such as T5 Exonuclease, which digests single- and double-stranded DNA in the 5′ to 3′ direction, could be used instead of Exo III and Exo I. We have found that T5 Exo is somewhat more sensitive to aptamer-ligand binding than Exo III;[13] in cases where Exo III and Exo I fail to detect any binding in the assay, T5 Exo can be used to rule out a false negative result. However, this will require altering the current conjugate design such that the aptamer is linked to R91−4bp at its 3′ end rather than the 5′ end. Second, Exo-RT could be used to assess the degree of conformational change that truncated structure-switching aptamers undergo upon target binding. This would simply entail connecting the truncated aptamer to R91−4bp and performing digestions in the absence and presence of ligand solely with Exo I.[31] Aptamers that are primarily unfolded in the absence of ligand are rapidly digested by Exo I, while ligand-bound, folded aptamers resist digestion. A large difference in the rate of digestion between the free and

https://doi.org/10.1021/jacs.5c17561
J. Am. Chem. Soc. 2026, 148, 10421−10436

ligand-bound aptamer would indicate that the aptamer undergoes a relatively large conformational change upon target binding. Third, it is possible that RNA aptamers could be adapted into the RT-Exo platform by switching Lettuce with fluorogenic RNA aptamers such as Spinach, and using RNA exonucleases such as Exonuclease T.[32] Fourth, there is certainly room for improving the signal-to-noise ratio of the assay. In the least sensitive system we tested here, the starting fluorescence signal was merely 3-fold above background. This could be improved by using alternative signal reporters in place of R91−4bp. For example, the Ferré-D'Amaré and Jaffrey groups designed a minimized Lettuce aptamer termed Bibb-Lettuce that may have more robust fluorogenic properties than R91−4bp, resulting in higher signal-to-noise ratios.[19] Finally, it may be possible to conduct RT-Exo assays in complex samples such as biological fluids if the fluorescent aptamer module can bind a previously reported derivative of DFHBI-1T which has excitation and emission wavelengths >500 nm.[33] With further enhancements and extensions of the method, we anticipate that the simplicity, reliability, versatility, and high-throughput nature of RT-Exo will make it a first-line choice for screening aptamer-ligand interactions and accelerate the discovery and development of aptamers suitable for a wide range of real-world applications.

■ ASSOCIATED CONTENT

Supporting Information

The Supporting Information is available free of charge at https://pubs.acs.org/doi/10.1021/jacs.5c17561.

DNA sequences and various buffer conditions employed in this work; summary of ITC experimental conditions and results; experimental setup of the first-generation exonuclease assay and RT-Exo assay; data analysis workflow for the RT-Exo assay, working principle of the first-generation exonuclease digestion assay; performance of the first-generation exonuclease digestion assay with or without SYBR Gold; secondary structures of aptamers used in this work; fluorescence yield of fluorogenic aptamers; effect of DMSO or Tris buffer on DFHBI-1T fluorescence; linearity of DFHBI-1T fluorescence with varying concentrations of R91−4bp; the first-generation exonuclease digestion of R91−4bp in the presence and absence of DFHBI-1T; RT-Exo fluorescence time course data of specificity experiments; ITC data of parent aptamers and their R91−4bp conjugates; DFHBI-1T binding affinity data; effect of linker length on the RT-Exo assay; biolayer interferometry data; fentanyl analog structures; RT-Exo fluorescence time course for F6 cross-reactivity; absorbance spectra for Cy7-displacement assay; NC195 structure−activity study with the first-generation exonuclease assay; RT-Exo fluorescence time course of NC195-R91−4bp and its mutant conjugates; TrpApt structure−activity study with the first-generation exonuclease assay; RT-Exo fluorescence time course of TrpApt-R91−4bp and its mutant conjugates (PDF)

■ AUTHOR INFORMATION

Corresponding Author

Yi Xiao − *Department of Chemistry, North Carolina State University, Raleigh, North Carolina 27695, United States;* orcid.org/0000-0001-7278-9811; Email: yxiao34@ncsu.edu

Authors

Caleb Byrd − *Department of Chemistry, North Carolina State University, Raleigh, North Carolina 27695, United States*

Obtin Alkhamis − *Department of Chemistry, North Carolina State University, Raleigh, North Carolina 27695, United States*

Gabriel Castro − *Department of Chemistry, North Carolina State University, Raleigh, North Carolina 27695, United States*

Thinh Phuc Nguyen − *Department of Chemistry, North Carolina State University, Raleigh, North Carolina 27695, United States*

Juan Canoura − *Department of Chemistry, North Carolina State University, Raleigh, North Carolina 27695, United States*

Complete contact information is available at: https://pubs.acs.org/10.1021/jacs.5c17561

Notes

The authors declare no competing financial interest.

■ ACKNOWLEDGMENTS

This work was supported by the National Institutes of Health [R01NS134365, Yi Xiao] and the National Institute of Justice, Grant Office of Justice Programs, U.S. Department of Justice, Award 2022-GG-04440-RESS.

■ REFERENCES

(1) Ellington, A. D.; Szostak, J. W. In Vitro Selection of RNA Molecules That Bind Specific Ligands. *Nature* **1990**, *346* (6287), 818−822.

(2) Tuerk, C.; Gold, L. Systematic Evolution of Ligands by Exponential Enrichment: RNA Ligands to Bacteriophage T4 DNA Polymerase. *Science* **1990**, *249* (4968), 505−510.

(3) Li, L.; Xu, S.; Yan, H.; Li, X.; Yazd, H. S.; Li, X.; Huang, T.; Cui, C.; Jiang, J.; Tan, W. Nucleic Acid Aptamers for Molecular Diagnostics and Therapeutics: Advances and Perspectives. *Angew. Chem. Int. Ed* **2021**, *60* (5), 2221−2231.

(4) Dunn, M. R.; Jimenez, R. M.; Chaput, J. C. Analysis of Aptamer Discovery and Technology. *Nat. Rev. Chem* **2017**, *1* (10), 0076.

(5) Slavkovic, S.; Johnson, P. E. Isothermal Titration Calorimetry Studies of Aptamer-Small Molecule Interactions: Practicalities and Pitfalls. *Aptamers* **2018**, *2*, 45−51.

(6) Chang, A. L.; McKeague, M.; Liang, J. C.; Smolke, C. D. Kinetic and Equilibrium Binding Characterization of Aptamers to Small Molecules Using a Label-Free, Sensitive, and Scalable Platform. *Anal. Chem* **2014**, *86* (7), 3273−3278.

(7) Entzian, C.; Schubert, T. Studying Small Molecule-Aptamer Interactions Using MicroScale Thermophoresis (MST). *Methods* **2016**, *97*, 27−34.

(8) Vignon, A.; Flaget, A.; Michelas, M.; Djeghdir, M.; Defrancq, E.; Coche-Guerente, L.; Spinelli, N.; van der Heyden, A.; Dejeu, J. Direct Detection of Low-Molecular-Weight Compounds in 2D and 3D Aptasensors by Biolayer Interferometry. *ACS Sens* **2020**, *5* (8), 2326−2330.

(9) Lou, X.; Egli, M.; Yang, X. Determining Functional Aptamer-Protein Interaction by Biolayer Interferometry. *Curr. Protoc. Nucleic Acid Chem* **2016**, *67* (1), 7.25.1−7.25.15.

(10) Yang, K.-A.; Barbu, M.; Halim, M.; Pallavi, P.; Kim, B.; Kolpashchikov, D. M.; Pecic, S.; Taylor, S.; Worgall, T. S.; Stojanovic, M. N. Recognition and Sensing of Low-Epitope Targets via Ternary

Complexes with Oligonucleotides and Synthetic Receptors. *Nat. Chem* **2014**, *6* (11), 1003−1008.
(11) Yang, K.; Mitchell, N. M.; Banerjee, S.; Cheng, Z.; Taylor, S.; Kostic, A. M.; Wong, I.; Sajjath, S.; Zhang, Y.; Stevens, J.; Mohan, S.; Landry, D. W.; Worgall, T. S.; Andrews, A. M.; Stojanovic, M. N. A Functional Group-Guided Approach to Aptamers for Small Molecules. *Science* **2023**, *380* (6648), 942−948.
(12) Canoura, J.; Wang, Z.; Yu, H.; Alkhamis, O.; Fu, F.; Xiao, Y. No Structure-Switching Required: A Generalizable Exonuclease-Mediated Aptamer-Based Assay for Small-Molecule Detection. *J. Am. Chem. Soc* **2018**, *140* (31), 9961−9971.
(13) Alkhamis, O.; Yang, W.; Farhana, R.; Yu, H.; Xiao, Y. Label-Free Profiling of DNA Aptamer-Small Molecule Binding Using T5 Exonuclease. *Nucleic Acids Res* **2020**, *48* (20), No. e120.
(14) Alkhamis, O.; Canoura, J.; Ly, P. T.; Xiao, Y. Using Exonucleases for Aptamer Characterization, Engineering, and Sensing. *Acc. Chem. Res* **2023**, *56* (13), 1731−1743.
(15) Canoura, J.; Alkhamis, O.; Liu, Y.; Willis, C.; Xiao, Y. High-Throughput Quantitative Binding Analysis of DNA Aptamers Using Exonucleases. *Nucleic Acids Res* **2023**, *51* (4), No. e19.
(16) Canoura, J.; Yu, H.; Alkhamis, O.; Roncancio, D.; Farhana, R.; Xiao, Y. Accelerating Post-SELEX Aptamer Engineering Using Exonuclease Digestion. *J. Am. Chem. Soc* **2021**, *143* (2), 805−816.
(17) Canoura, J.; Liu, Y.; Alkhamis, O.; Xiao, Y. Aptamer-Based Fentanyl Detection in Biological Fluids. *Anal. Chem* **2023**, *95* (49), 18258−18267.
(18) VarnBuhler, B. S.; Moon, J.; Dey, S. K.; Wu, J.; Jaffrey, S. R. Detection of SARS-CoV-2 RNA Using a DNA Aptamer Mimic of Green Fluorescent Protein. *ACS Chem. Biol* **2022**, *17* (4), 840−853.
(19) Passalacqua, L. F. M.; Banco, M. T.; Moon, J. D.; Li, X.; Jaffrey, S. R.; Ferré-D'Amaré, A. R. Intricate 3D Architecture of a DNA Mimic of GFP. *Nature* **2023**, *618* (7967), 1078−1084.
(20) Chen, H.; Meisburger, S. P.; Pabit, S. A.; Sutton, J. L.; Webb, W. W.; Pollack, L. Ionic Strength-Dependent Persistence Lengths of Single-Stranded RNA and DNA. *Proc. Natl. Acad. Sci.* **2012**, *109* (3), 799−804.
(21) Yu, H.; Luo, Y.; Alkhamis, O.; Canoura, J.; Yu, B.; Xiao, Y. Isolation of Natural DNA Aptamers for Challenging Small-Molecule Targets, Cannabinoids. *Anal. Chem* **2021**, *93* (6), 3172−3180.
(22) Stojanovic, M. N.; de Prada, P.; Landry, D. W. Aptamer-Based Folding Fluorescent Sensor for Cocaine. *J. Am. Chem. Soc* **2001**, *123* (21), 4928−4931.
(23) Alkhamis, O.; Canoura, J.; Wang, L.; Xiao, Y. Nuclease-Assisted Selection of Slow-Off Rate Aptamers. *Sci. Adv* **2024**, *10* (24), No. eadl3426.
(24) Cheung, K. M.; Yang, K.-A.; Nakatsuka, N.; Zhao, C.; Ye, M.; Jung, M. E.; Yang, H.; Weiss, P. S.; Stojanović, M. N.; Andrews, A. M. Phenylalanine Monitoring via Aptamer-Field-Effect Transistor Sensors. *ACS Sens* **2019**, *4* (12), 3308−3317.
(25) Nakatsuka, N.; Yang, K.-A.; Abendroth, J. M.; Cheung, K. M.; Xu, X.; Yang, H.; Zhao, C.; Zhu, B.; Rim, Y. S.; Yang, Y.; Weiss, P. S.; Stojanović, M. N.; Andrews, A. M. Aptamer−Field-Effect Transistors Overcome Debye Length Limitations for Small-Molecule Sensing. *Science* **2018**, *362* (6412), 319−324.
(26) Tasset, D. M.; Kubik, M. F.; Steiner, W. Oligonucleotide Inhibitors of Human Thrombin That Bind Distinct Epitopes. *J. Mol. Biol* **1997**, *272* (5), 688−698.
(27) Stojanovic, M. N.; Landry, D. W. Aptamer-Based Colorimetric Probe for Cocaine. *J. Am. Chem. Soc* **2002**, *124* (33), 9678−9679.
(28) Alkhamis, O.; Canoura, J.; Bukhryakov, K. V.; Tarifa, A.; DeCaprio, A. P.; Xiao, Y. DNA Aptamer−Cyanine Complexes as Generic Colorimetric Small-Molecule Sensors. *Angew. Chem. Int. Ed* **2022**, *61* (3), No. e202112305.
(29) Alkhamis, O.; Canoura, J.; Wu, Y.; Emmons, N. A.; Wang, Y.; Honeywell, K. M.; Plaxco, K. W.; Kippin, T. E.; Xiao, Y. High-Affinity Aptamers for In Vitro and In Vivo Cocaine Sensing. *J. Am. Chem. Soc* **2024**, *146* (5), 3230−3240.
(30) Zadeh, J. N.; Steenberg, C. D.; Bois, J. S.; Wolfe, B. R.; Pierce, M. B.; Khan, A. R.; Dirks, R. M.; Pierce, N. A. NUPACK: Analysis and Design of Nucleic Acid Systems. *J. Comput. Chem* **2011**, *32* (1), 170−173.
(31) Liu, Y.; Yu, H.; Alkhamis, O.; Moliver, J.; Xiao, Y. Tuning Biosensor Cross-Reactivity Using Aptamer Mixtures. *Anal. Chem* **2020**, *92* (7), 5041−5047.
(32) Deutscher, M. P.; Marlor, C. W.; Zaniewski, R. Ribonuclease T: New Exoribonuclease Possibly Involved in End-Turnover of tRNA. *Proc. Natl. Acad. Sci.* **1984**, *81* (14), 4290−4293.
(33) Li, X.; Mo, L.; Litke, J. L.; Dey, S. K.; Suter, S. R.; Jaffrey, S. R. Imaging Intracellular S-Adenosyl Methionine Dynamics in Live Mammalian Cells with a Genetically Encoded Red Fluorescent RNA-Based Sensor. *J. Am. Chem. Soc* **2020**, *142* (33), 14117−14124.

https://doi.org/10.1021/jacs.5c17561
J. Am. Chem. Soc. 2026, 148, 10421−10436

Supporting information for:

High-Throughput Aptamer Characterization via Real-Time Nuclease Digestion

Caleb Byrd, Obtin Alkhamis, Gabriel Castro, Thinh Phuc Nguyen, Juan Canoura and Yi Xiao*

Department of Chemistry, North Carolina State University, 2620 Yarbrough Dr., Raleigh, NC, USA, 27695.

*Corresponding author: yxiao34@ncsu.edu

Table S1. List of oligonucleotides and aptamers used in this work.

Sequence ID	Sequence (5' to 3')
Lettuce	AACGTGCTCAAGGTGTCTTAGTAGGGATGATGCGGCAGTGGGCTTCGC AGAACAGTGTTTATTCTGCGAGGGGACTAAGACTCCTTCAGCAAGTTAAGC
Lettuce-4bp	TAGTAGGGATGATGCGGCAGTGGGCTTCGCAGAACAGTGTTTATT CTGCGAGGGGACTA
Lettuce-mini	TAGTAGGGATGATGCGGCAGTGGGCTTCGCTTTGCGAGGGGACTA
R91	GGAGGCTCTCGGGACGACAGGGATCAGGGATGTAGCGGCAGTGGGTGA GTCGTCCCGATGCTGCAATCGTAA
R91-4bp	CGACAGGGATCAGGGATGTAGCGGCAGTGGGTGAGTCG
E1	GGGACGACTGCTTGGGTAGGTCGGGCTTGGGTTCGGCGGTCGTCCC
E1-R91-4bp	CGACAGGGATCAGGGATGTAGCGGCAGTGGGTGAGTCGTTTGGGACGACTGC TTGGGTAGGTCGGGCTTGGGTTCGGCGGTCGTCCC
E1-R91-4bp-1T	CGACAGGGATCAGGGATGTAGCGGCAGTGGGTGAGTCGTGGGACGACTGC TTGGGTAGGTCGGGCTTGGGTTCGGCGGTCGTCCC
E1-R91-4bp-6T	CGACAGGGATCAGGGATGTAGCGGCAGTGGGTGAGTCGTTTTTTGGGACGACTGC TTGGGTAGGTCGGGCTTGGGTTCGGCGGTCGTCCC
A23T	CGCACCTGGGGGAGTATTGCGGTGGAAGGTGCG
A23T-R91-4bp	CGACAGGGATCAGGGATGTAGCGGCAGTGGGTGAGTCGTTTCGCACCTGGGG GAGTATTGCGGTGGAAGGTGCG
THC1.2	CTTACGACCCAGGGGGGTGGACAGGCGGGGGTTAGGGGGGTCGTAAG
THC1.2-R91-4bp	CGACAGGGATCAGGGATGTAGCGGCAGTGGGTGAGTCGTTTCTTACGACCCA GGGGGGTGGACAGGCGGGGGTTAGGGGGGTCGTAAG
MNS4.1	GGGAGACAAGGATAAATCCTTCAATGAAGTGGGTCGATA
MNS4.1-R91-4bp	CGACAGGGATCAGGGATGTAGCGGCAGTGGGTGAGTCGTTTGGGAGACA AGGATAAATCCTTCAATGAAGTGGGTCGATA
SER	GGGACGACTGGTAGGCAGATAGGGGAAGCTGATTCGATGCGTGGGTCGTCCC
SER-R91-4bp	CGACAGGGATCAGGGATGTAGCGGCAGTGGGTGAGTCGTTTGGGACGACTGG TAGGCAGATAGGGGAAGCTGATTCGATGCGTGGGTCGTCCC
Phe1	GGGACGACCGCGTTTCCCAAGAAAGCAAGTATTGGTTGGTCGTCCC
Phe1-R91-4bp	CGACAGGGATCAGGGATGTAGCGGCAGTGGGTGAGTCGTTTGGGACGACCGC GTTTCCCAAGAAAGCAAGTATTGGTTGGTCGTCCC
Tasset	AGTCCGTGGTAGGGCAGGTTGGGGTGACT
Tasset-R91-4bp	CGACAGGGATCAGGGATGTAGCGGCAGTGGGTGAGTCGTTTAGTCCGT GGTAGGGCAGGTTGGGGTGACT
F6	CTTACGACTAGTGGAGTAGGGTCGGGTAGTGGGCCTCAGTCGTAAG
F6-R91-4bp	CGACAGGGATCAGGGATGTAGCGGCAGTGGGTGAGTCGTTTCTTACGACT AGTGGAGTAGGGTCGGGTAGTGGGCCTCAGTCGTAAG
NC195	CTTACGACAGGTTCTGAGGAATCAACGTCGGTGTAGTTGTCGTAAG
NC195-mut1	CTTACGACGGGTTCTGAGGAATCAACGTCGGTGTAGTCGTCGTAAG
NC195-mut2	CTTACGACAGGTTCTGAGGAACCAACGTCGGTGTAGTTGTCGTAAG
NC195-mut3	CTTACGACAGGTCTGAGGATCAACGTCGGTGTAGTTGTCGTAAG
NC195-mut4	CTTACGACAGGTTCTGAGGAATCTACGTCGGTGTAGTTGTCGTAAG
NC195-mut5	CTTACGACAGGTTCTGAGGAATCAACCTCGGTGTAGTTGTCGTAAG
NC195-mut6	CTTACGACAGGTTCTGAGGAATCAACGTCGGTTTAGTTGTCGTAAG
NC195-R91-4bp	CGACAGGGATCAGGGATGTAGCGGCAGTGGGTGAGTCGTTTCTTACGACAGGTTCTG AGGAATCAACGTCGGTGTAGTTGTCGTAAG
NC195-mut1-R91	CGACAGGGATCAGGGATGTAGCGGCAGTGGGTGAGTCGTTTCTTACGACGGGTTCTG AGGAATCAACGTCGGTGTAGTCGTCGTAAG

NC195-mut2-R91	CGACAGGGATCAGGGATGTAGCGGCAGTGGGTGAGTCGTTTCTTACGACAGGTTCTGAGGAACCAACGTCGGTGTAGTTGTCGTAAG
NC195-mut3-R91	CGACAGGGATCAGGGATGTAGCGGCAGTGGGTGAGTCGTTTCTTACGACAGGTCTGAGGATCAACGTCGGTGTAGTTGTCGTAAG
NC195-mut4-R91	CGACAGGGATCAGGGATGTAGCGGCAGTGGGTGAGTCGTTTCTTACGACAGGTTCTGAGGAATCTACGTCGGTGTAGTTGTCGTAAG
NC195-mut5-R91	CGACAGGGATCAGGGATGTAGCGGCAGTGGGTGAGTCGTTTCTTACGACAGGTTCTGAGGAATCAACCTCGGTGTAGTTGTCGTAAG
NC195-mut6-R91	CGACAGGGATCAGGGATGTAGCGGCAGTGGGTGAGTCGTTTCTTACGACAGGTTCTGAGGAATCAACGTCGGTTTAGTTGTCGTAAG
TrpApt	GACGACGGAACCGGTGGTGTAGTTCCGGCGTGGGGAAGGTTCGTCGTC
TrpApt-mut1	GACGACGAACCGGTGGTGTAGTTCCGGCGTGGGGAAGGTTCGTCGTC
TrpApt-mut2	GACGACGGAATCGGTGGTGTAGTTCCGGCGTGGGGAAGATTCGTCGTC
TrpApt-mut3	GACGACGGAACCGGTGTTGTAGTTCCGGCGTGGGGAAGGTTCGTCGTC
TrpApt-mut4	GACGACGGAACCGGTGGTGAAGTTCCGGCGTGGGGAAGGTTCGTCGTC
TrpApt-mut5	GACGACGGAACCGGTGGTGTAGTTCCTGCGTGGGGAAGGTTCGTCGTC
TrpApt-mut6	GACGACGGAACCGGTGGTGTAGTTCCGGCGTTGGGAAGGTTCGTCGTC
TrpApt-R91	CGACAGGGATCAGGGATGTAGCGGCAGTGGGTGAGTCGTTTGACGACGGAACCGGTGGTGTAGTTCCGGCGTGGGGAAGGTTCGTCGTC
TrpApt-mut1-R91	CGACAGGGATCAGGGATGTAGCGGCAGTGGGTGAGTCGTTTGACGACGAACCGGTGGTGTAGTTCCGGCGTGGGGAAGGTTCGTCGTC
TrpApt-mut2-R91	CGACAGGGATCAGGGATGTAGCGGCAGTGGGTGAGTCGTTTGACGACGGAATCGGTGGTGTAGTTCCGGCGTGGGGAAGATTCGTCGTC
TrpApt-mut3-R91	CGACAGGGATCAGGGATGTAGCGGCAGTGGGTGAGTCGTTTGACGACGGAACCGGTGTTGTAGTTCCGGCGTGGGGAAGGTTCGTCGTC
TrpApt-mut4-R91	CGACAGGGATCAGGGATGTAGCGGCAGTGGGTGAGTCGTTTGACGACGGAACCGGTGGTGAAGTTCCGGCGTGGGGAAGGTTCGTCGTC
TrpApt-mut5-R91	CGACAGGGATCAGGGATGTAGCGGCAGTGGGTGAGTCGTTTGACGACGGAACCGGTGGTGTAGTTCCTGCGTGGGGAAGGTTCGTCGTC
TrpApt-mut6-R91	CGACAGGGATCAGGGATGTAGCGGCAGTGGGTGAGTCGTTTGACGACGGAACCGGTGGTGTAGTTCCGGCGTTGGGAAGGTTCGTCGTC
SCA2.1	CTTACGACCTTAAGTGGGGTTCGGGTGGAGTTTATGGGGTCGTAAG
F27	CTTACGACGAGCGCGTGTGGCCGGCGTGAGGGAGGTGAGTCGTAAG
F17	CTTACGACCGGTGGGGAGGCCGGAGTTGGGAACGGGGGGTCGTAAG
HM1	GGGACGACGGGATTCGGATCGTGGAACAGTGCCTCGTCGTCGTCCC
HM20	GGGACGACATGCGTCGAAAAGACCCCTGAGGGCAGCTGGTCGTCCC
OM1	GGGACGACAAGTCAGGCCTGTCTCAGCGAGTTCGACATGTCGTCCC
OM4	GGGACGACGAGTGCGGGGAGTGTGTTTCTGTGGGGGTCGTCGTCCC
MMC1	CTTACGACCAGGGTTGGTTTCATCGGTGGTGTAATATGGTCGTAAG
E2	GGGACGACAAAATGGCAGCATTGGTGACGGAGTTGCTTGTCGTCCC
E7	GGGACGACAGAATGGCAGCATTGGTGAGTTATTTGCCTGTCGTCCC
E5	GGGACGACGTAATGGGAGCATTGGTCACGCAGGTGCACGTCGTCCC
FX1	GGGACGACGGCCCCTTTTAAGGAGGTAGAGGTGTTCGCTGTCGTCCC
FX5	GGGACGACGGTACCCGGCGATCTTTAGTTGGAGGTAGGGTCGTCCC
FX40	GGGACGACGGCCCCCGGAGAGGAGGTAGAGGTGTTCGCTGTCGTCCC
OBA-3	CGGGGCGAAGCGGGTCCCG
NC48	CTTACGACGCGGACGTTGTGGGGCGTGGCAGTCGGTGAGTCGTAAG
NC69	CTTACGACATGGGATGTGTAGTTAGTGGTCGGATCCGGGTCGTAAG

ATP-33	CGCACCTGGGGGAGTATTGCGGAGGAAGGTGCG
ATP-7	CTTACGACGGGGATGAGGAGAGTGGTCGGGGAAAGGAAGTCGTAAG
FUB2	GGGACGACCTAGGGCTTGGGTTTAGGTGTGGGGTGTTGGGTCGTCCC
FUB4	GGGACGACGGGGGGCTTTAGGGTGTAGGAGTGGGGTGAGTCGTCCC
AMB2F	GGGACGACTAGCGGTGTTGGTCGGAGTGGTGGAATCTAGTCGTCCC
XA1	CTTACGACTGTGGTCGGGTGGTGGGCCTCTAGAGGGGTGTCGTAAG
GLU	ACGACCGTGTGTGTTGCTCTGTAACAGTGTCCATTGTCGT
EF1	TTCAAATCTAGCGCAGGTAGGGGTGTAGGTGTGGGGGTAAGTCTAGATTTGAA
EF5	TTCAAATCTCGCGCAGGTAGGGGTGTAGGTGTGGGGGTAAGTCTAGATTTGAA

Table S2. Composition of buffers used for studying fluorogenic aptamers.

Experiment	Buffer Conditions
Lettuce selection buffer	40 mM HEPES (pH 7.4), 20 mM NaCl, 100 mM KCl, 1 mM $MgCl_2$, 0.1% (v/v) DMSO
DMSO study	40 mM HEPES (pH 7.4), 20 mM NaCl, 100 mM KCl, 1 mM $MgCl_2$, 0.1–5.0% (v/v) DMSO
Buffering agent study	20 mM Tris or 40 mM HEPES (pH 7.4), 20 mM NaCl, 100 mM KCl, 1 mM $MgCl_2$, 1% (v/v) DMSO
KCl study	20 mM Tris (pH 7.4), 20 mM NaCl, 0–100 mM KCl, 1 mM $MgCl_2$, 1% (v/v) DMSO
NaCl study	20 mM Tris (pH 7.4), 0–200 mM NaCl, 4 mM KCl, 1 mM $MgCl_2$, 1% (v/v) DMSO
$MgCl_2$ study	20 mM Tris (pH 7.4), 20 or 140 mM NaCl, 4 mM KCl, 0–10 mM $MgCl_2$, 1% (v/v) DMSO
BSA study (high salt)	20 mM Tris (pH 7.4), 140 mM NaCl, 4 mM KCl, 1 mM $MgCl_2$, 1% (v/v) DMSO, 1.5 μM BSA
BSA study (low salt)	10 mM Tris (pH 7.4), 20 mM NaCl, 4 mM KCl, 0.5 mM $MgCl_2$, 1% (v/v) DMSO, 1.5 μM BSA
BSA study (FEN1)	20 mM Tris (pH 7.4), 140 mM NaCl, 4 mM KCl, 5 mM $MgCl_2$, 1% (v/v) DMSO, 1.5 μM BSA
BSA study (1× PBS)	1× PBS, 1 mM $MgCl_2$, 1% (v/v) DMSO, 1.5 μM BSA

Table S3. Composition of buffers used to study aptamer cross-reactivity to DFHBI-1T.

Buffer Name	Buffer Conditions
Low-salt Tris	10 mM Tris (pH 7.4), 20 mM NaCl, 4 mM KCl, 0.5 mM $MgCl_2$, 1% (v/v) DMSO, 1.5 μM BSA
FEN 1 buffer	20 mM Tris (pH 7.4), 140 mM NaCl, 4 mM KCl, 5 mM $MgCl_2$, 1% (v/v) DMSO, 1.5 μM BSA
THC buffer	10 mM Tris (pH 7.4), 20 mM NaCl, 4 mM KCl, 0.5 mM $MgCl_2$, 5% (v/v) DMSO, 1.5 μM BSA
AB-FUB buffer	10 mM Tris (pH 7.4), 137 mM NaCl, 4 mM KCl, 1 mM $MgCl_2$, 5% (v/v) DMSO, 1.5 μM BSA
ATP buffer	20 mM Tris (pH 7.4), 140 mM NaCl, 4 mM KCl, 2 mM $MgCl_2$, 1% (v/v) DMSO, 1.5 μM BSA
1x PBS	1× PBS, 1 mM $MgCl_2$, 1% (v/v) DMSO, 1.5 μM BSA
*Eco*R1 buffer	0.5× PBS, 5 mM $MgCl_2$, 0.005% Triton X-100, 4% (v/v) DMSO, 1.5 μM BSA
Glucose buffer	20 mM HEPES (pH 7.4), 20 mM NaCl, 10 mM KCl, 5 mM $MgCl_2$, 1% (v/v) DMSO, 1.5 μM BSA

Table S4. Composition of buffers used for the real-time exonuclease digestion assays.

Aptamer ID	[Target] (μM)	Buffer Conditions
E1 & E1-R91-4bp	25	1× PBS, 1 mM $MgCl_2$, 1.0% DMSO
A23T & A23T-R91-4bp	500	10 mM Tris, 20 mM NaCl, 1.5 mM $MgCl_2$, 4 mM KCl, 1% DMSO
THC1.2 & THC1.2-R91-4bp	10	20 mM Tris, 20 mM NaCl, 0.5 mM $MgCl_2$, 4 mM KCl, 5% DMSO
MNS4.1 & MNS4.1-R91-4bp	100	1× PBS, 1 mM $MgCl_2$, 1% DMSO
SER & SER-R91-4bp	2	1× PBS, 2 mM $MgCl_2$, 1% DMSO
Phe1 & Phe1-R91-4bp	2,000	1× PBS, 2 mM $MgCl_2$, 1% DMSO
Tasset & Tasset-R91-4bp	1	1× PBS, 1 mM $MgCl_2$, 1% DMSO
F6 & F6-R91-4bp	25	10 mM Tris, 20 mM NaCl, 0.5 mM $MgCl_2$, 4 mM KCl, 1% DMSO
NC195 & NC195-R91-4bp	500	20 mM Tris, 140 mM NaCl, 2 mM $MgCl_2$, 4 mM KCl, 1% DMSO
TrpApt & TrpApt-R91-4bp	25	1× PBS, 2 mM $MgCl_2$, 1% DMSO

Table S5. Parameters used for ITC experiments.

Aptamer ID	[Aptamer] (μM)	Target	[Target] (μM)	Injection Spacing	# Titrations
E1 & E1-R91-4bp	10	Fentanyl	100	180	1
A23T & A23T-R91-4bp	20	Adenosine	500	180	2
MNS4.1 & MNS4.1-R91-4bp	20	Cocaine	400	180	1
SER & SER-R91-4bp	10	Serotonin	50	180	1
Phe1 & Phe1-R91-4bp	20	Phenylalanine	500	180	1
F6 & F6-R91-4bp	10	Fentanyl	100	180	1
F6	10	Cyclopropyl Fentanyl	100	120	1
F6	10	Ortho-methyl Phenylfentanyl	150	120	1
F6	20	(±)-cis-3-methyl Thiofentanyl	300	120	1
NC195, NC195-mut1, NC195-mut4, NC195-mut5, & NC195-mut6	15	Cocaine	150	180	1
NC195-mut2	20	Cocaine	300	180	1
NC195-mut3	50	Cocaine	1000	120	2
TrpApt & TrpApt-mutants	10	Tryptophan	200	150	1

Table S6. Binding affinity of parent aptamers and related constructs determined by ITC experiments.

Aptamer	K_D	ΔH (kcal/mol)	ΔS (cal/mol/K)
E1	79 ± 7 nM	-22.5 ± 0.1	-43.5
E1-R91-4bp	67 ± 6 nM	-20.8 ± 0.2	-37.3
E1-R91-4bp-1T	56 ± 8 nM	-36.5 ± 0.4	-90.2
E1-R91-4bp-6T	36 ± 2 nM	-34.7 ± 0.1	-93.1
A23T	K_{D1} =14.8 ± 1.1 μM K_{D2} = 28.6 ± 0.5 μM	ΔH_1 = -12.9 ± 1.1 ΔH_2 = -23.2 ± 1.4	ΔS_1 = -21.3 ΔS_2 = -57.7
A23T-R91-4bp	K_{D1} = 14.9 ± 0.9 μM K_{D2} = 26.1 ± 0.4 μM	ΔH_1 = -13.1 ± 0.9 ΔH_2 = -21.5 ± 1.2	ΔS_1 = -22.1 ΔS_2 = -51.7
MNS4.1	8.9 ± 0.9 μM	-11.8 ± 0.8	-16.7
MNS4.1-R91-4bp	10.7 ± 0.8 μM	-8.5 ± 0.5	-5.9
SER	50 ± 5 nM	-17.1 ± 0.2	-24.2
SER-R91-4bp	47 ± 4 nM	-13.9 ± 0.1	-13.7
Phe1	8.2 ± 0.3 μM	-31.5 ± 0.9	-83.1
Phe1-R91-4bp	8.8 ± 0.3 μM	-31.3 ± 0.7	-82.4
F6 – Fentanyl	33 ± 5 nM	-30.8 ± 0.3	-69.6
F6 – Cyclopropyl Fentanyl	29 ± 2 nM	-22.4 ± 0.1	-40.9
F6 – ortho-methyl Phenylfentanyl	452 ± 46 nM	-13.3 ± 0.2	-15.8
F6 – (±)-cis-3-methyl Thiofentanyl	3.0 ± 0.2 μM	-11.7 ± 0.2	-14.1
F6-R91-4bp	76 ± 9 nM	-17.1 ± 0.2	-25.2
NC195	39 ± 8 nM	-26.3 ± 0.3	-54.7
NC195-mut1	82 ± 9 nM	-19.7 ± 0.2	-34.1
NC195-mut2	9.8 ± 0.3 μM	-22.0 ± 0.8	-51.3
NC195-mut3	79 ± 1 μM	-32.4 ± 0.1	-90.5
NC195-mut4	No Binding	N/A	N/A
NC195-mut5	No Binding	N/A	N/A
NC195-mut6	No Binding	N/A	N/A
TrpApt	387 ± 15 nM	-31.1 ± 0.2	-75.5
TrpApt-mut1	282 ± 28 nM	-30.5 ± 0.5	-73.0
TrpApt-mut2	210 ± 24 nM	-28.7 ± 0.5	-66.4
TrpApt-mut3	No Binding	N/A	N/A
TrpApt-mut4	No Binding	N/A	N/A
TrpApt-mut5	No Binding	N/A	N/A
TrpApt-mut6	2.3 ± 0.2 μM	-20.2 ± 1.1	-44.1

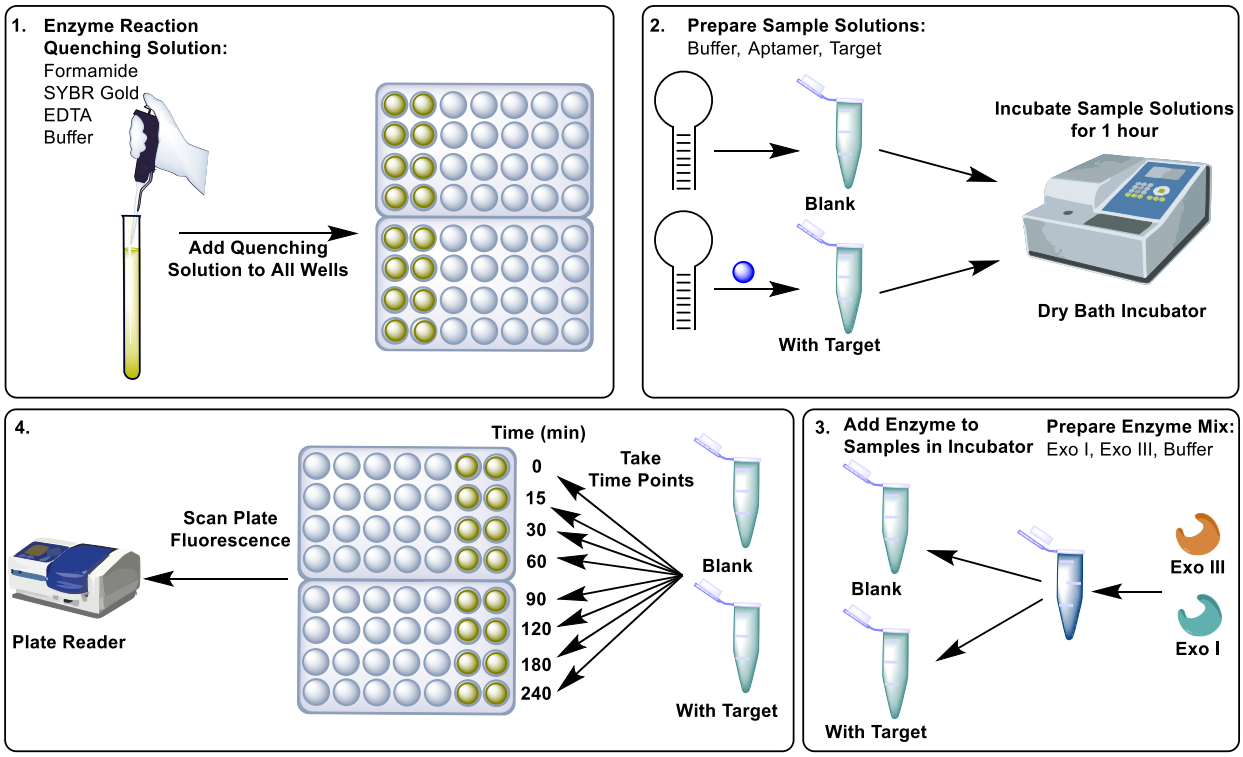

Figure S1. A schematic experimental setup of the first-generation of exonuclease assay.

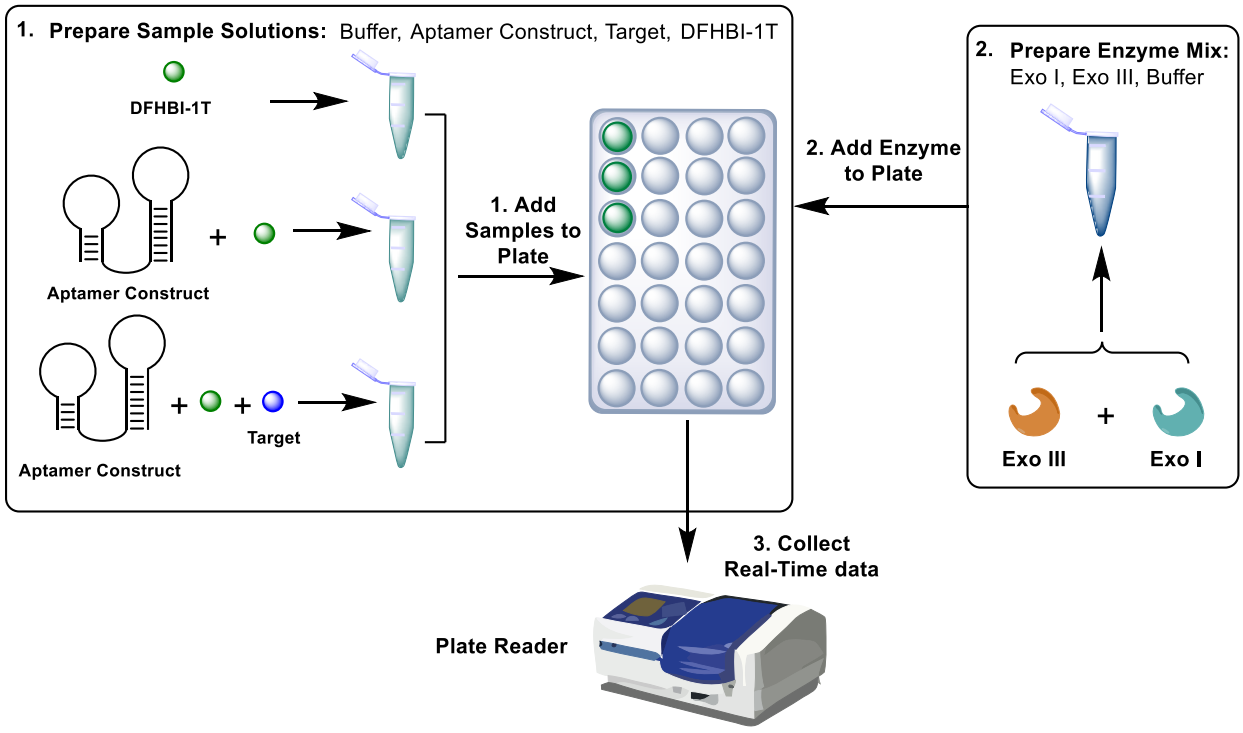

Figure S2. A schematic experimental setup of the second-generation of RT-Exo assay.

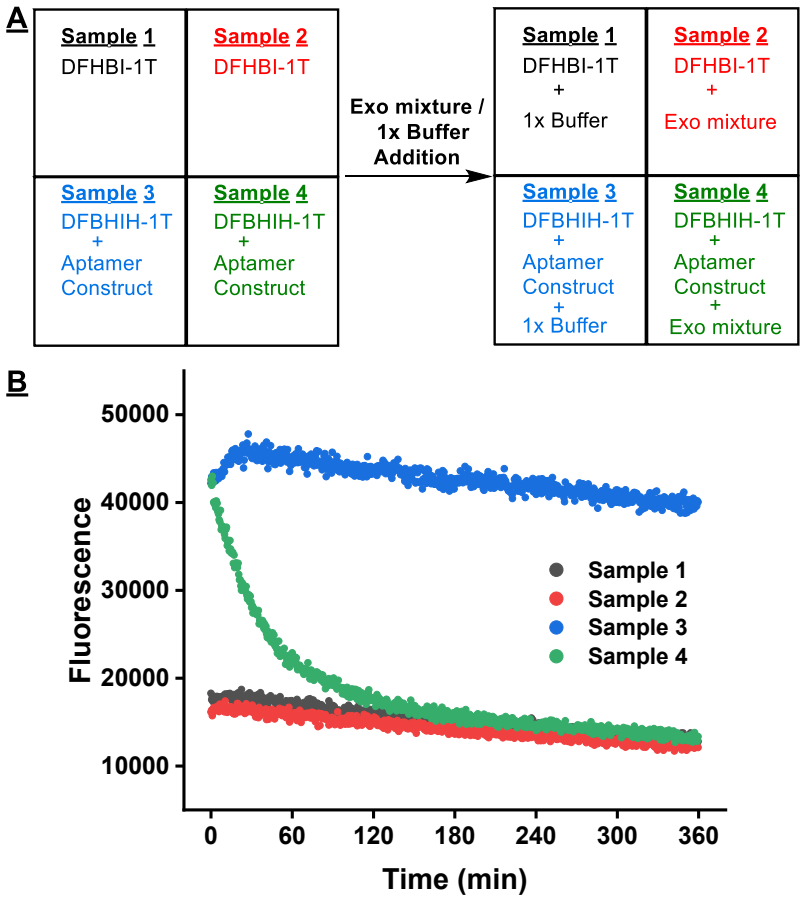

Figure S3. Samples created for the RT-Exo assay. (**A**) Schematic of experimental samples and how they are prepared. Sample 1 is a negative control that contains DFHBI-1T in buffer. Sample 2, another negative control, contains DFHBI-1T and exonuclease mixture in buffer. Sample 3 (a negative control) contains DFHBI-1T and aptamer in buffer. Sample 4 (the main test sample) has the same species but also has exonuclease mixture. (**B**) Raw fluorescence of these samples monitored over time during a typical RT-Exo experiment.

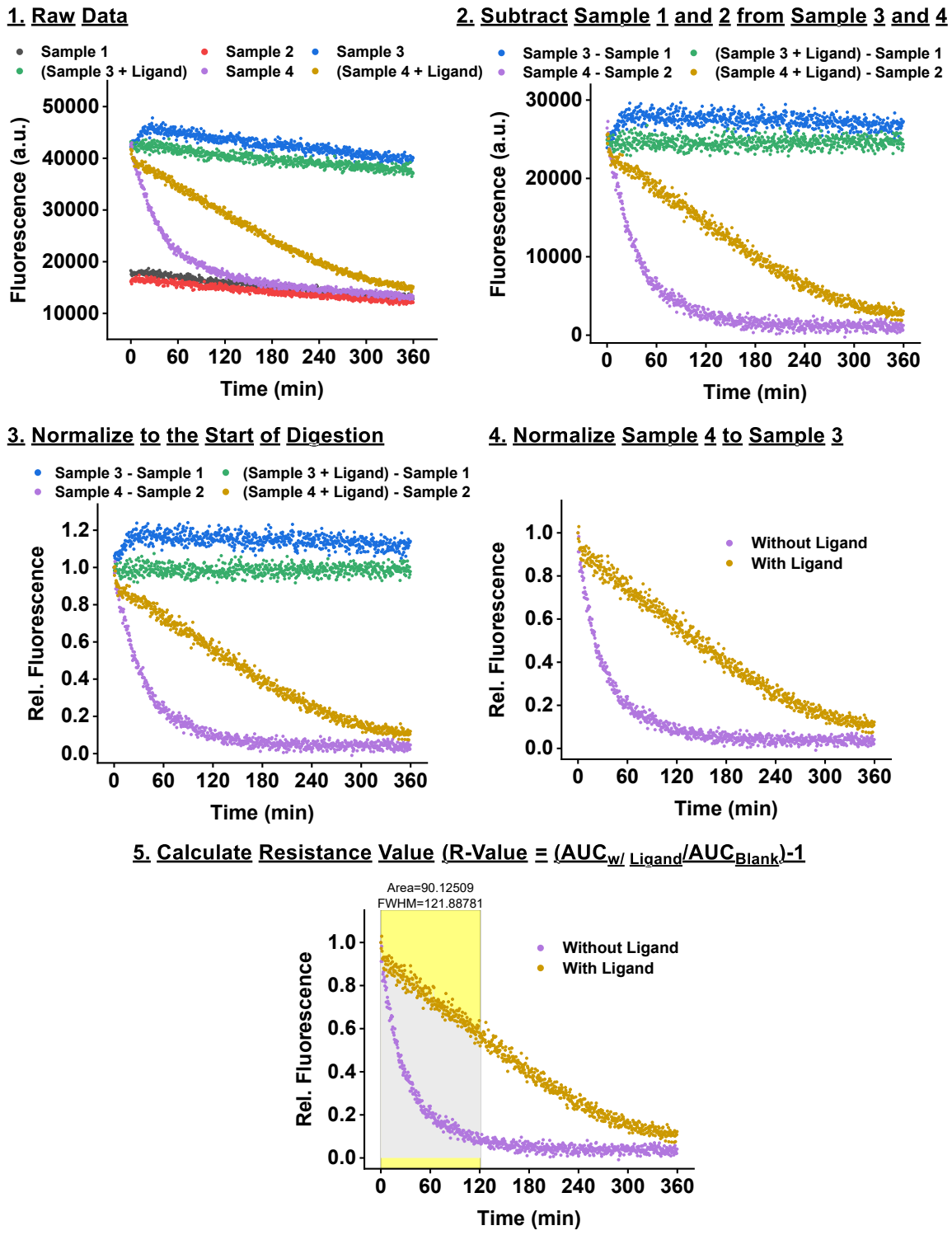

Figure S4. Workflow for analyzing the raw data obtained from the RT-Exo assay. (1) For a given aptamer-ligand pair, the raw data consists of fluorescence measurements of six different samples over time. The identity of the samples is described in **Figure S3**. (2) Because the background fluorescence of DFHBI-1T (*i.e.*, its fluorescence without aptamer) is non-zero and drifts over time, this background fluorescence is subtracted from all samples at every time-point. To do so, the fluorescence reads from Sample 1 (DFHBI-

1T and exonuclease mixture) are subtracted from those of Sample 3 (aptamer, DFHBI-1T, and exonuclease mixture) and Sample 3 + ligand. Fluorescence reads from Sample 2 (only DFHBI-1T) are subtracted from those of Sample 4 (aptamer and DFHBI-1T) and Sample 4 + ligand. (3) Next, the resulting fluorescence values for each sample are normalized with respect to each sample's starting fluorescence read (*i.e.*, the fluorescence read at t = 0 min). (4) Then, to account for the drift in the fluorescence of aptamer-bound DFHBI-1T, the normalized fluorescence reads of Sample 4 (without and with ligand) are normalized relative to Sample 3 (without and with ligand, respectively). This dataset can now be further analyzed to assess relative aptamer binding strength. (5) As a proxy of this, we use the metric termed 'resistance value' which is equal to the area under the curve (AUC) for the ligand-containing sample subtracted by the AUC of the ligand-free sample up until the time that the normalized fluorescence of the sample without ligand reaches zero; the resulting difference is then subtracted by 1. We determined AUCs using the integration function in the OriginPro software.

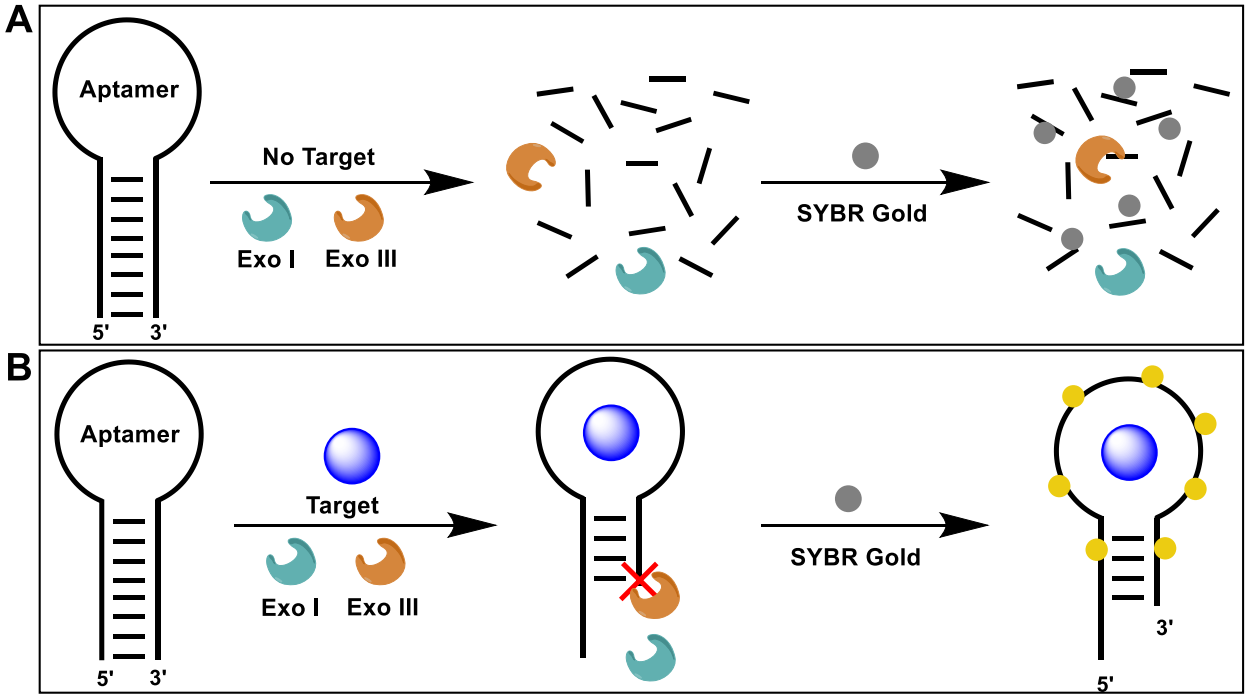

Figure S5. Scheme of exonuclease digestion assay with a mixture of exonuclease III (Exo III) and exonuclease I (Exo I) in the (**A**) absence and (**B**) presence of ligand.

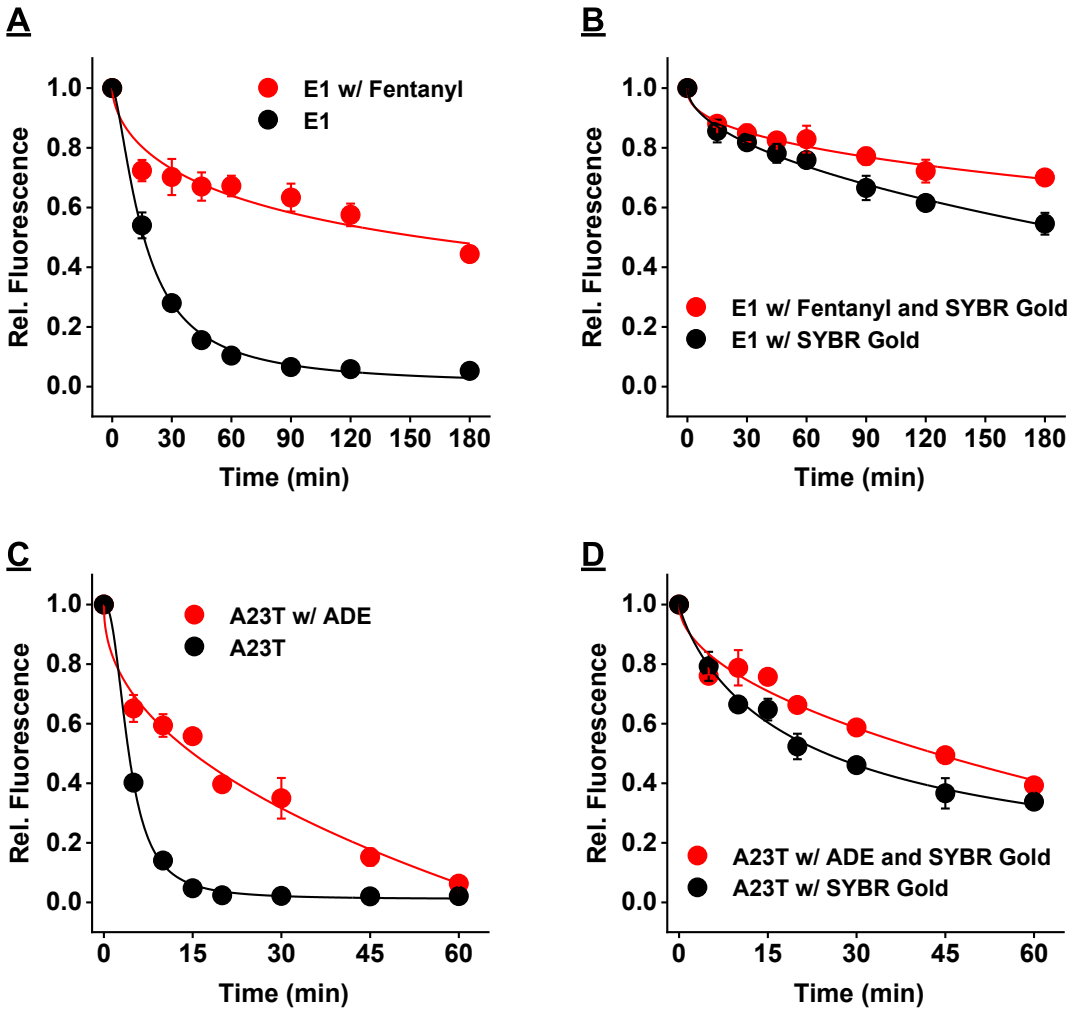

Figure S6. Evaluating whether SYBR Gold can be used to continuously monitor the exonuclease digestion assay. We evaluated the DNA aptamers (**A, B**) E1 and (**C, D**) A23T with SYBR Gold either added after the digestion reaction was quenched (**A, C**) or included in the exonuclease reaction mixture (**B, D**).

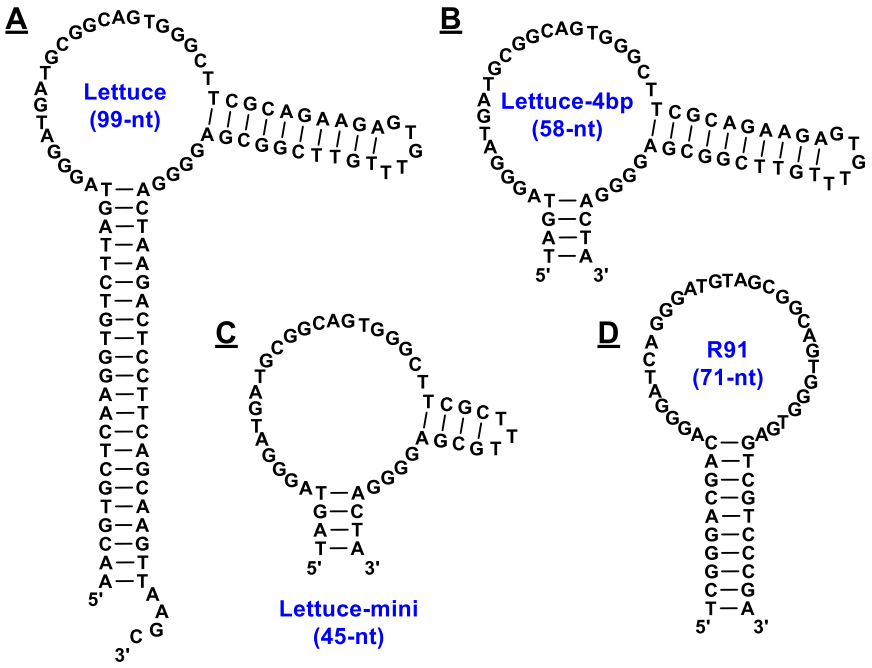

Figure S7. Secondary structures of fluorogenic aptamers reported by the Jaffrey group and some truncated derivatives.

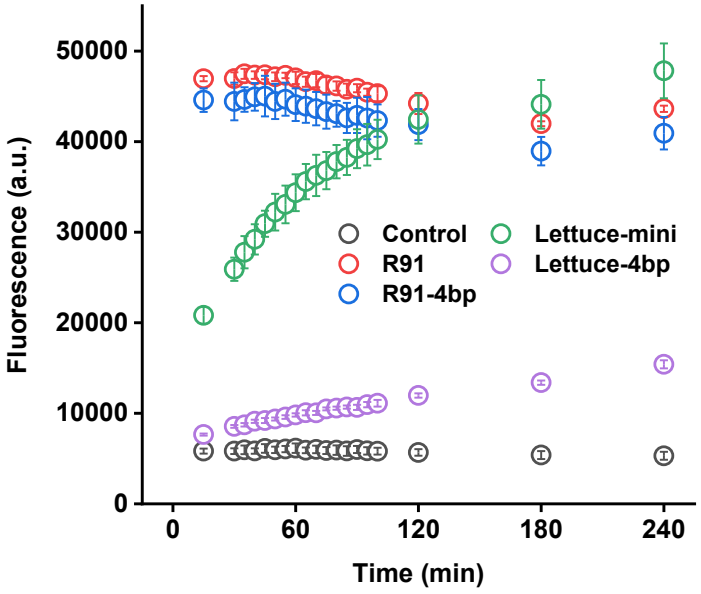

Figure S8. Fluorescence of 5 μM DFHBI-1T at 505 nm (λ_{ex} = 460 nm) in the absence (black) and presence of 1 μM aptamer R91 (red), R91-4bp (blue), Lettuce-mini (green), or Lettuce-4bp (purple) plotted versus time after mixing the dye and aptamer (or buffer as control).

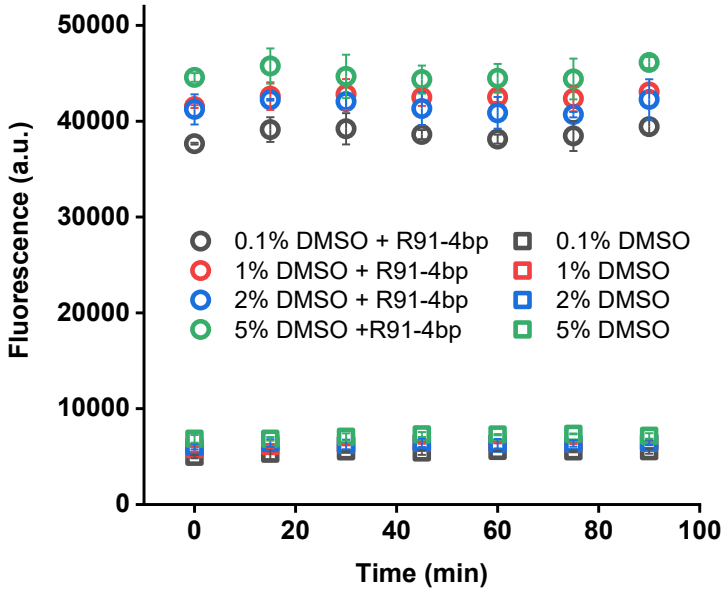

Figure S9. Fluorescence of 5 μM DFHBI-1T at 505 nm (λ_{ex} = 460 nm) in the absence and presence of 1 μM R91-4bp at various concentrations of DMSO plotted versus time after mixing the dye and aptamer (or buffer as control).

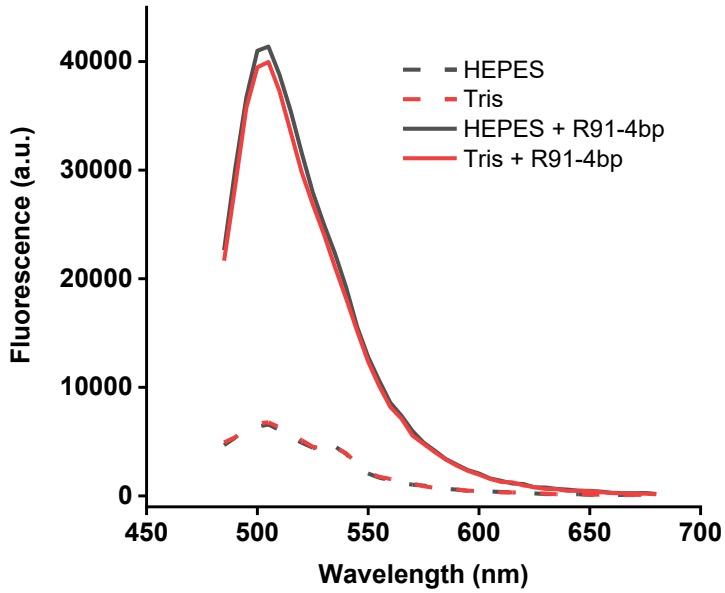

Figure S10. Fluorescence emission spectrum of 5 μM DFHBI-1T (λ_{ex} = 460 nm) in the absence (dashed lines) and presence (solid lines) of 1 μM R91-4bp in Tris-based (red) and HEPES-based (black) buffer.

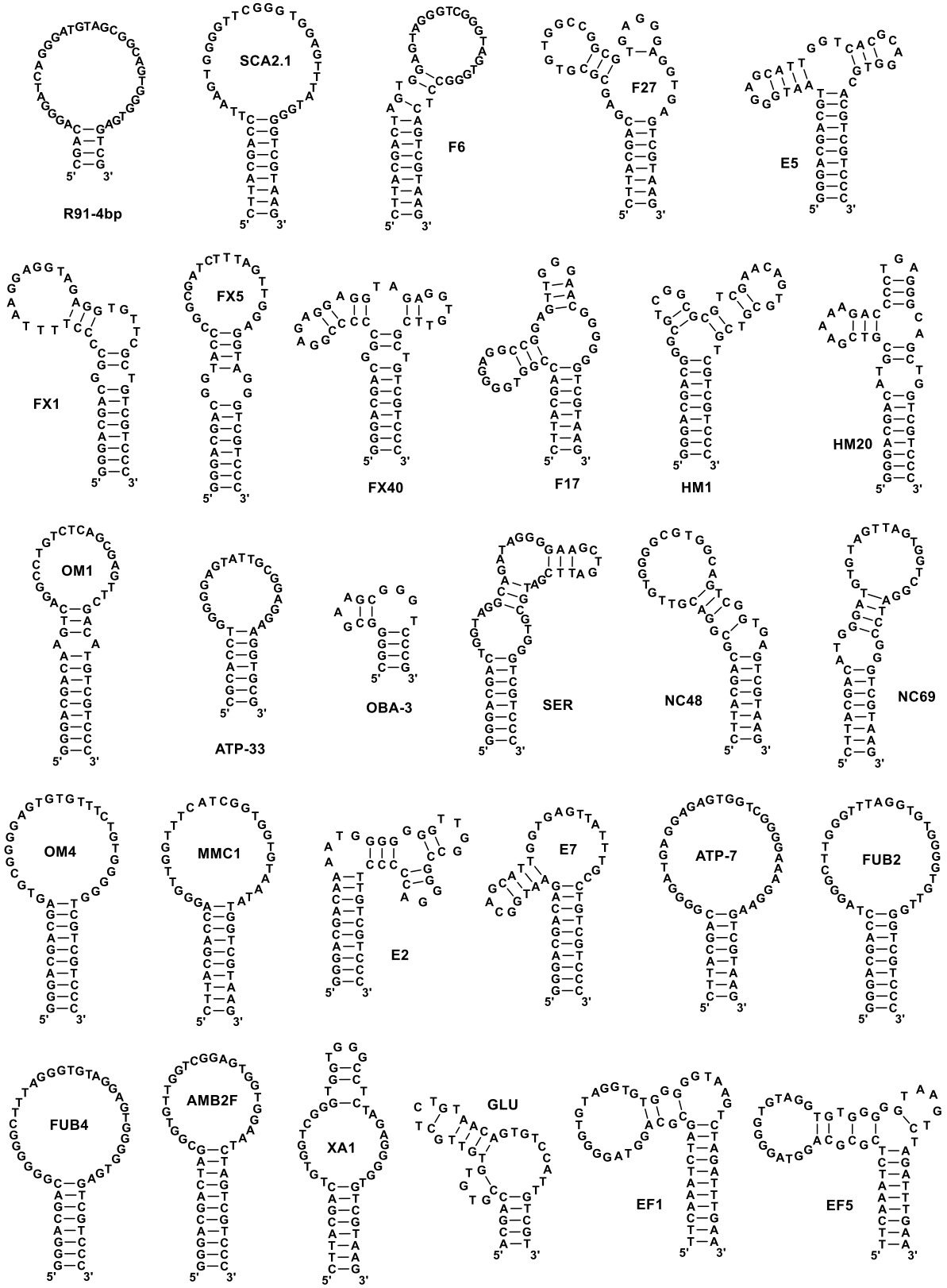

Figure S11. Secondary structures of aptamers used in this work.

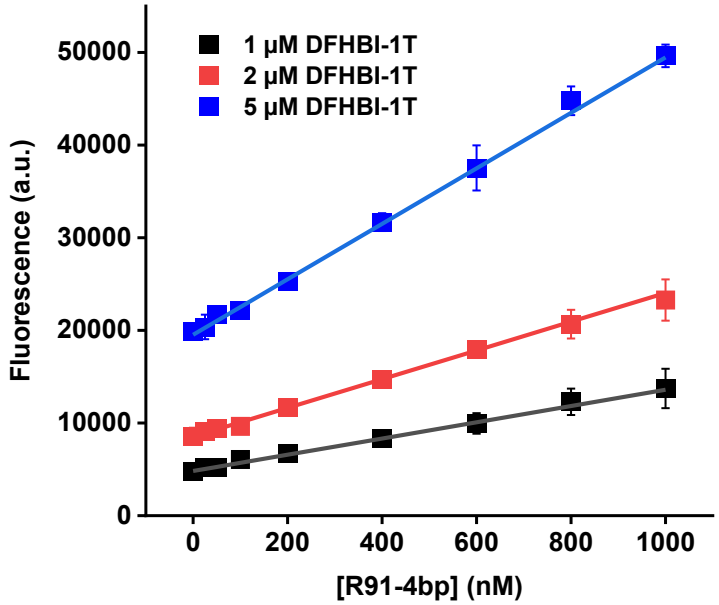

Figure S12. Fluorescence of DFHBI-1T at 505 nm (λ_{ex} = 460 nm) in the presence of various concentrations of R91-4bp.

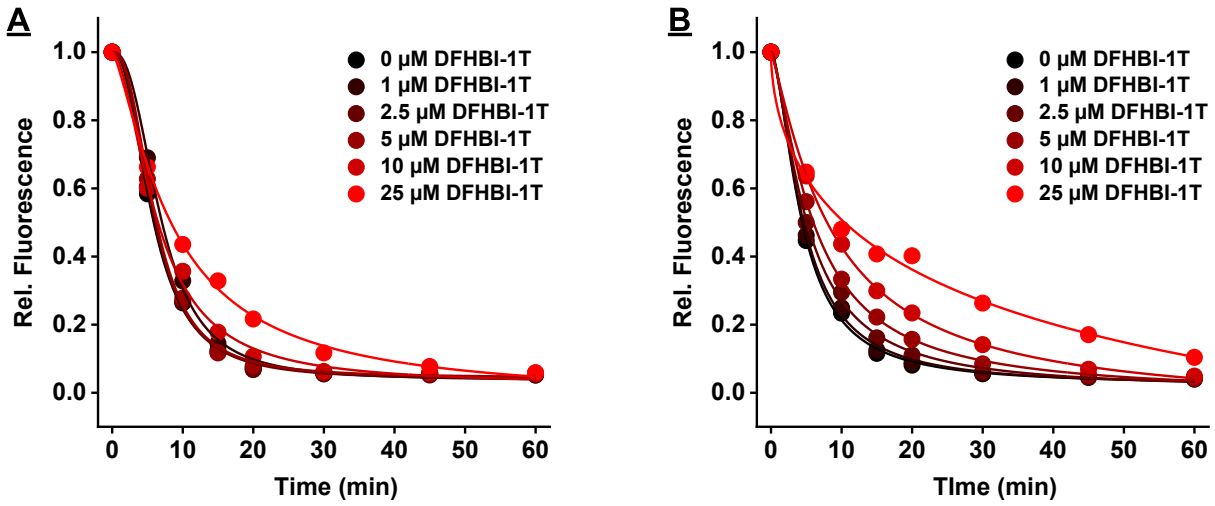

Figure S13. Digestion of R91-4bp by a mixture of Exo I and Exo III. Digestion of R91-4bp by the exonucleases in the presence of various concentrations of DFHBI-1T in (**A**) PBS buffer and (**B**) low salt Tris buffer. The progress of the digestion process is monitored by staining aliquots of the reaction mixture with SYBR Gold.

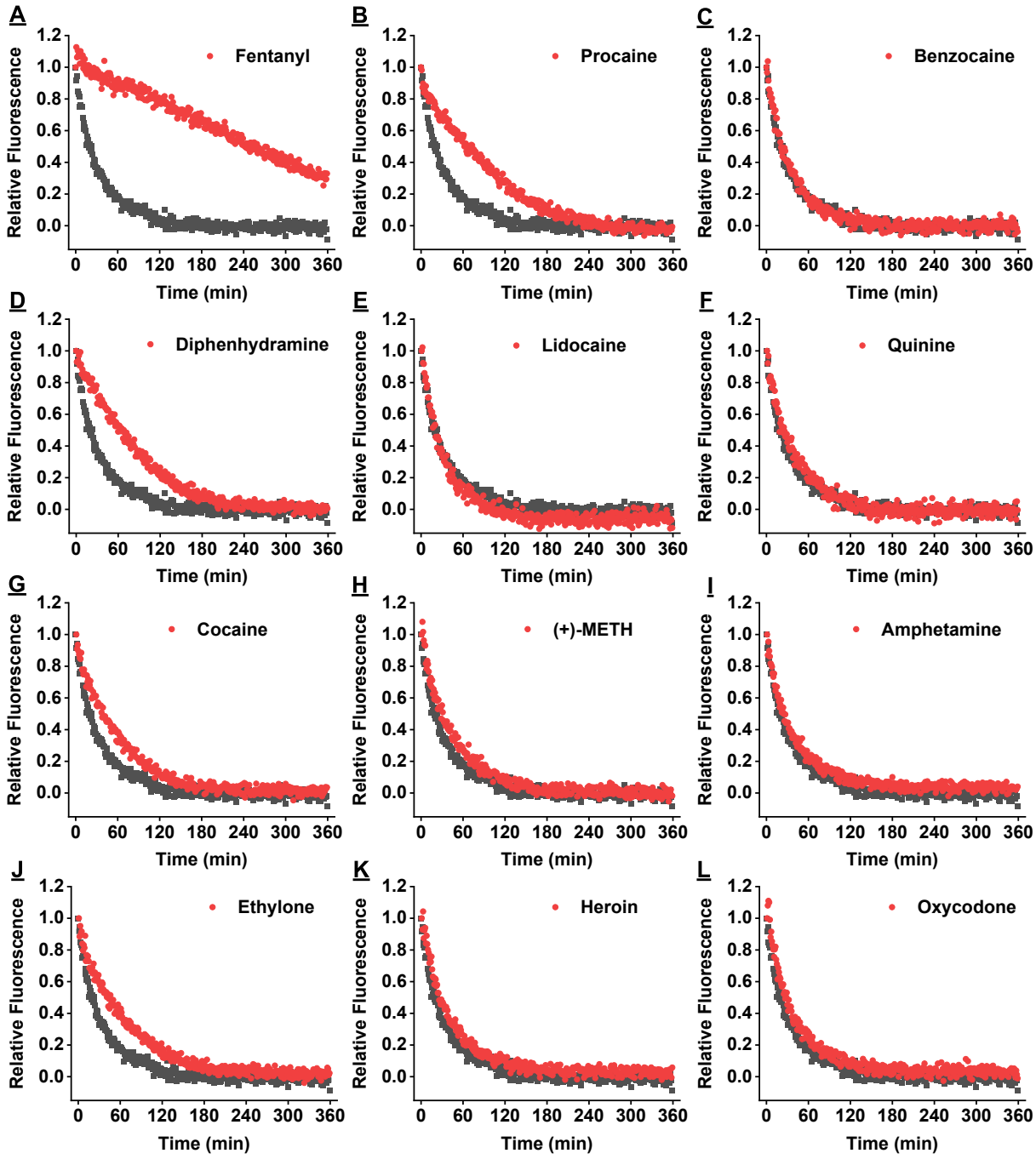

Figure S14. Fluorescence time-course data from the RT-Exo assay for the E1-R91-4bp and the ligands (**A**) fentanyl, (**B**) procaine, (**C**) benzocaine, (**D**) diphenhydramine, (**E**) lidocaine, (**F**) quinine, (**G**) cocaine, (**H**) (+)-methamphetamine, (**I**) amphetamine, (**J**) ethylone, (**K**) heroin, and (**L**) oxycodone. The red and black datapoints respectively indicate data for samples with and without ligand.

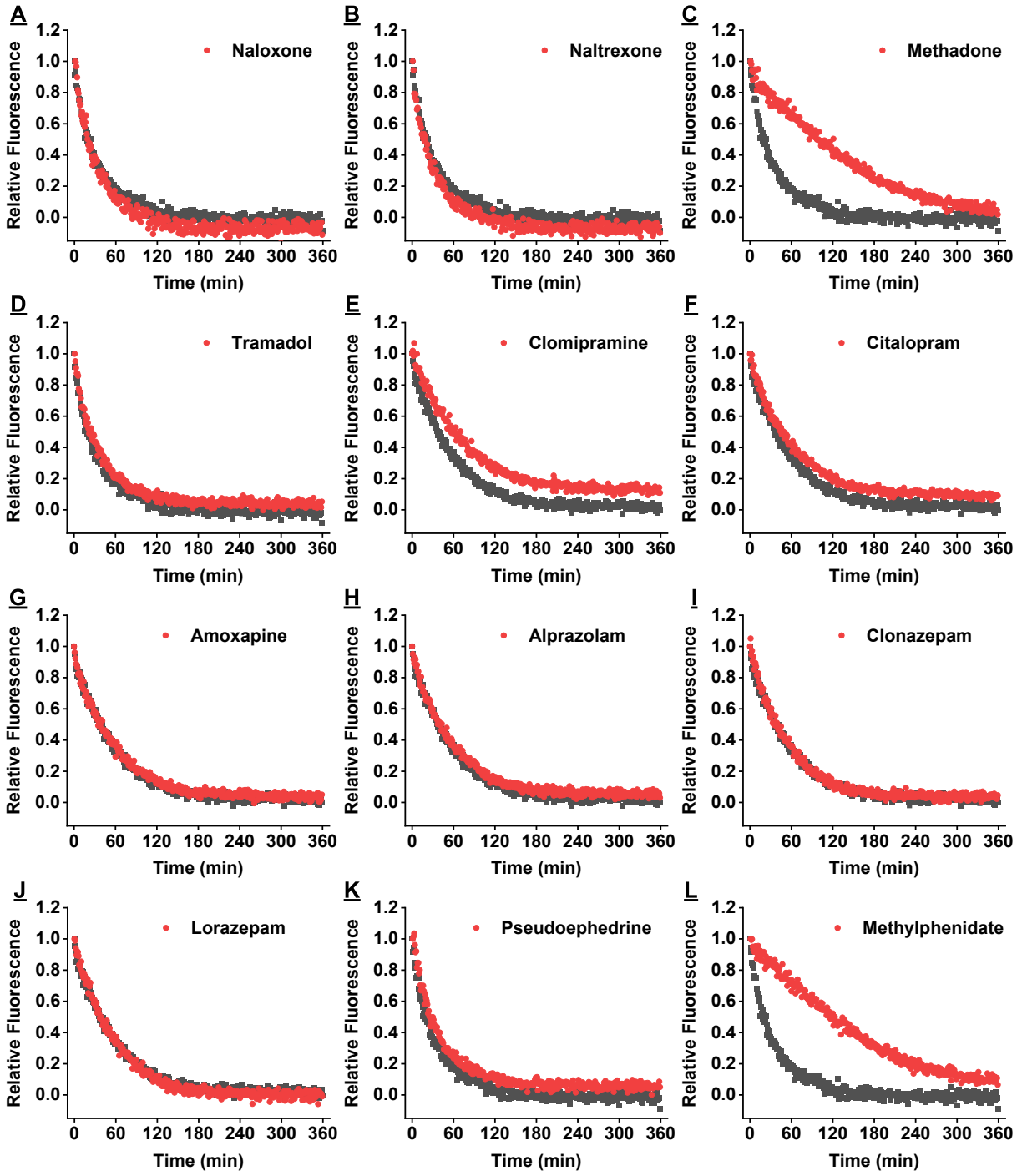

Figure S15. Fluorescence time-course data from the RT-Exo assay for the E1-R91-4bp and the ligands (**A**) naloxone, (**B**) naltrexone, (**C**) methadone, (**D**) tramadol, (**E**) clomipramine, (**F**) citalopram, (**G**) amoxapine, (**H**) alprazolam, (**I**) clonazepam, (**J**) lorazepam, (**K**) pseudoephedrine, and (**L**) methylphenidate. The red and black datapoints respectively indicate data for samples with and without ligand.

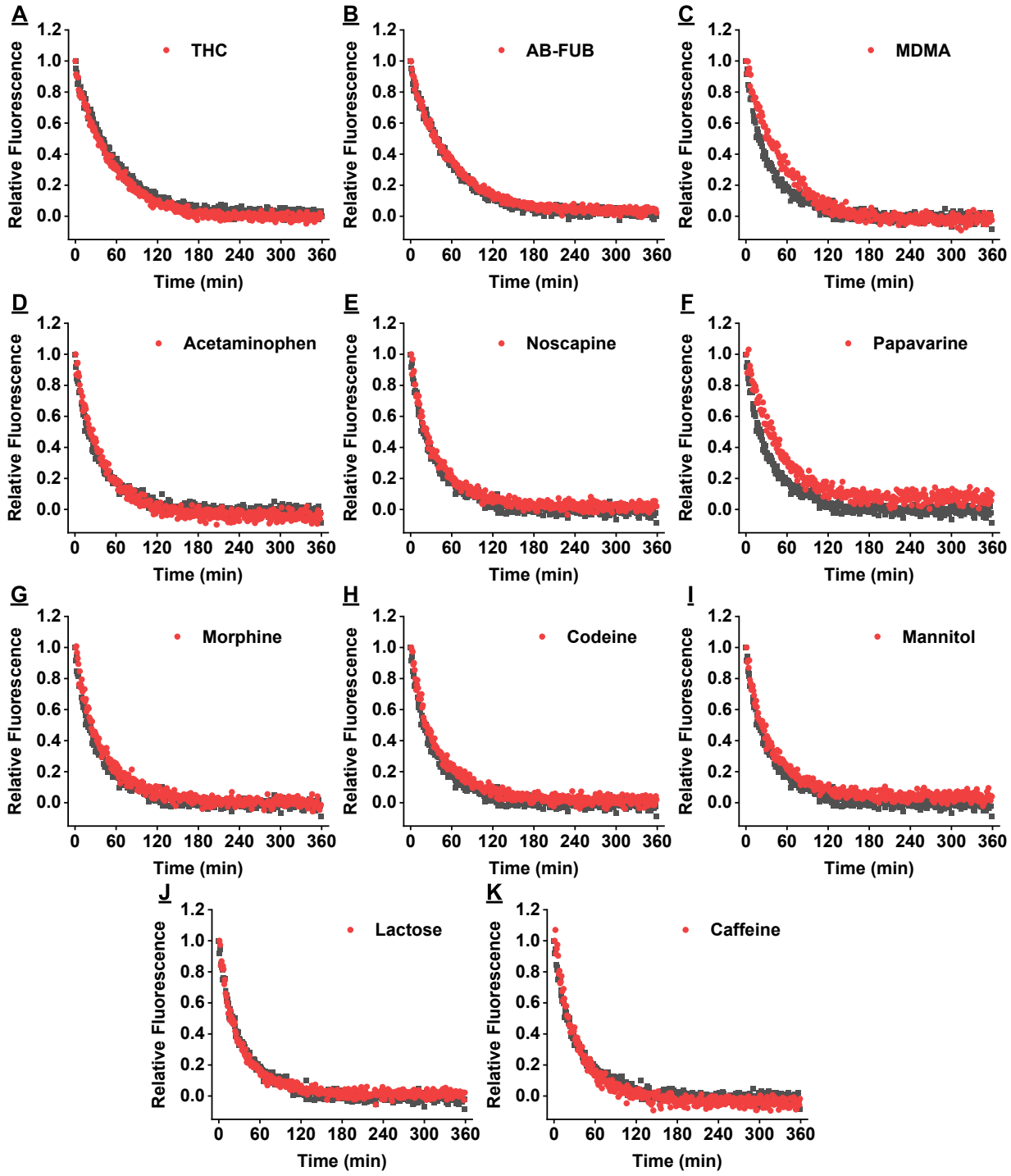

Figure S16. Fluorescence time-course data from the RT-Exo assay for the E1-R91-4bp and the ligands (**A**) tetrahydrocannabinol, (**B**) AB-FUBINACA, (**C**) methylenedioxymethamphetamine, (**D**) acetaminophen, (**E**) noscapine, (**F**) papaverine, (**G**) morphine, (**H**) codeine, (**I**) mannitol, (**J**) lactose, and (**K**) caffeine. The red and black datapoints respectively indicate data for samples with and without ligand.

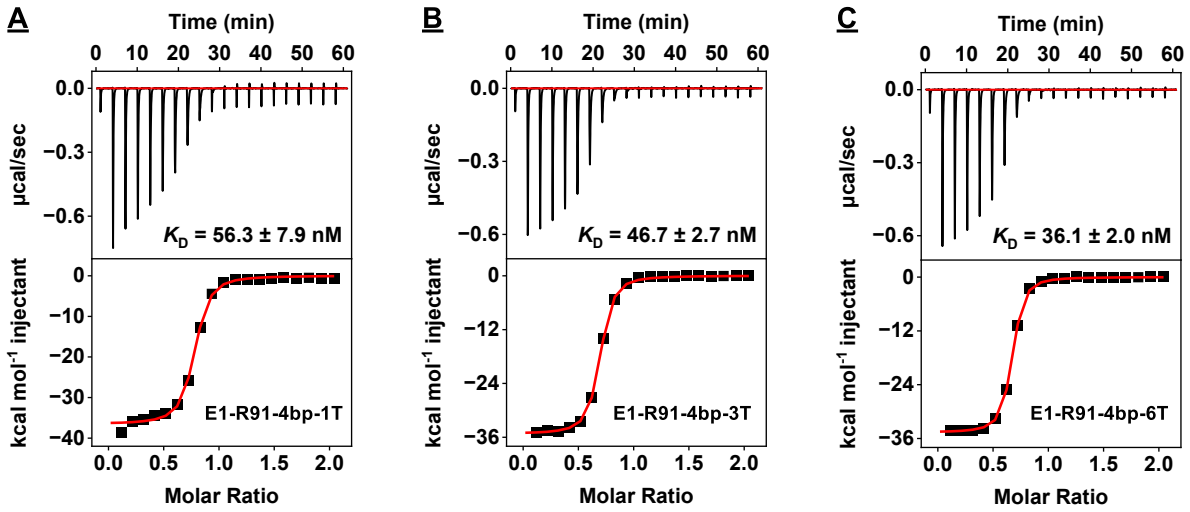

Figure S17. Determining the affinity of various E1-R91-4bp conjugates for fentanyl using ITC. Data are presented for (**A**) E1-R91-4bp-1T, (**B**) E1-R91-4bp-3T, and (**C**) E1-R91-4bp-6T. Top panels show the raw heat from the titration of fentanyl into the aptamer. Bottom panels show integrated heat values per mole of injectant plotted as a function of the molar ratio of target to aptamer after correcting for the heat of dilution of the titrant. Data were fitted with a one-site binding model.

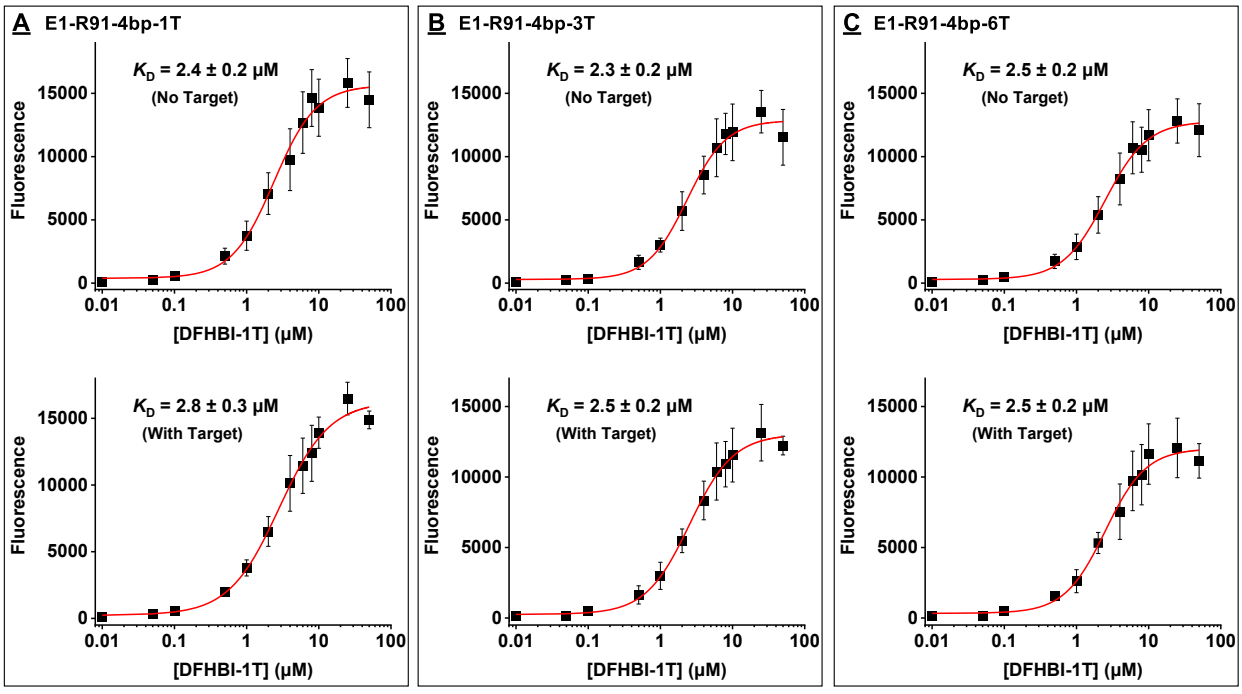

Figure S18. Affinity of E1-R91-4bp conjugates for DFHBI-1T. Titrating various concentrations of DFHBI-1T to a fixed concentration of (**A**) E1-R91-4bp-1T, (**B**) E1-R91-4bp-3T, and (**C**) E1-R91-4bp-6T and plots the resulting fluorescent signal. Top and bottom panels show experiments performed in absence and presence of fentanyl, respectively. Data were fitted using the Langmuir-Hill equation to obtain K_D.

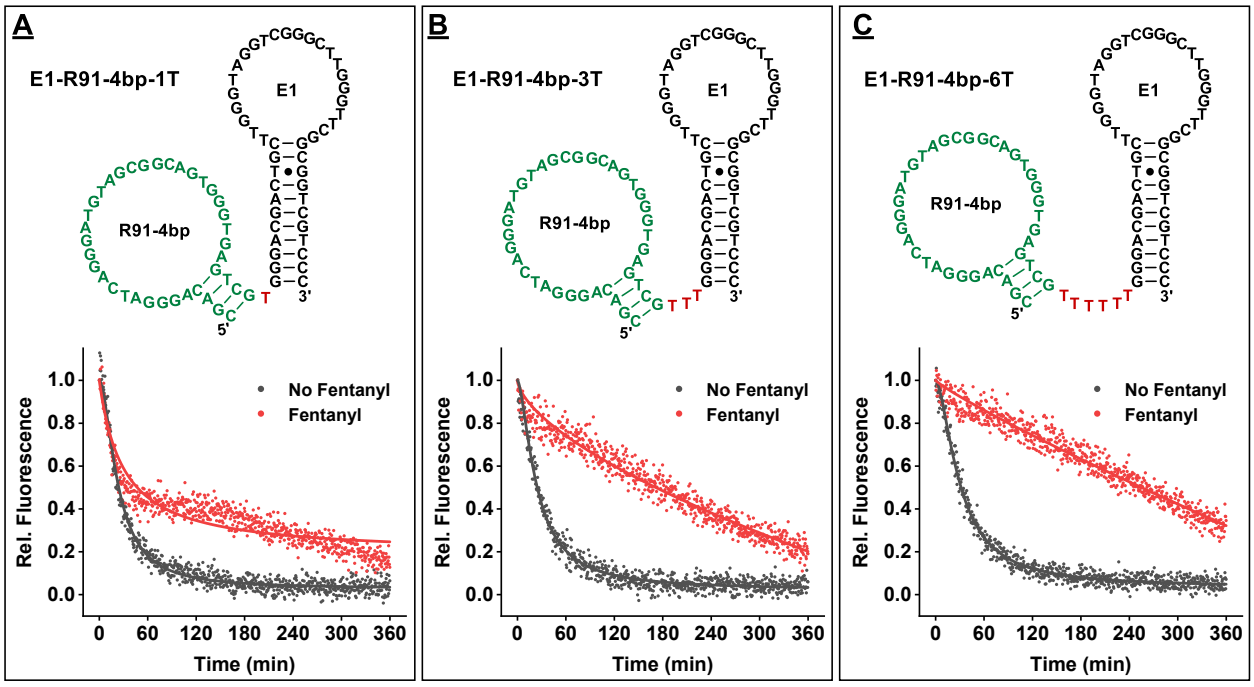

Figure S19. Assessing the effect of linker length in the RT-Exo assay. Digestion results for (**A**) E1-R91-4bp-1T, (**B**) E1-R91-4bp-3T, and (**C**) E1-R91-4bp-6T. Top panels show secondary structure of the conjugates. Bottom panels show the progress of digestion in terms of DFHBI-1T fluorescence over time.

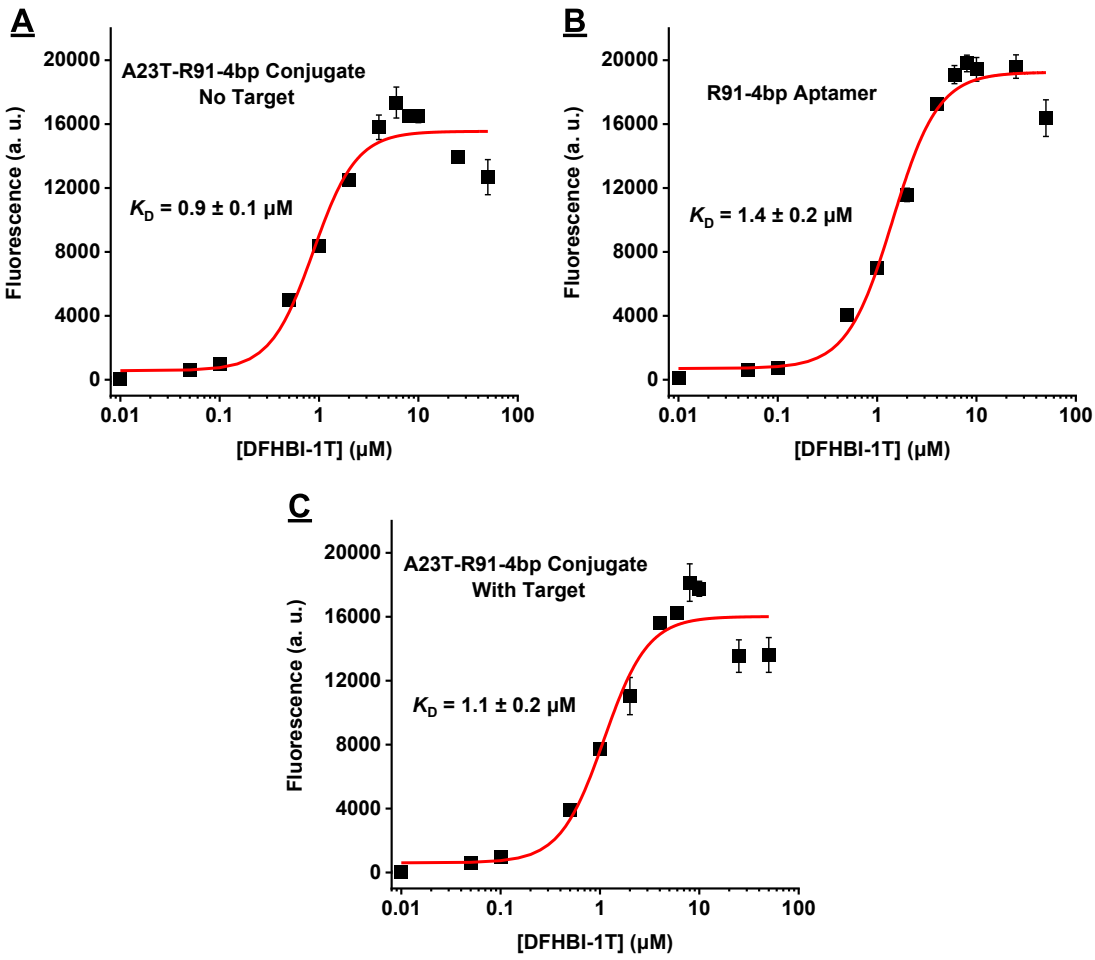

Figure S20. Determining the DFHBI-1T-binding affinity of R91-4bp and the adenosine aptamer A23T conjugated to R91-4bp. Fluorescence of DFHBI-1T at 505 nm (λ_{ex} = 460 nm) was measured in the presence of various concentrations of DFHBI-1T and with a fixed concentration (1 µM) of (**A**) A23T-R91-4bp without adenosine, (**B**) R91-4bp, and (**C**) A23T-R91-4bp with 500 µM adenosine.

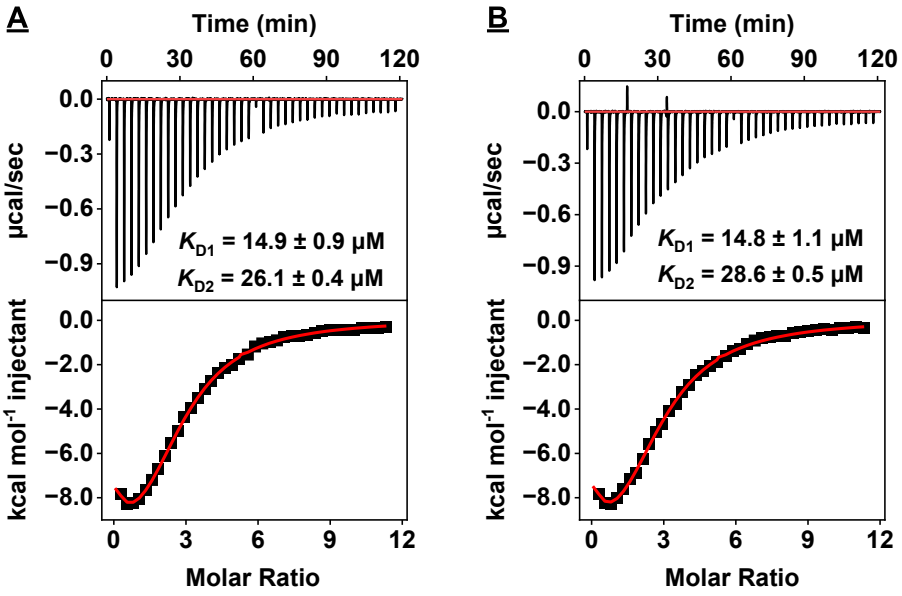

Figure S21. The binding affinity of (**A**) A23T-R91-4bp and (**B**) A23T to adenosine as determined using isothermal titration calorimetry (ITC). Top panels display the heat generated from each titration of ligand into aptamer. Bottom panels show the integrated heat of each titration after correcting for the heat of dilution of the titrant.

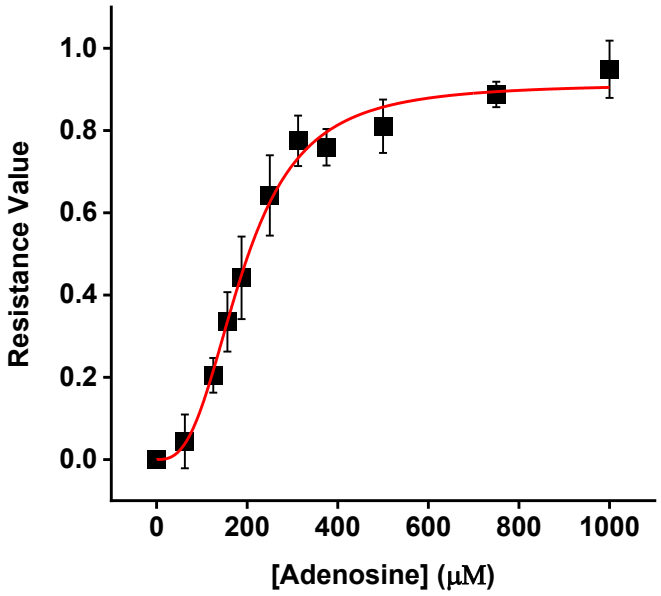

Figure S22. Resistance values for A23T-R91-4bp at various concentrations of adenosine as determined by the RT-Exo assay.

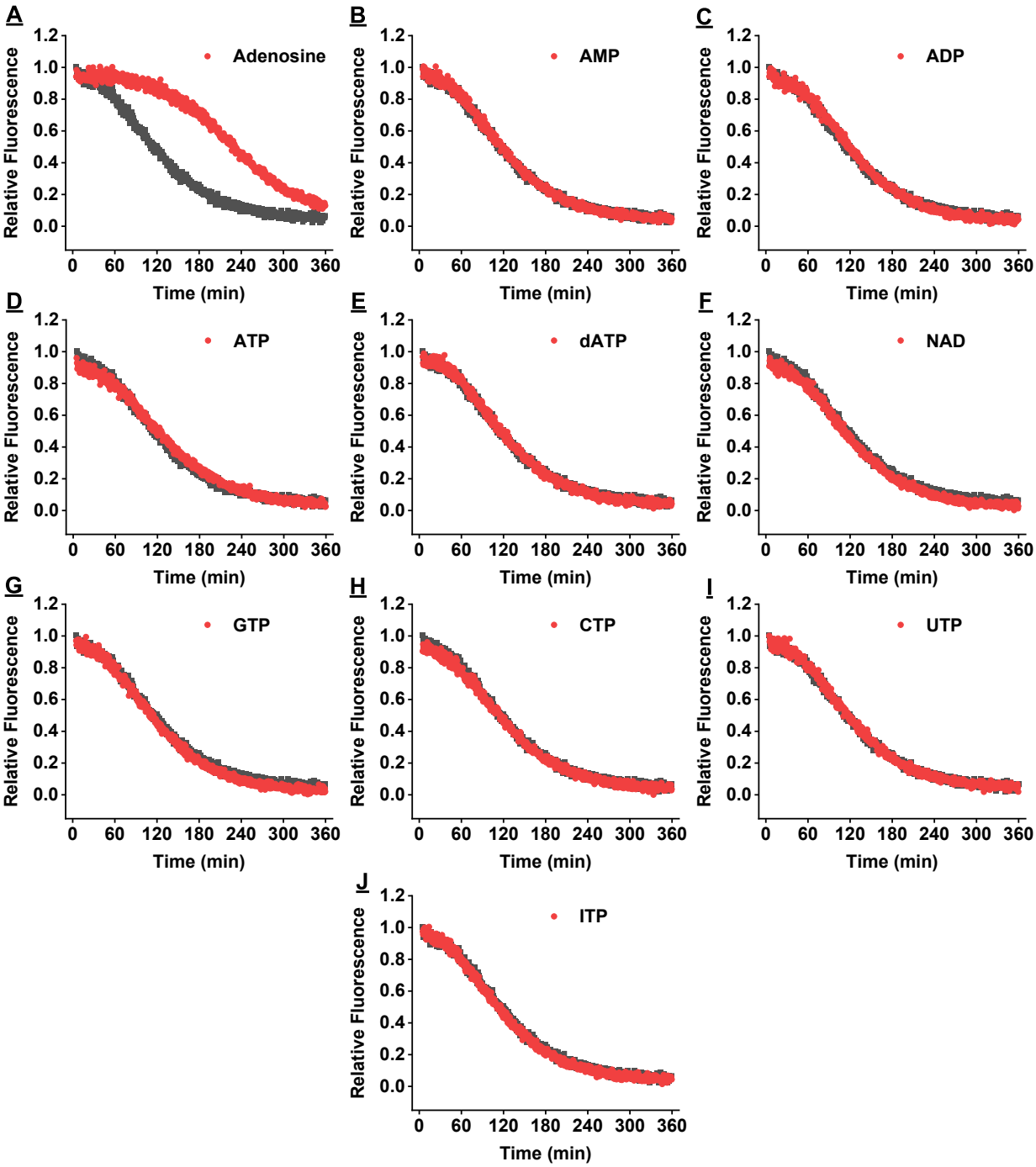

Figure S23. Fluorescence time-course data from the RT-Exo assay for the A23T-R91-4bp and the ligands (**A**) adenosine, (**B**) adenosine monophosphate, (**C**) adenosine diphosphate, (**D**) adenosine triphosphate, (**E**) deoxyadenosine triphosphate, (**F**) nicotinamide adenine dinucleotide, (**G**) guanosine triphosphate, (**H**) cytidine triphosphate, (**I**) uridine triphosphate, and (**J**) inosine triphosphate. The red and black datapoints respectively indicate data for samples with and without ligand.

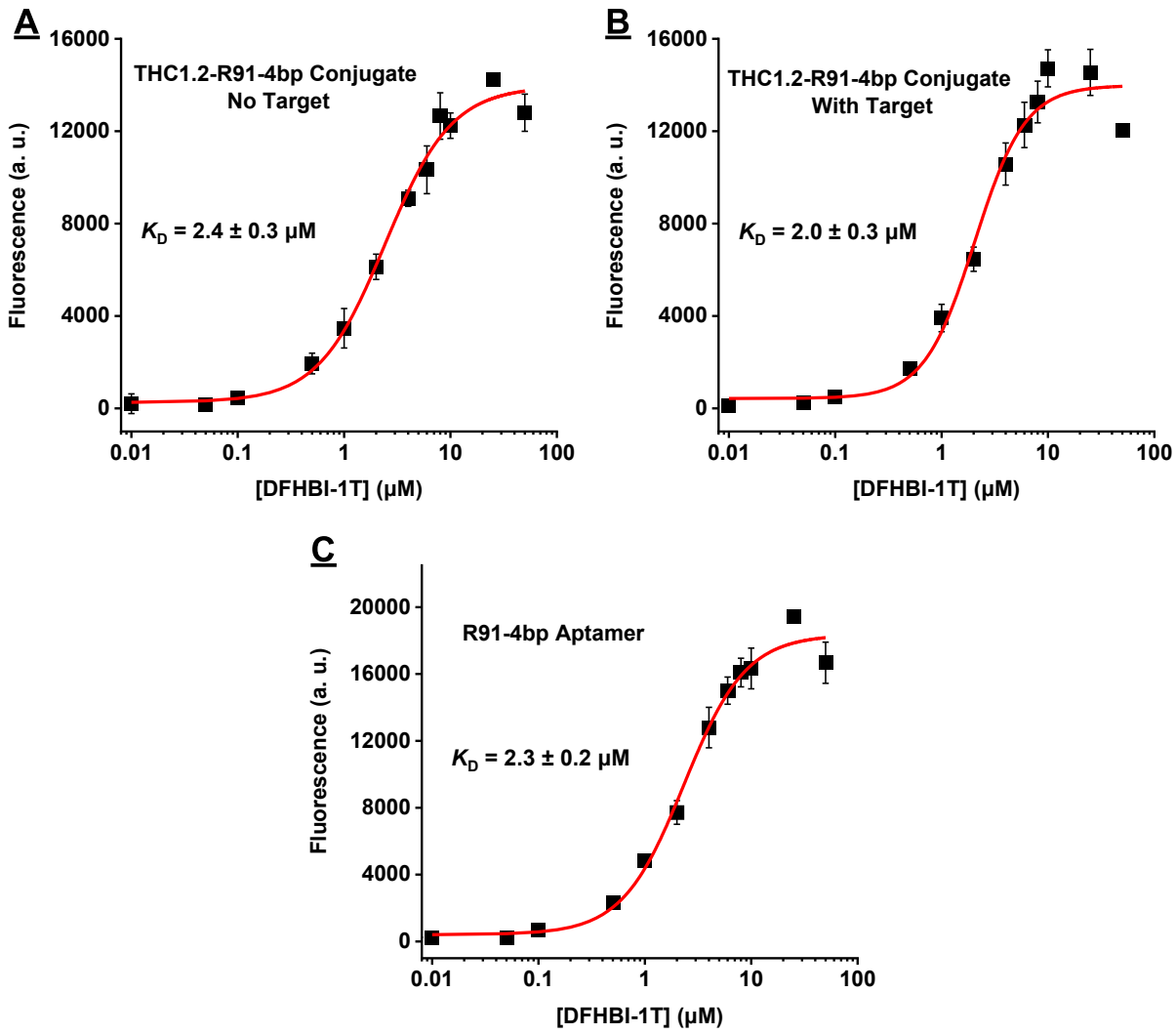

Figure S24. Determining the DFHBI-1T-binding affinity of R91-4bp and the THC aptamer THC1.2 conjugated to R91-4bp. We measured the fluorescence of DFHBI-1T at 505 nm (λ_{ex} = 460 nm) in the presence of various concentrations of DFHBI-1T and with a fixed concentration (1 μM) of (**A**) THC1.2-R91-4bp without THC, (**B**) THC1.2-R91-4bp with 10 μM THC, and (**C**) R91-4bp.

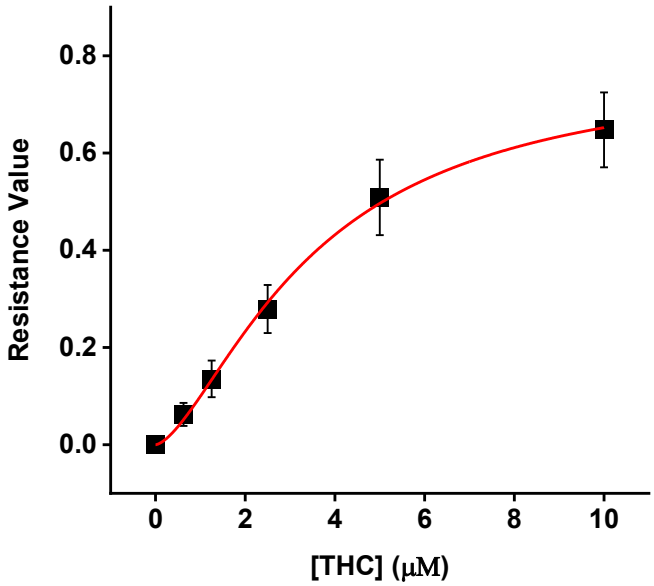

Figure S25. Resistance values for THC1.2-R91-4bp at various concentrations of THC as determined by the RT-Exo assay.

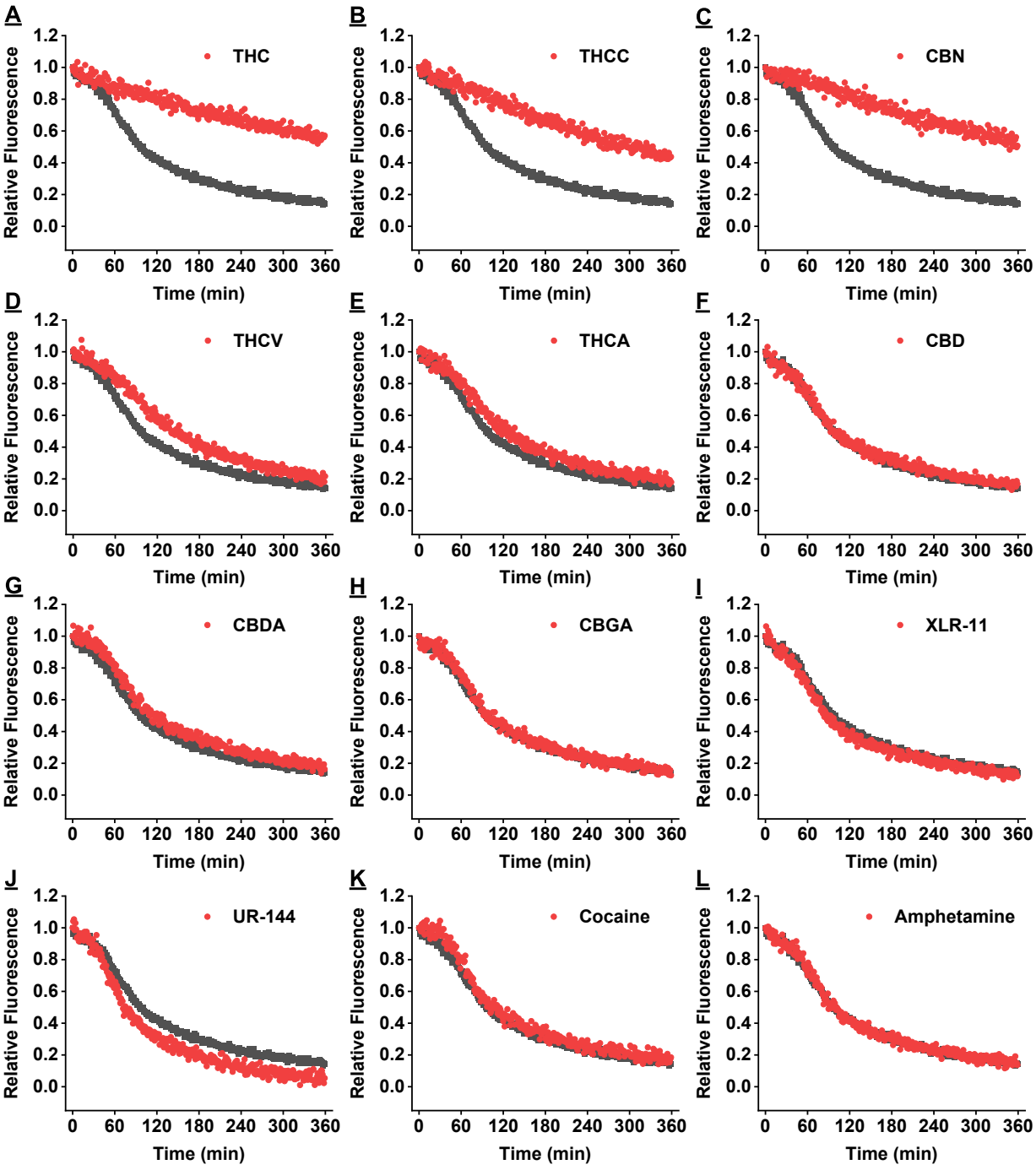

Figure S26. Fluorescence time-course data from the RT-Exo assay for the THC1.2-R91-4bp and the ligands (**A**) THC, (**B**) 11-nor-9-carboxy-THC, (**C**) cannabinol, (**D**) tetrahydrocannabivarin, (**E**) tetrahydrocannabinolic acid, (**F**) cannabidiol, (**G**) cannabidiolic acid, (**H**) cannabigerolic acid, (**I**) XLR-11, (**J**) UR-144, (**K**) cocaine, and (**L**) amphetamine. The red and black datapoints respectively indicate data for samples with and without ligand.

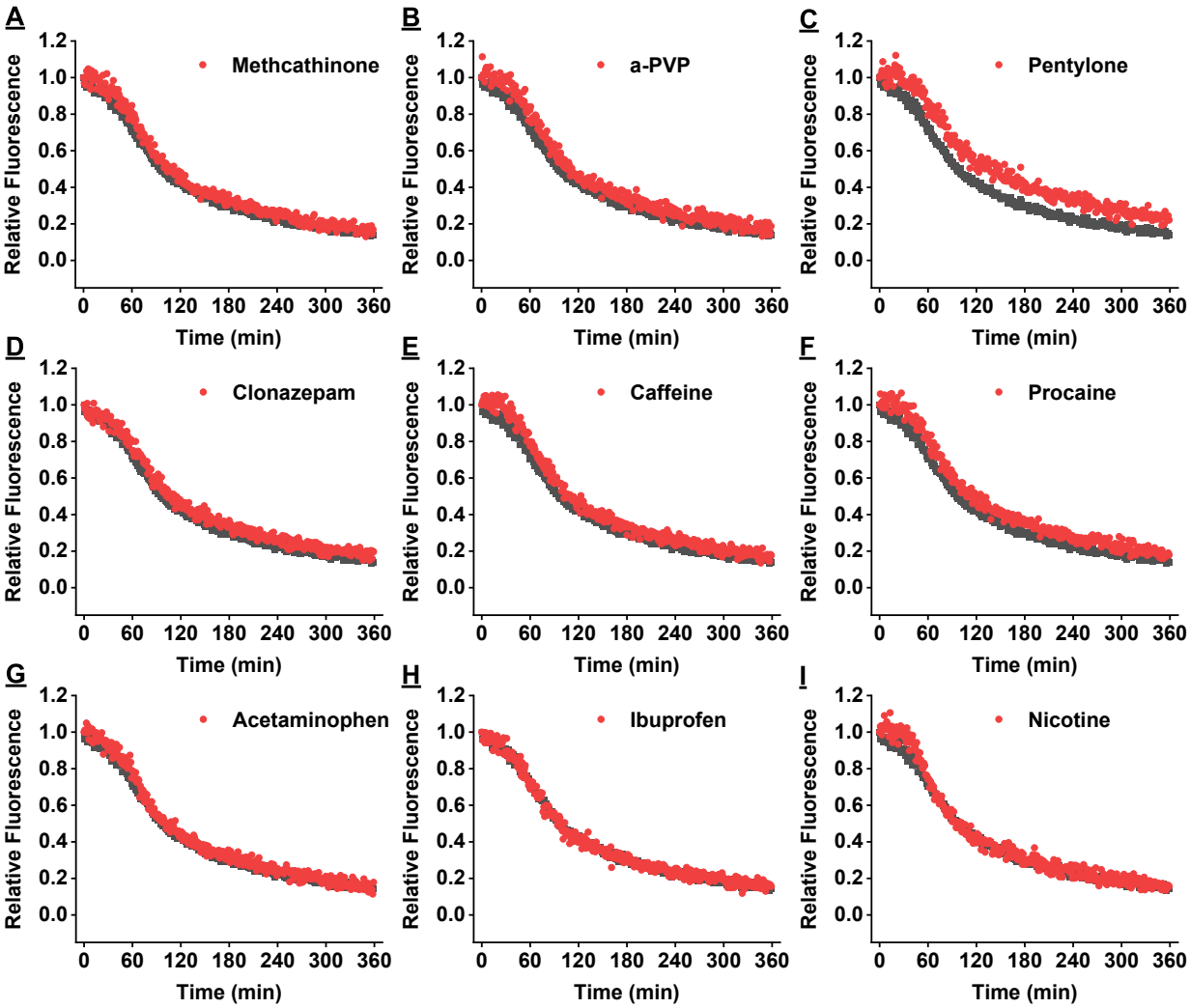

Figure S27. Fluorescence time-course data from the RT-Exo assay for the THC1.2-R91-4bp and the ligands (**A**) methcathinone, (**B**) α-PVP, (**C**) pentylone, (**D**) clonazepam, (**E**) caffeine, (**F**) procaine, (**G**) acetaminophen, (**H**) ibuprofen, and (**I**) nicotine. The red and black datapoints respectively indicate data for samples with and without ligand.

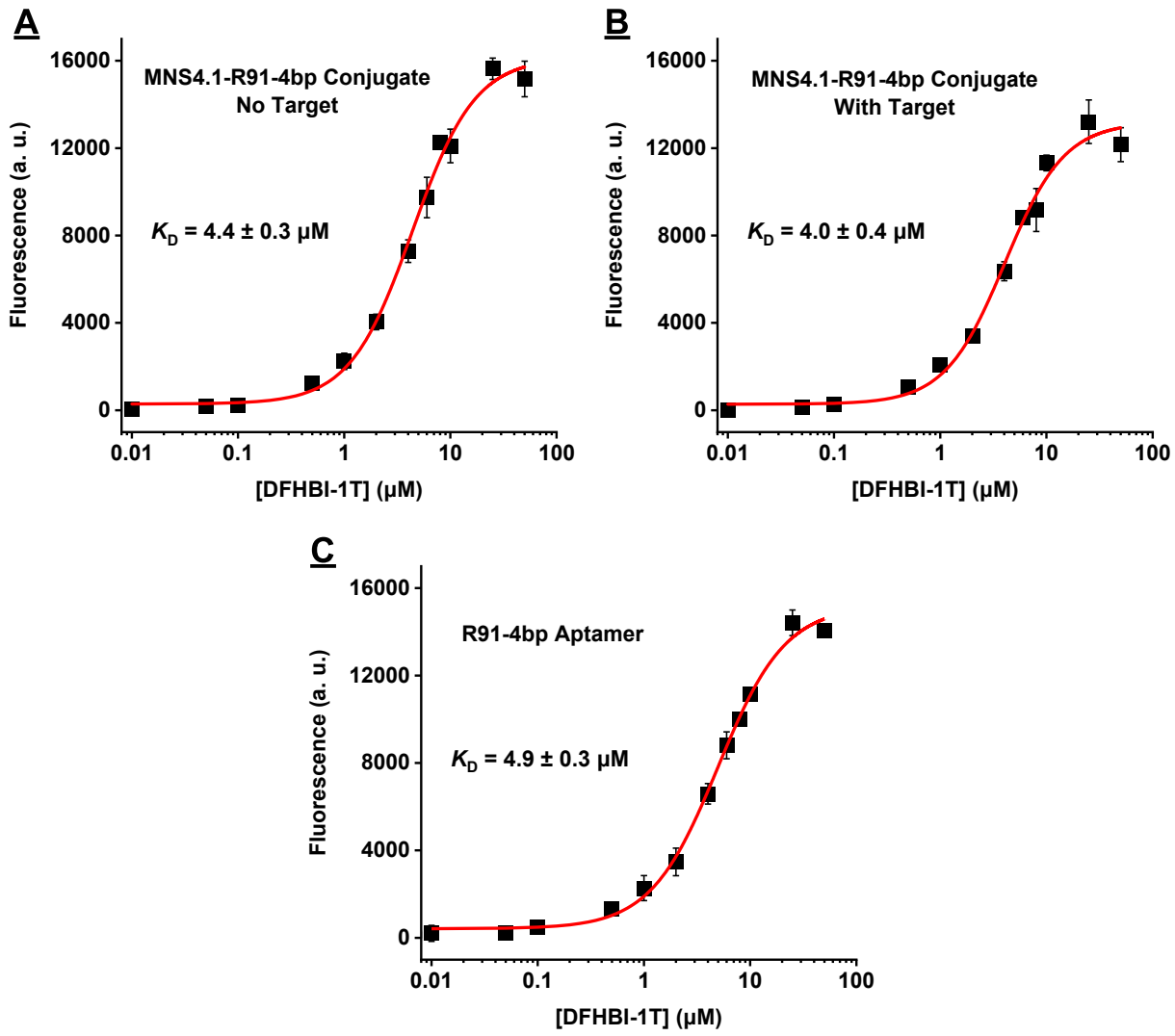

Figure S28. Determining the DFHBI-1T-binding affinity of R91-4bp and the cocaine aptamer MNS4.1 conjugated to R91-4bp. We measured the fluorescence of DFHBI-1T at 505 nm (λ_{ex} = 460 nm) in the presence of various concentrations of DFHBI-1T and with a fixed concentration (1 μM) of (**A**) MNS4.1-R91-4bp without cocaine, (**B**) MNS4.1-R91-4bp with 100 μM cocaine, and (**C**) R91-4bp.

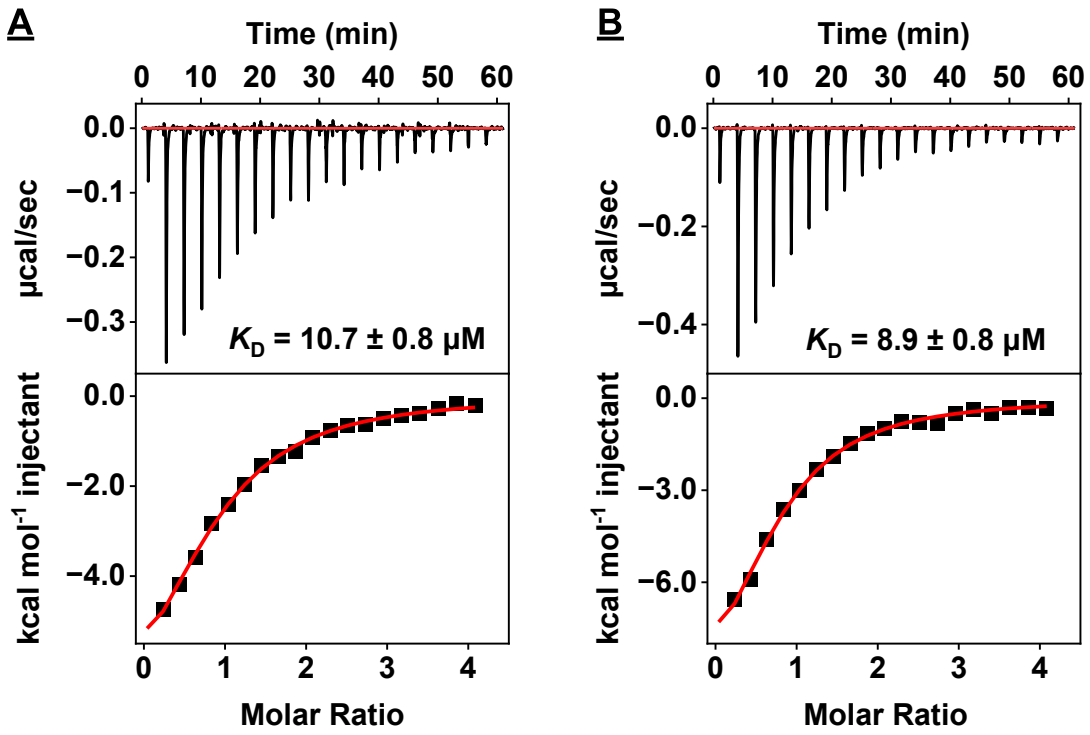

Figure S29. The binding affinity of (**A**) MNS4.1-R91-4bp and (**B**) MNS4.1 to cocaine as determined using ITC. Top panels display the heat generated from each titration of ligand into aptamer. Bottom panels show the integrated heat of each titration after correcting for the heat of dilution of the titrant.

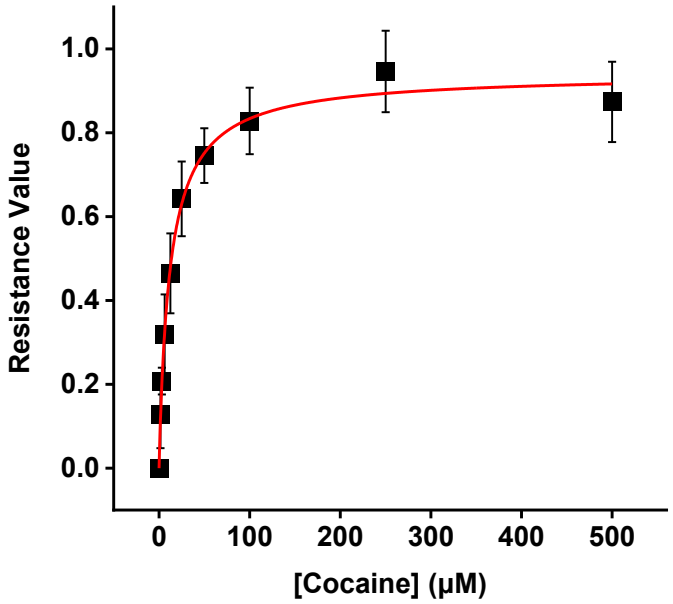

Figure S30. Resistance values for MNS4.1-R91-4bp at various concentrations of cocaine as determined by the RT-Exo assay.

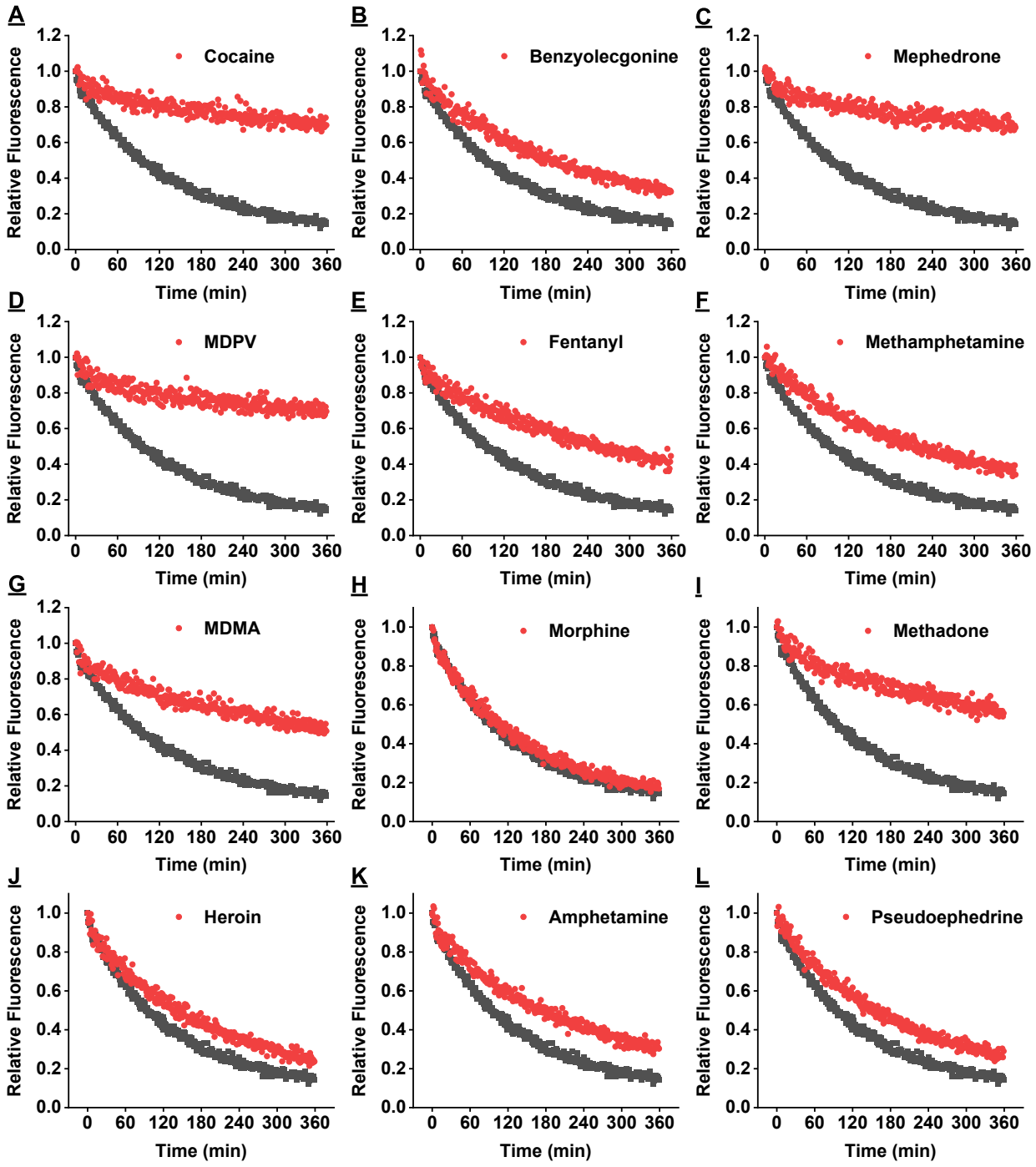

Figure S31. Fluorescence time-course data from the RT-Exo assay for the MNS4.1-R91-4bp and the ligands (**A**) cocaine, (**B**) benzoylecgonine, (**C**) mephedrone, (**D**) methylenedioxypyrovalerone, (**E**) fentanyl, (**F**) methamphetamine, (**G**) methylenedioxymethamphetamine, (**H**) morphine, (**I**) methadone, (**J**) heroin, (**K**) amphetamine, and (**L**) pseudoephedrine. The red and black datapoints respectively indicate data for samples with and without ligand.

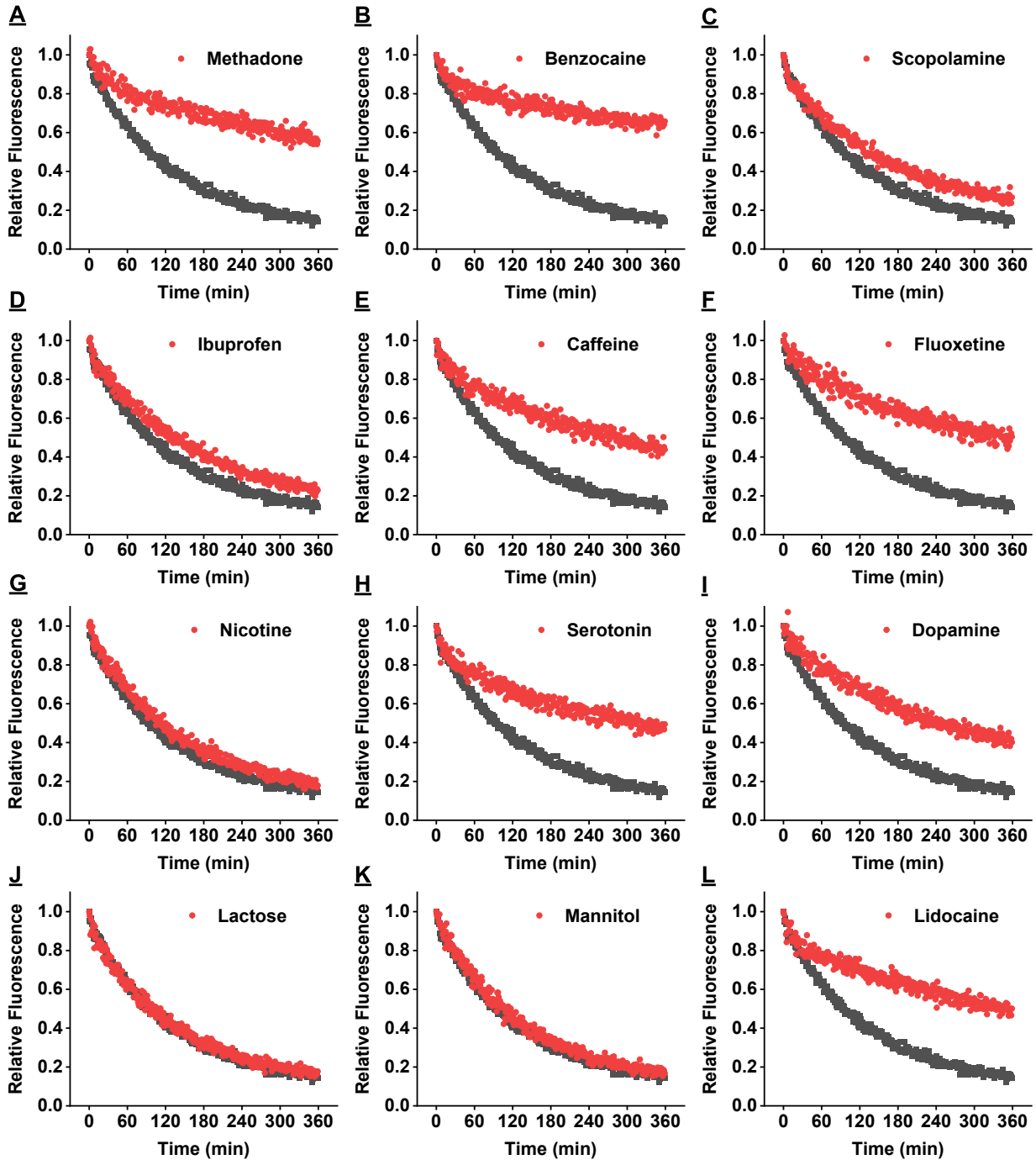

Figure S32. Fluorescence time-course data from the RT-Exo assay for the MNS4.1-R91-4bp and the ligands (**A**) methadone, (**B**) benzocaine, (**C**) scopolamine, (**D**) ibuprofen, (**E**) caffeine, (**F**) fluoxetine, (**G**) nicotine, (**H**) serotonin, (**I**) dopamine, (**J**) lactose, (**K**) mannitol, and (**L**) lidocaine. The red and black datapoints respectively indicate data for samples with and without ligand.

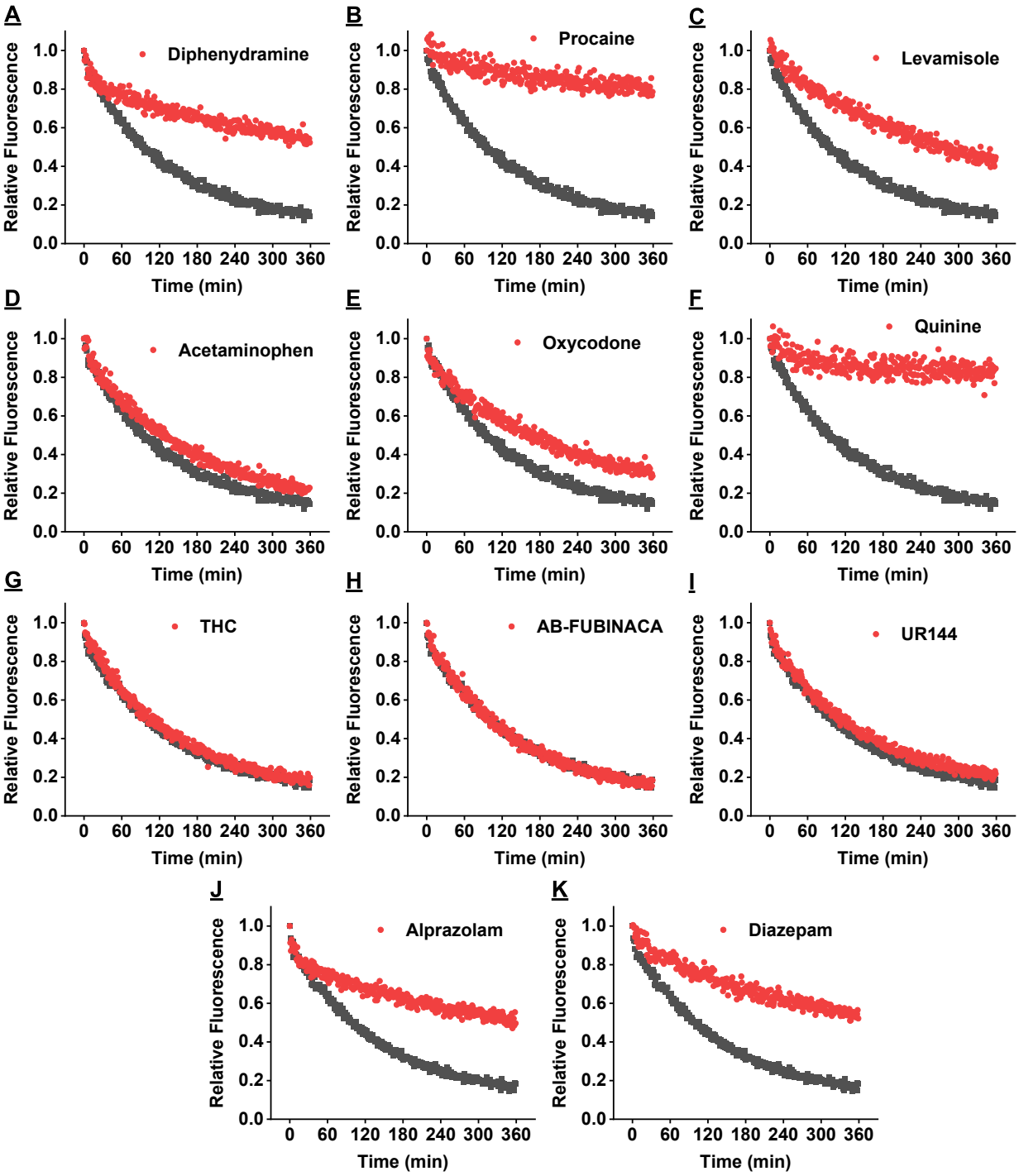

Figure S33. Fluorescence time-course data from the RT-Exo assay for the MNS4.1-R91-4bp and the ligands (**A**) diphenhydramine, (**B**) procaine, (**C**) levamisole, (**D**) acetaminophen, (**E**) oxycodone, (**F**) quinine, (**G**) THC, (**H**) AB-FUBINACA, (**I**) UR-144, (**J**) alprazolam, and (**K**) diazepam. The red and black datapoints respectively indicate data for samples with and without ligand.

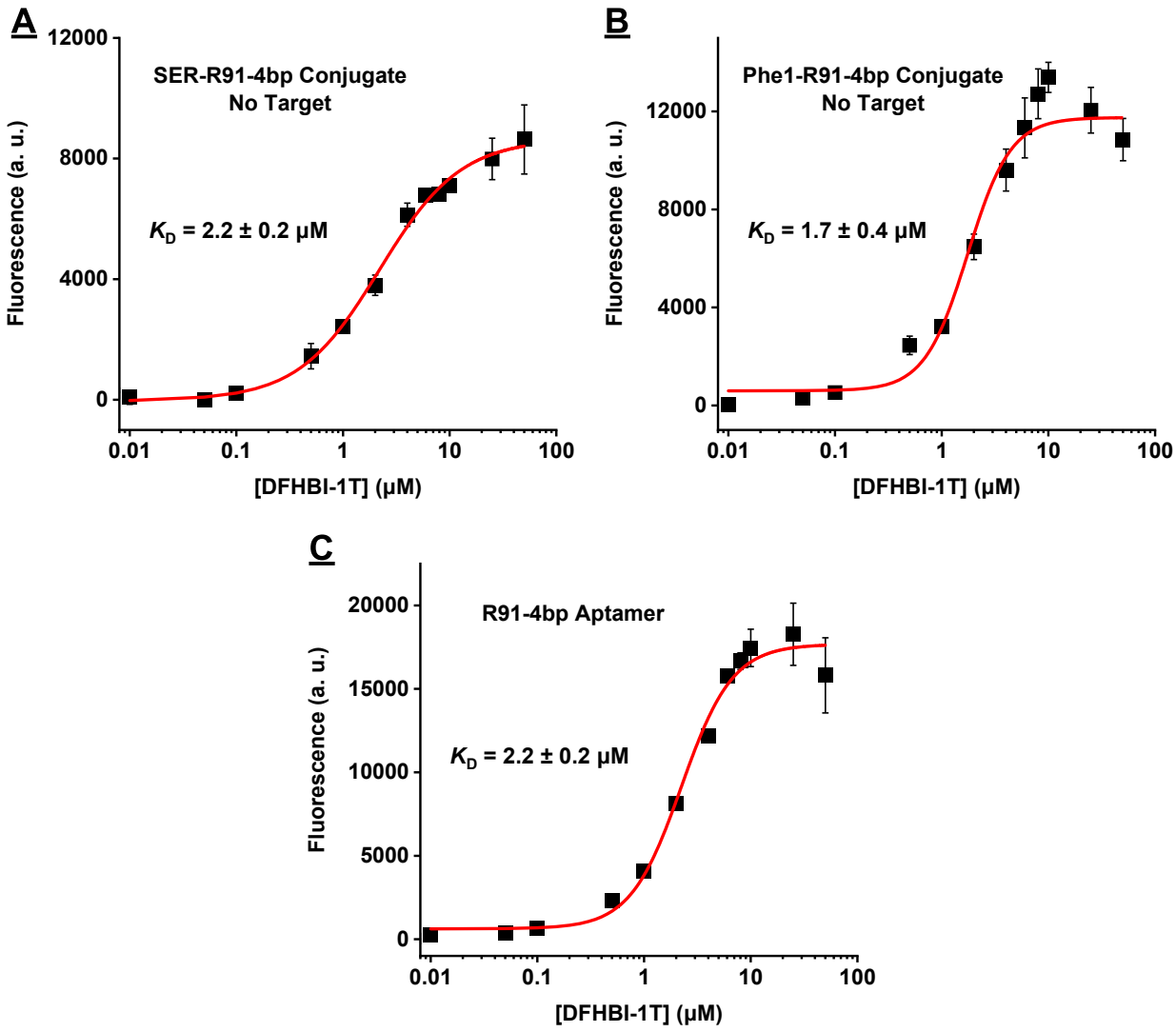

Figure S34. Determining the DFHBI-1T-binding affinity of R91-4bp and the serotonin aptamer SER and phenylalanine aptamer Phe1 conjugated to R91-4bp. We measured the fluorescence of DFHBI-1T at 505 nm (λ_{ex} = 460 nm) in the presence of various concentrations of DFHBI-1T and with a fixed concentration (1 μM) of (**A**) SER-R91-4bp without serotonin, (**B**) Phe1-R91-4bp without phenylalanine, and (**C**) R91-4bp.

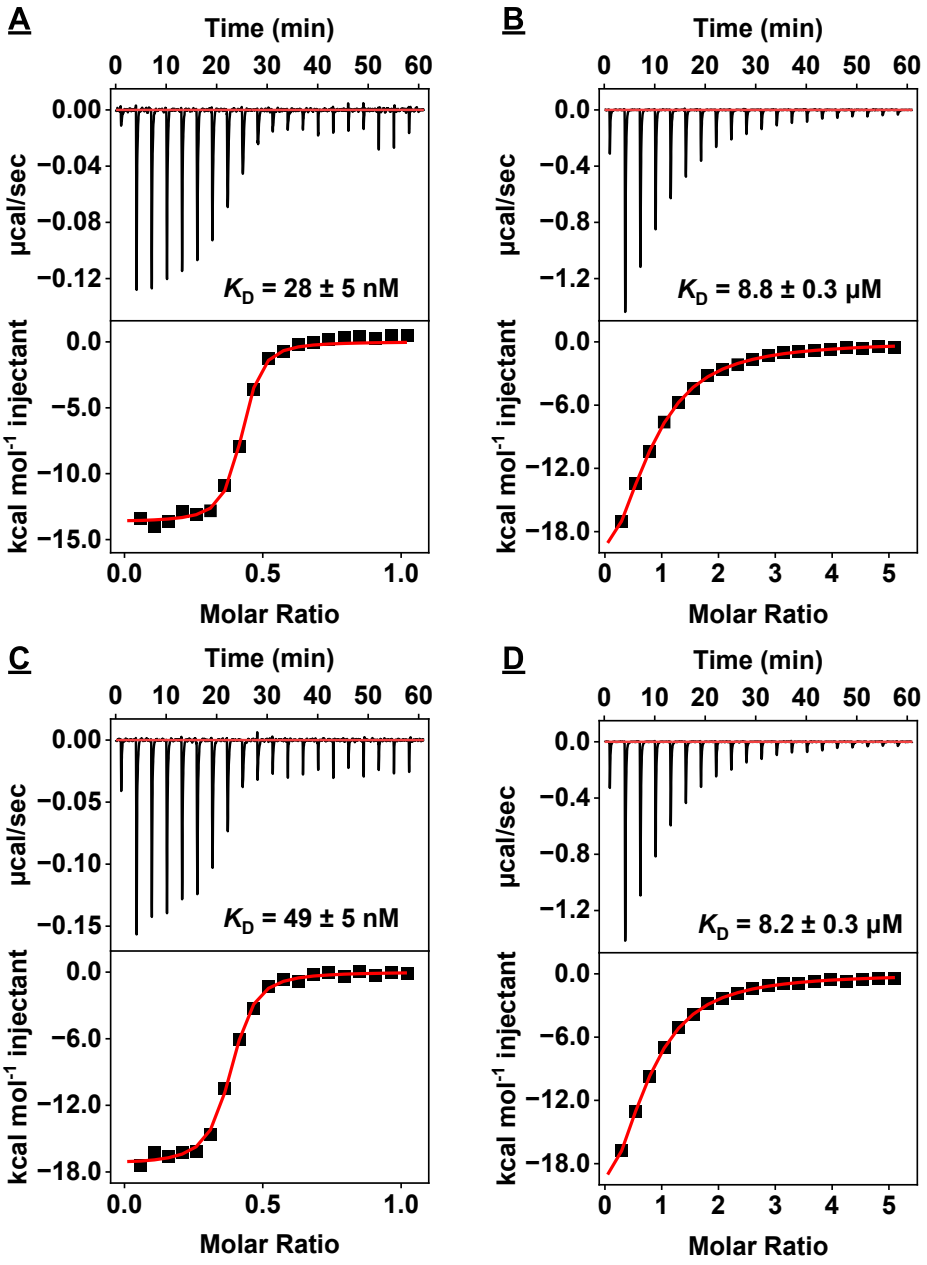

Figure S35. The binding affinity of (**A**) SER-R91-4bp to serotonin, (**B**) Phe1-R91-4bp to phenylalanine, (**C**) SER to serotonin, and (**D**) Phe1 to phenylalanine as determined using ITC. Top panels display the heat generated from each titration of ligand into aptamer. Bottom panels show the integrated heat of each titration after correcting for the heat of dilution of the titrant.

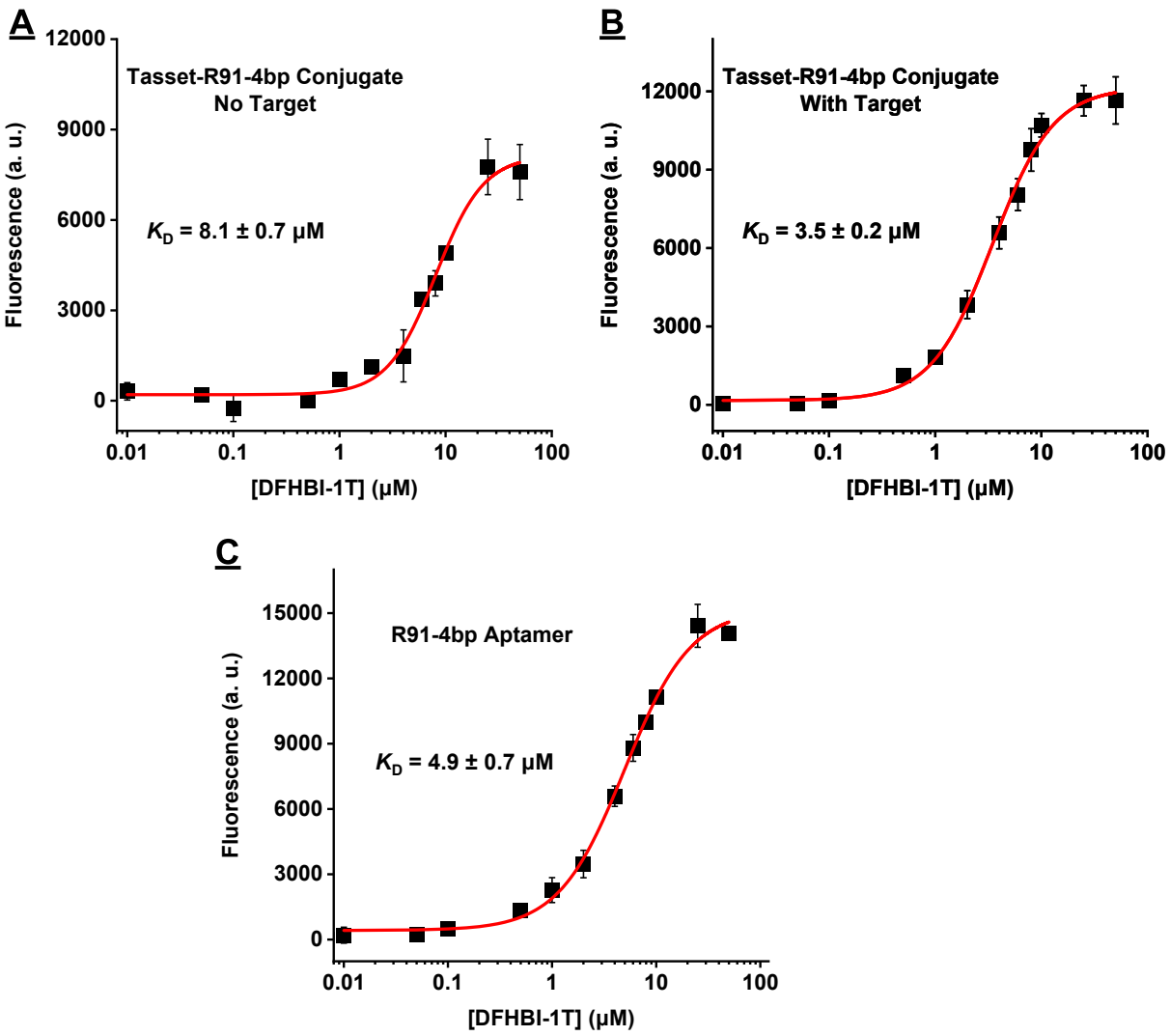

Figure S36. Determining the DFHBI-1T-binding affinity of R91-4bp and the thrombin-binding aptamer Tasset conjugated to R91-4bp. We measured the fluorescence of DFHBI-1T at 505 nm (λ_{ex} = 460 nm) in the presence of various concentrations of DFHBI-1T and with a fixed concentration (1 μM) of (**A**) Tasset-R91-4bp without thrombin, (**B**) Tasset-R91-4bp with 1 μM thrombin, and (**C**) R91-4bp.

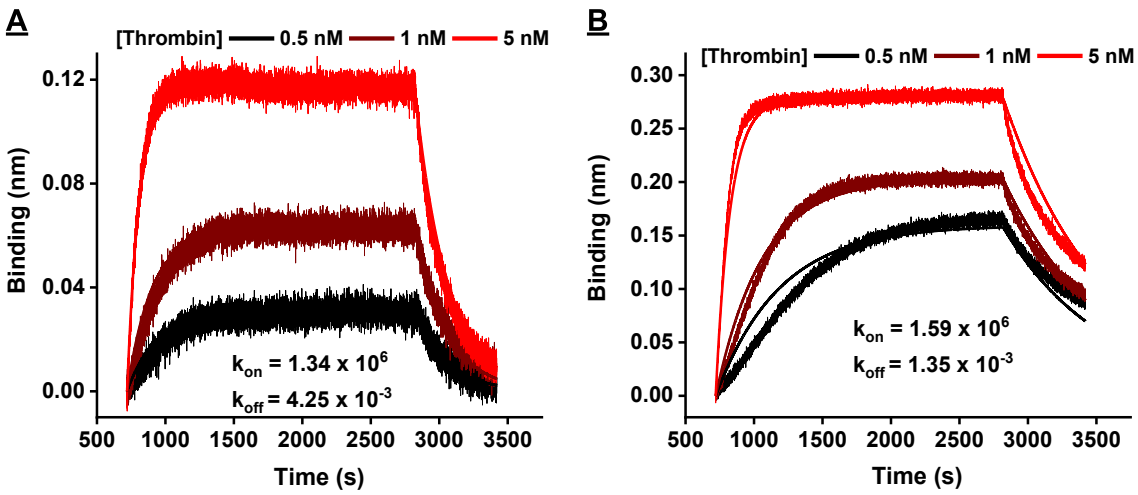

Figure S37. Determining the binding affinity of the Tasset aptamer for thrombin using biolayer interferometry. Binding data for (**A**) Tasset-R91-4bp and (**B**) Tasset aptamer alone. K_D was calculated using the equation: $K_D = \frac{k_{on}}{k_{off}}$

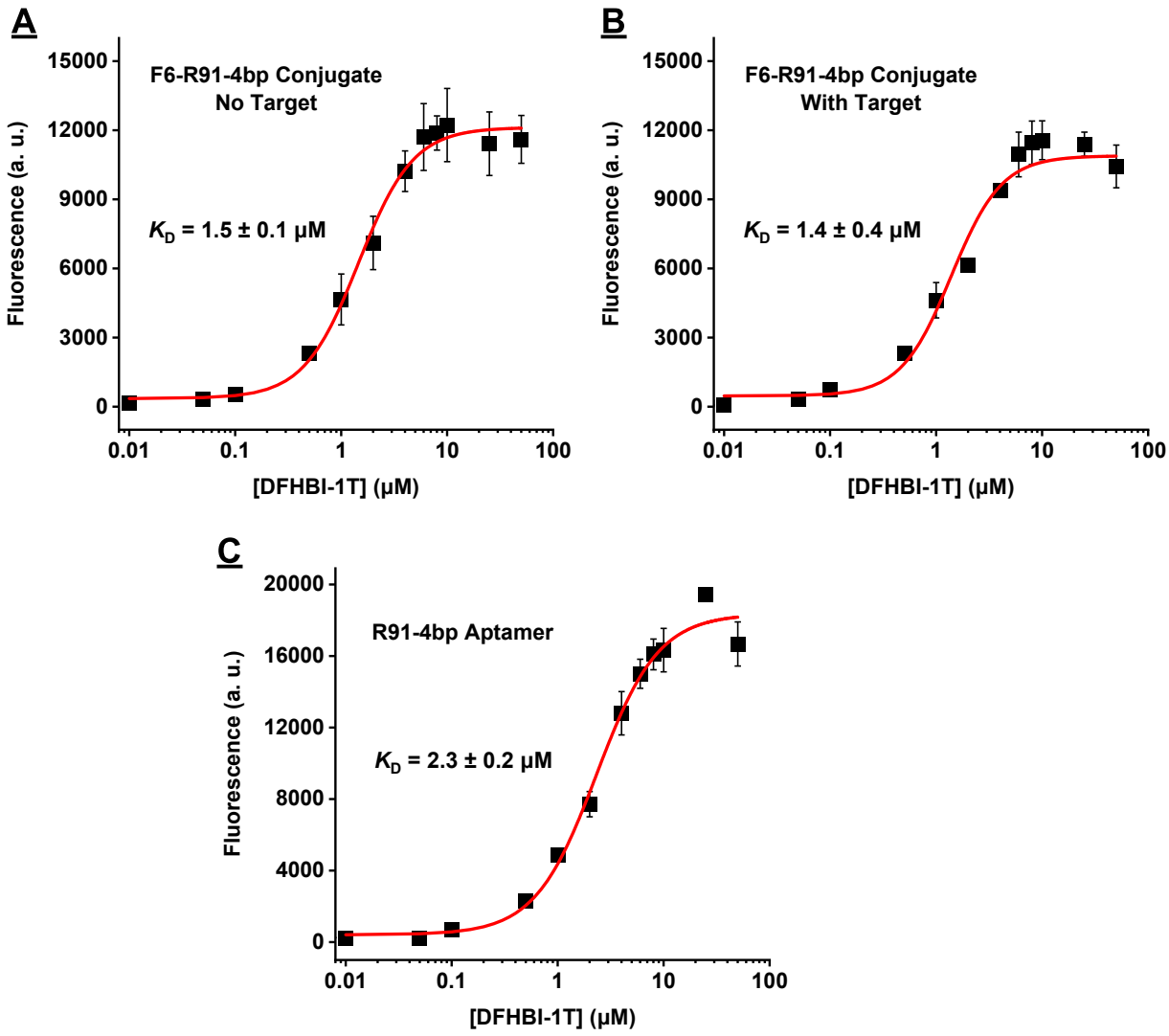

Figure S38. Determining the DFHBI-1T-binding affinity of R91-4bp and the fentanyl-binding aptamer F6 conjugated to R91-4bp. We measured the fluorescence of DFHBI-1T at 505 nm (λ_{ex} = 460 nm) in the presence of various concentrations of DFHBI-1T and with a fixed concentration (1 μM) of (**A**) F6-R91-4bp without fentanyl, (**B**) F6-R91-4bp with 25 μM fentanyl, and (**C**) R91-4bp.

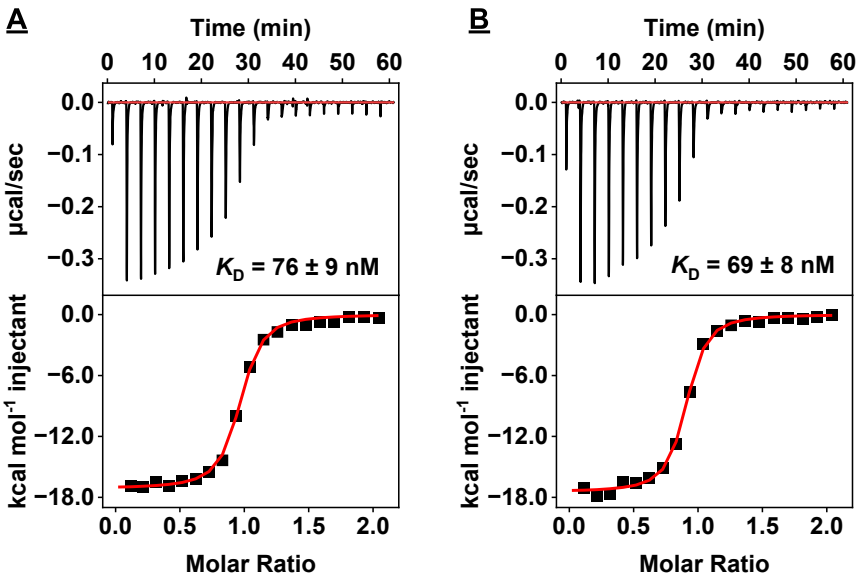

Figure S39. Determining the binding affinity of (**A**) F6-R91-4bp and (**B**) F6 to fentanyl using ITC. Top panels display the heat generated from each titration of ligand into aptamer. Bottom panels show the integrated heat of each titration after correcting for the heat of dilution of the titrant.

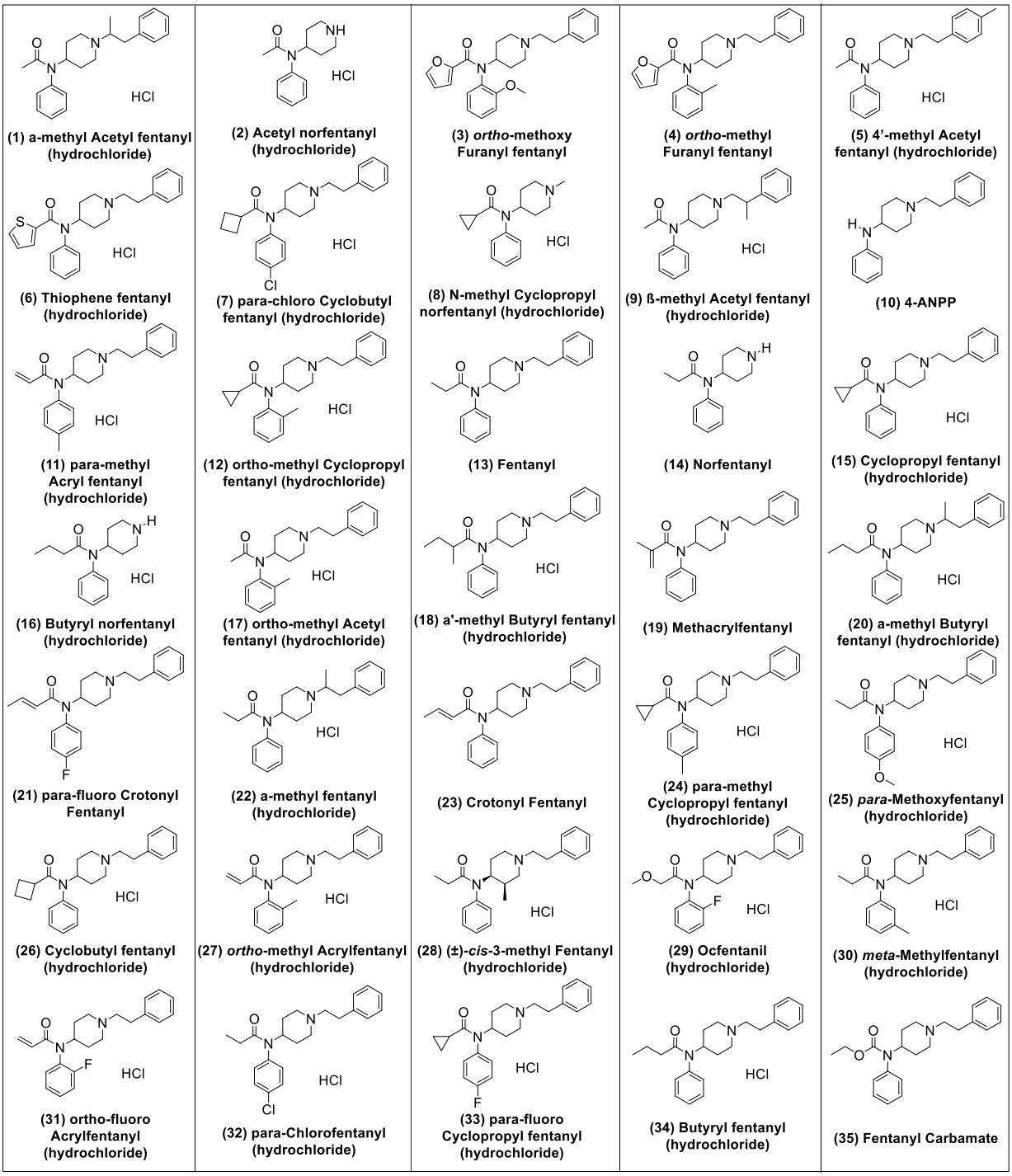

Figure S40. Structures of fentanyl analogs used in this work.

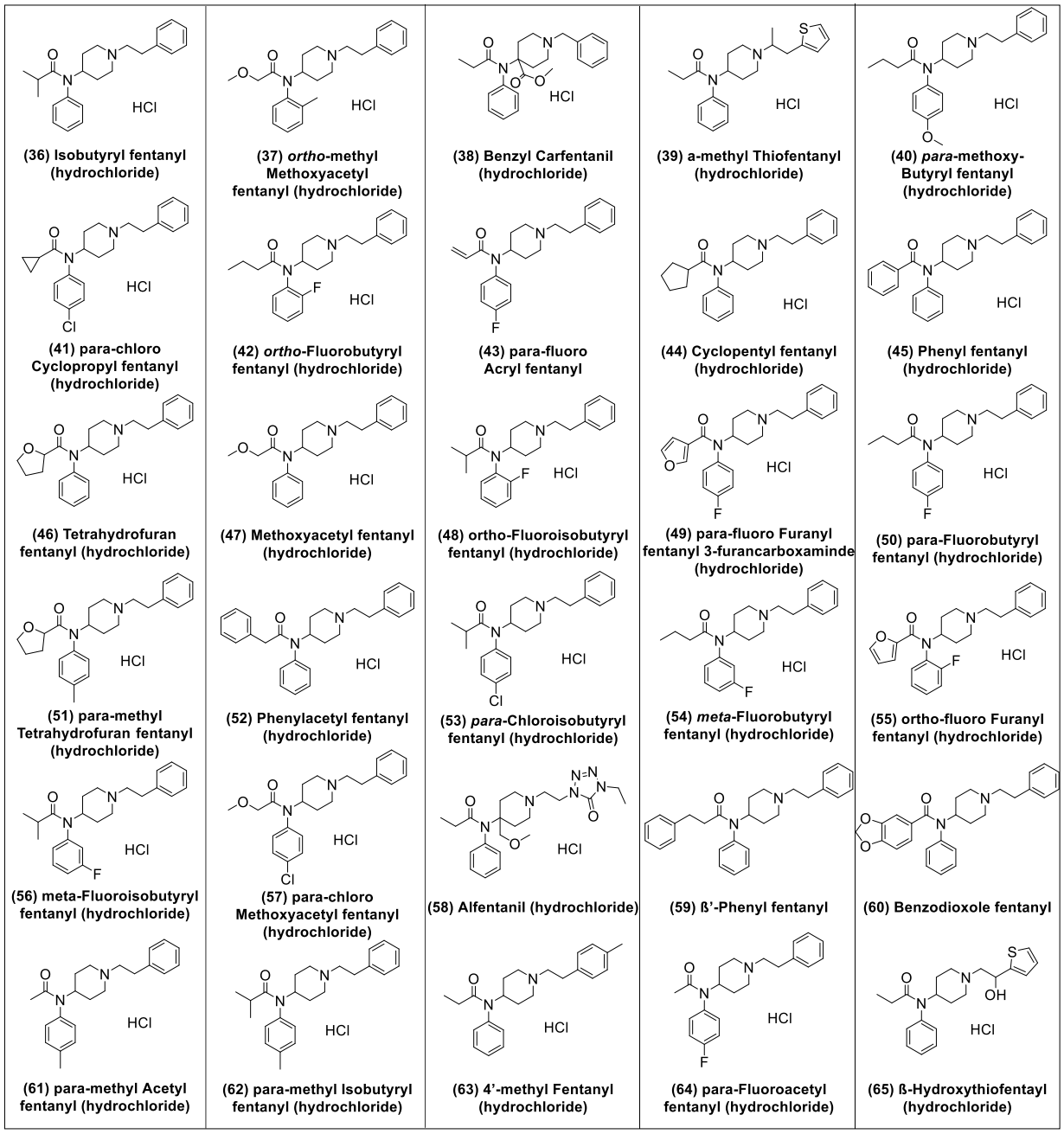

Figure S41. Structures of fentanyl analogs used in this work.

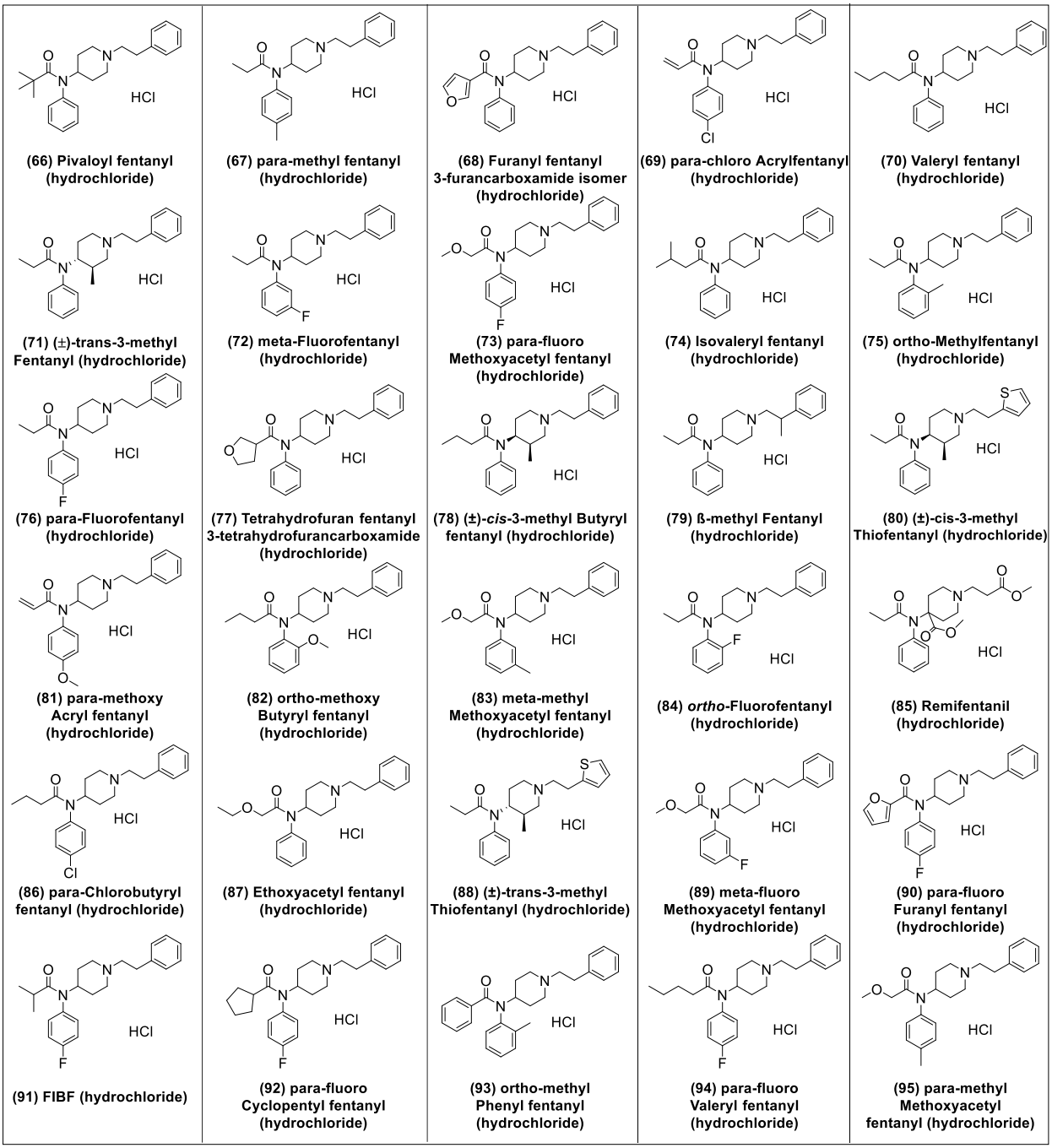

Figure S42. Structures of fentanyl analogs used in this work.

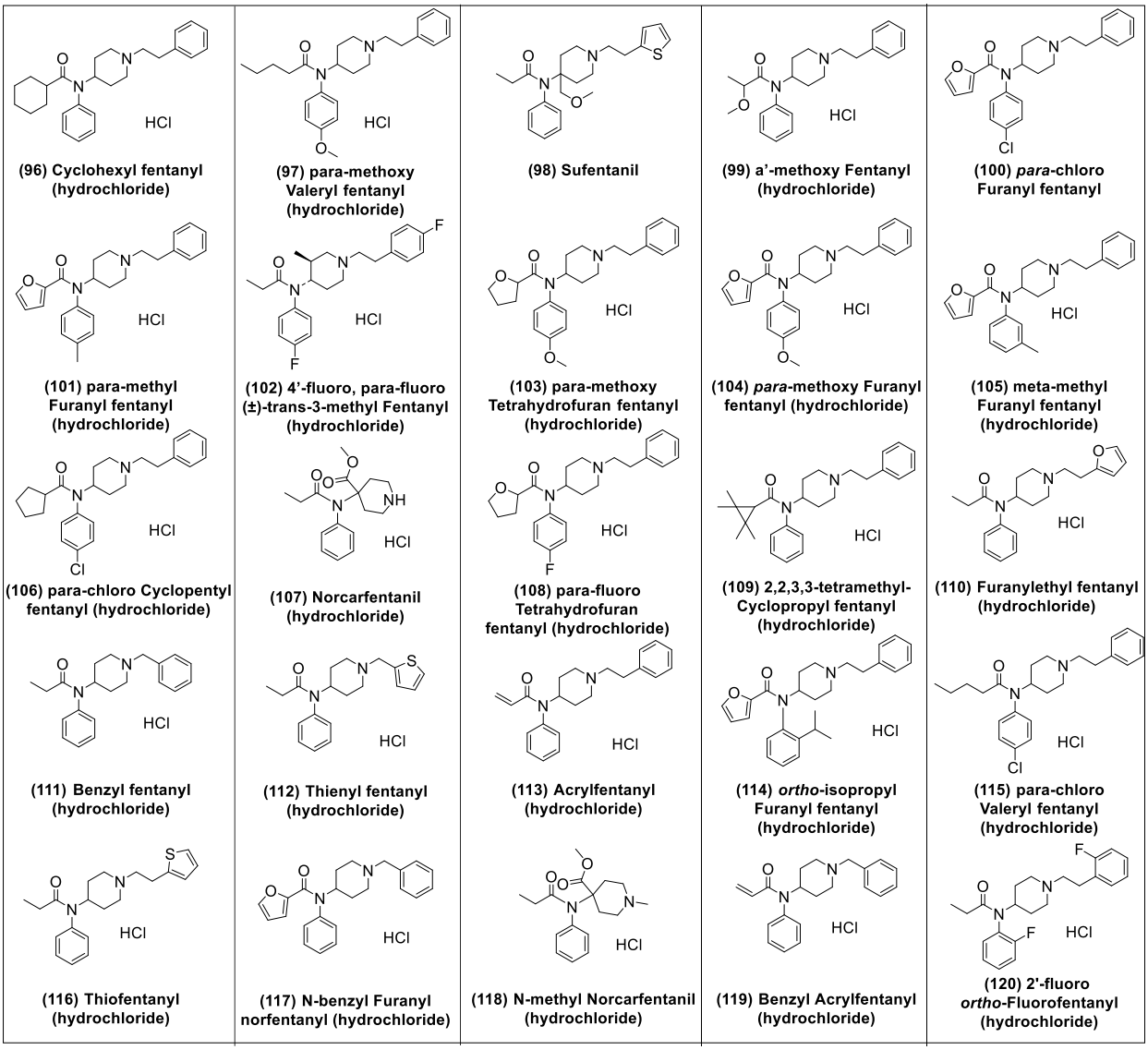

Figure S43. Structures of fentanyl analogs used in this work.

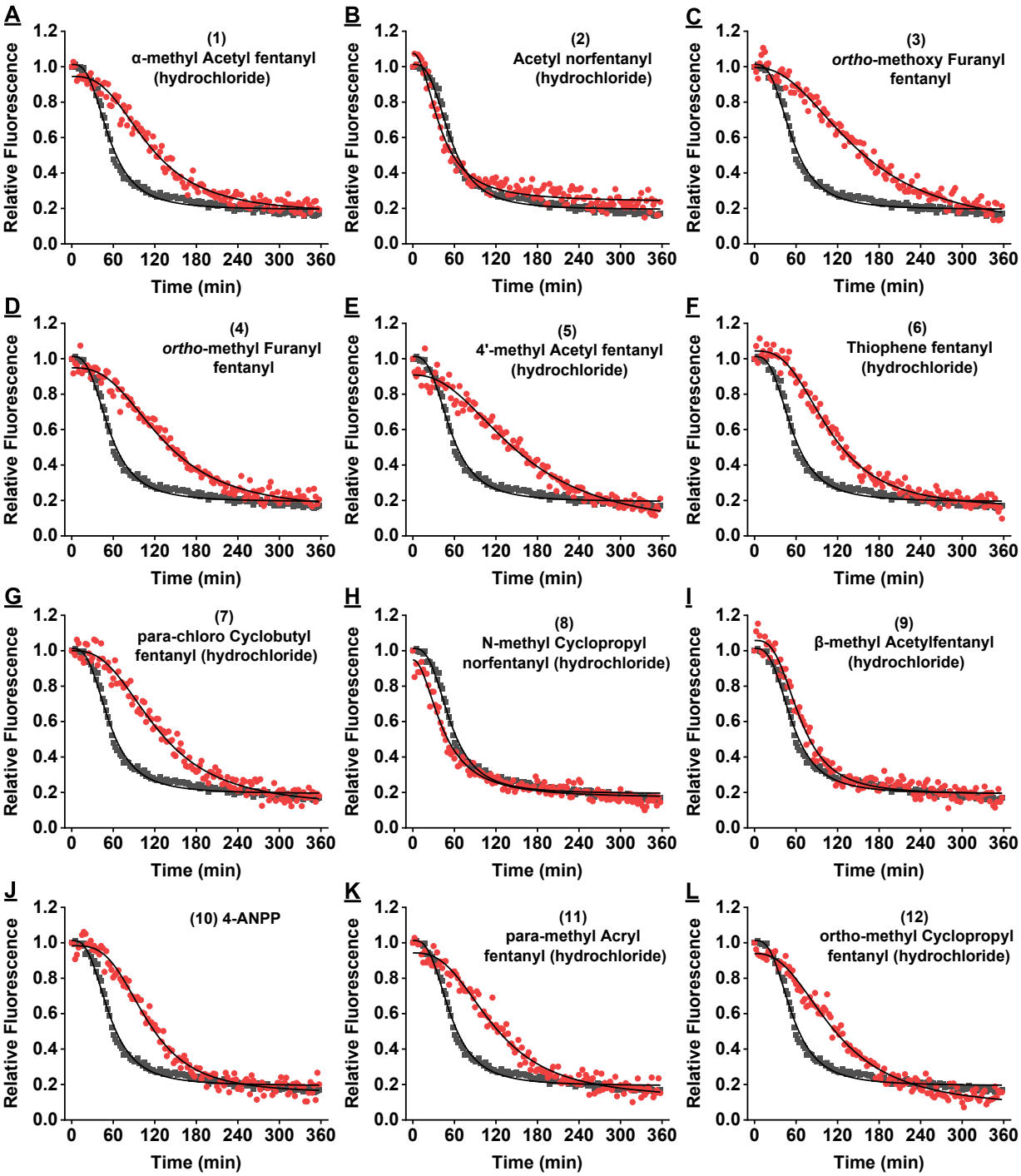

Figure S44. Fluorescence time-course data from the RT-Exo assay for F6-R91-4bp and fentanyl analog (**A**) 1, (**B**) 2, (**C**) 3, (**D**) 4, (**E**) 5, (**F**) 6, (**G**) 7, (**H**) 8, (**I**) 9, (**J**) 10, (**K**) 11, and (**L**) 12. The red and black datapoints respectively indicate data for samples with and without ligand.

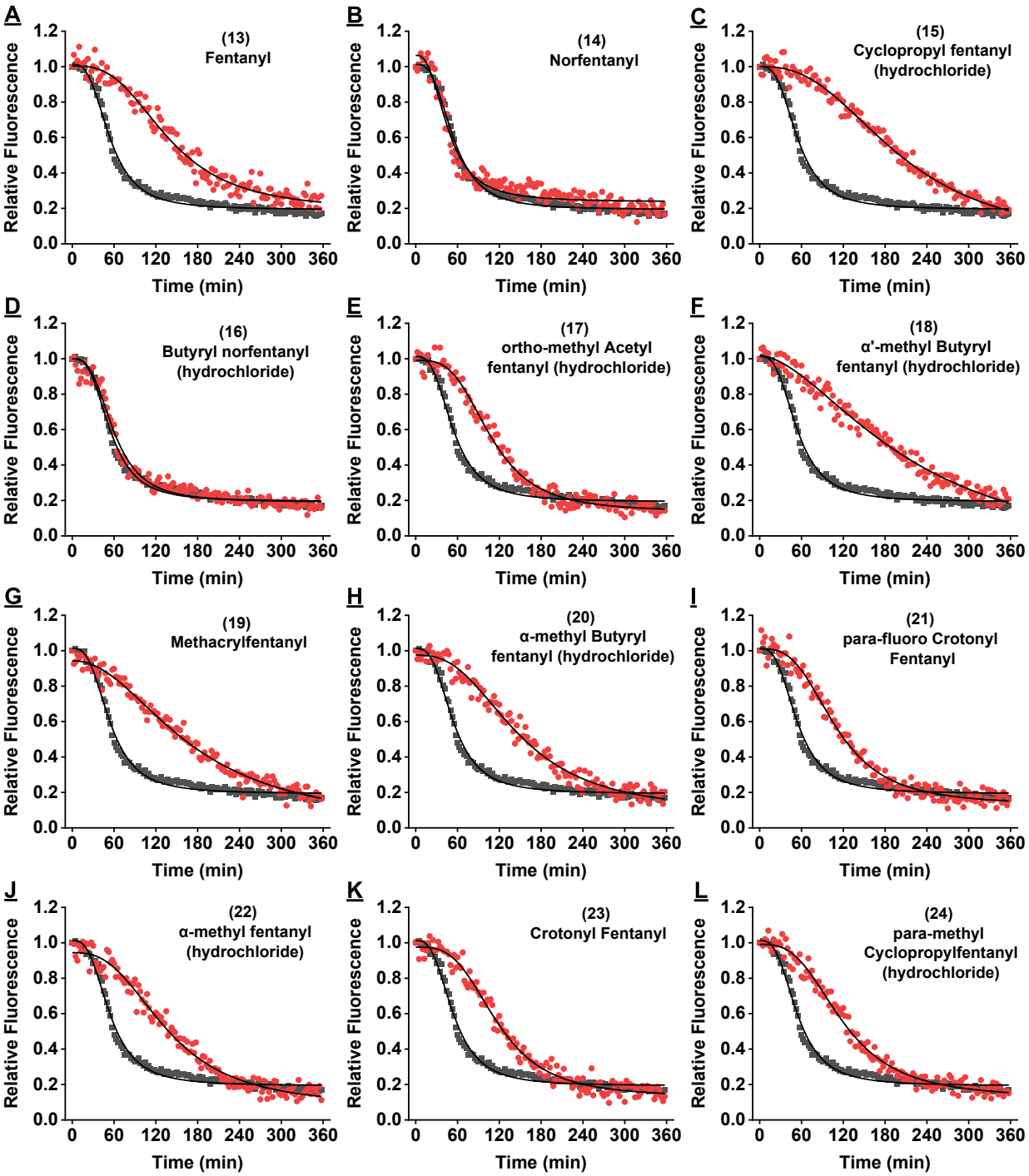

Figure S45. Fluorescence time-course data from the RT-Exo assay for F6-R91-4bp and fentanyl analog (**A**) 13, (**B**) 14, (**C**) 15, (**D**) 16, (**E**) 17, (**F**) 18, (**G**) 19, (**H**) 20, (**I**) 21, (**J**) 22, (**K**) 23, and (**L**) 24. The red and black datapoints respectively indicate data for samples with and without ligand.

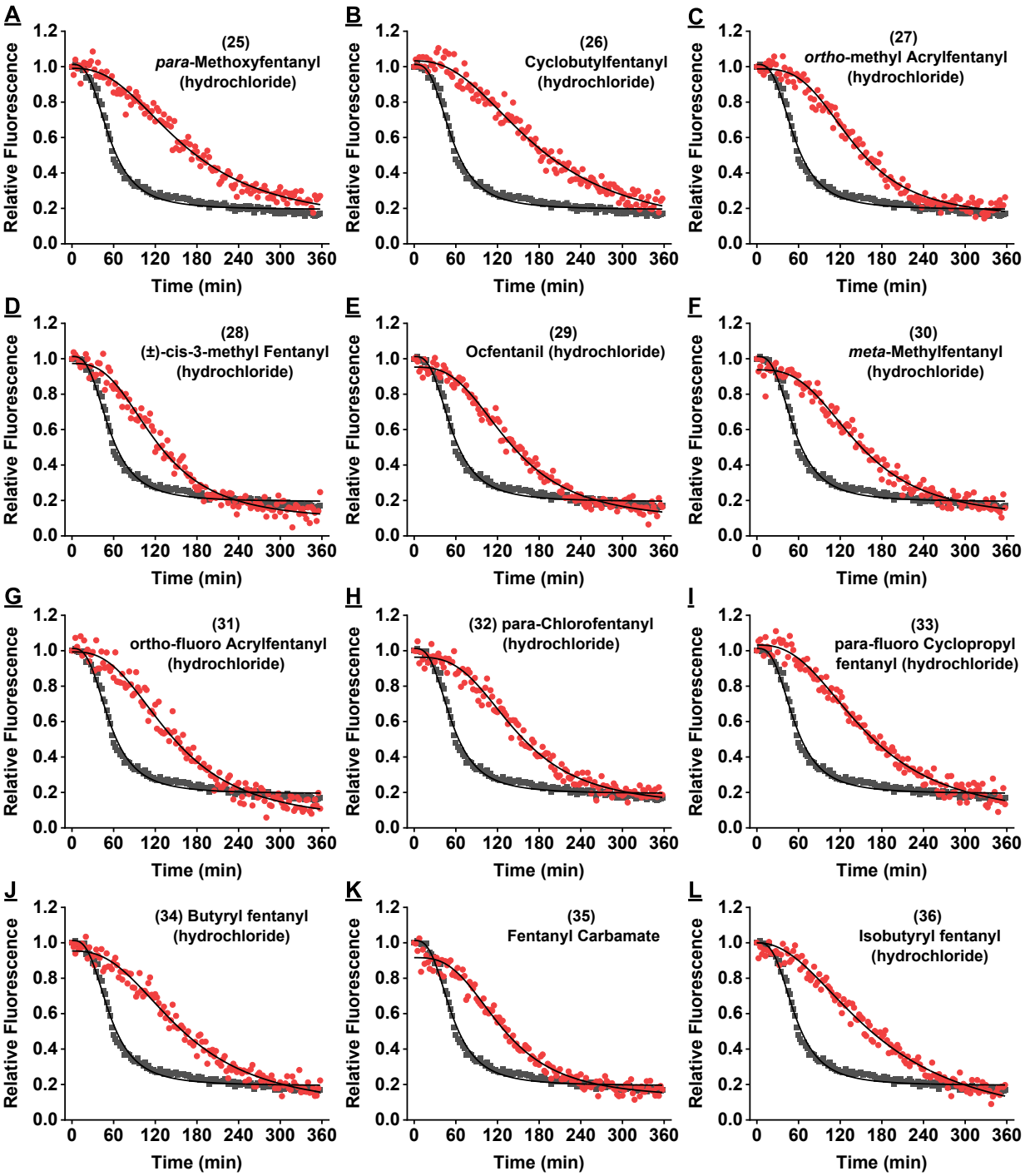

Figure S46. Fluorescence time-course data from the RT-Exo assay for F6-R91-4bp and fentanyl analog (**A**) 25, (**B**) 26, (**C**) 27, (**D**) 28, (**E**) 29, (**F**) 30, (**G**) 31, (**H**) 32, (**I**) 33, (**J**) 34, (**K**) 35, and (**L**) 36. The red and black datapoints respectively indicate data for samples with and without ligand.

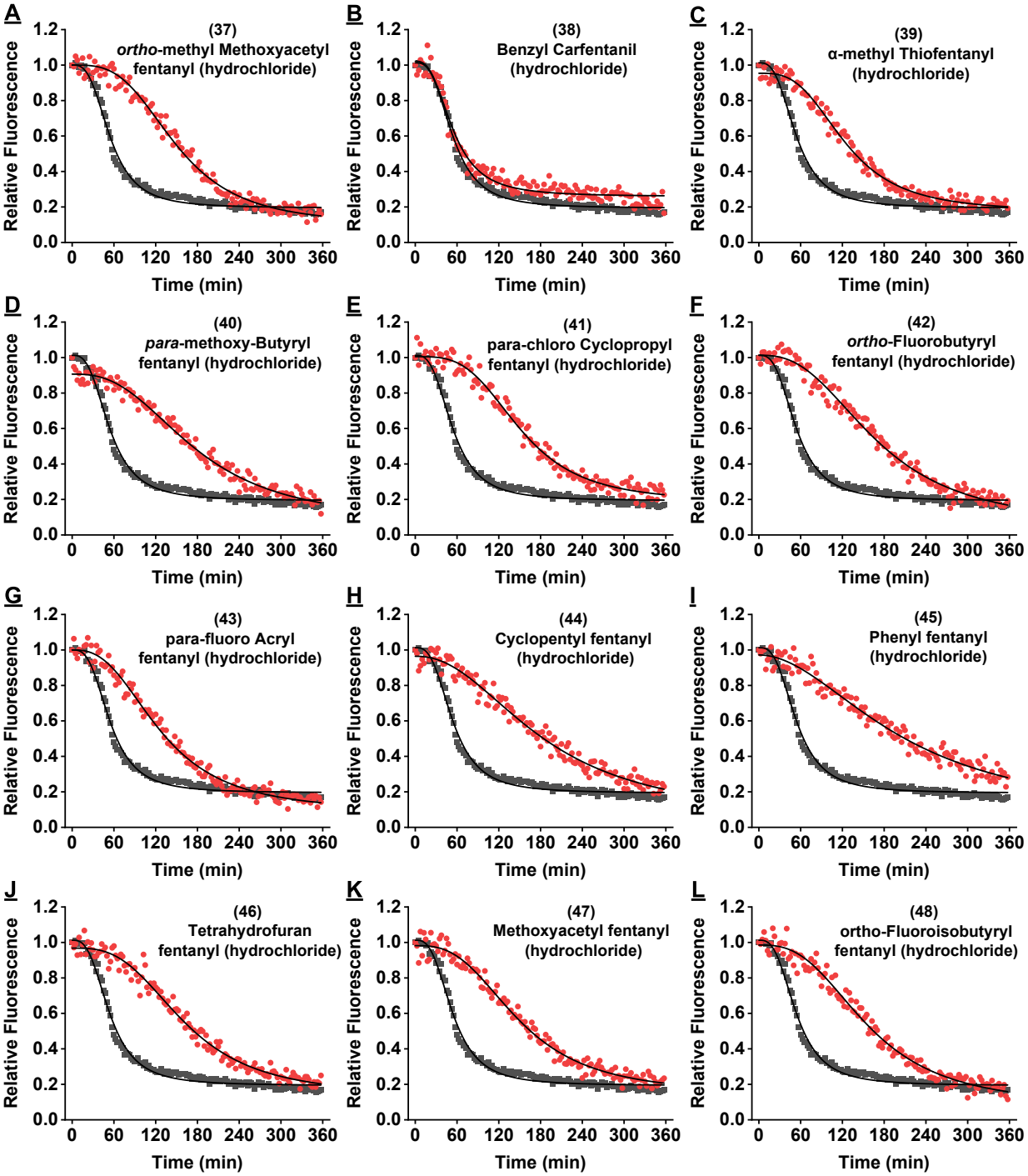

Figure S47. Fluorescence time-course data from the RT-Exo assay for F6-R91-4bp and fentanyl analog (**A**) 37, (**B**) 38, (**C**) 39, (**D**) 40, (**E**) 41, (**F**) 42, (**G**) 43, (**H**) 44, (**I**) 45, (**J**) 46, (**K**) 47, and (**L**) 48. The red and black datapoints respectively indicate data for samples with and without ligand.

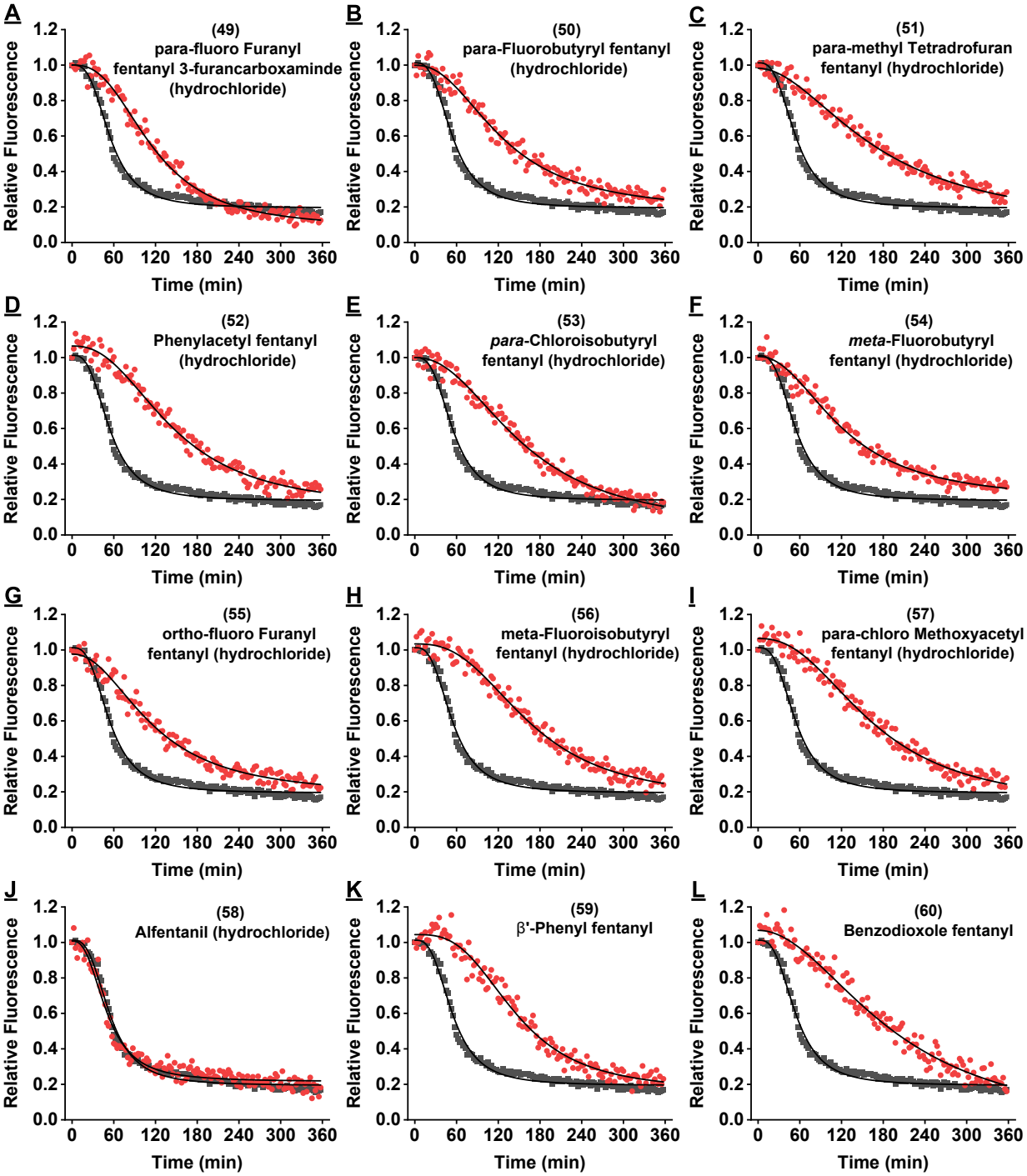

Figure S48. Fluorescence time-course data from the RT-Exo assay for F6-R91-4bp and fentanyl analog (**A**) 49, (**B**) 50, (**C**) 51, (**D**) 52, (**E**) 53, (**F**) 54, (**G**) 55, (**H**) 56, (**I**) 57, (**J**) 58, (**K**) 59, and (**L**) 60. The red and black datapoints respectively indicate data for samples with and without ligand.

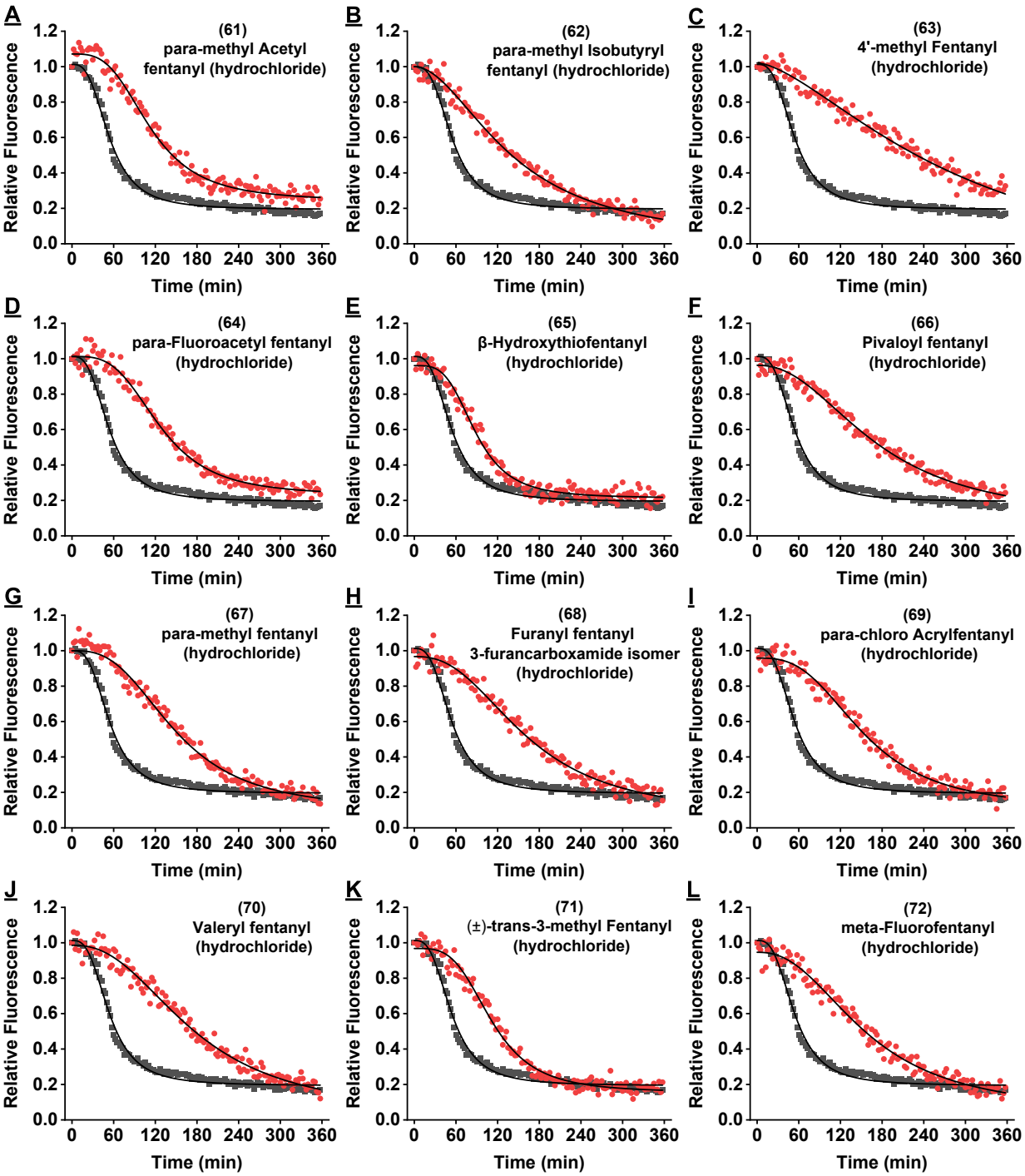

Figure S49. Fluorescence time-course data from the RT-Exo assay for F6-R91-4bp and fentanyl analog (**A**) 61, (**B**) 62, (**C**) 63, (**D**) 64, (**E**) 65, (**F**) 66, (**G**) 67, (**H**) 68, (**I**) 69, (**J**) 70, (**K**) 71, and (**L**) 72. The red and black datapoints respectively indicate data for samples with and without ligand.

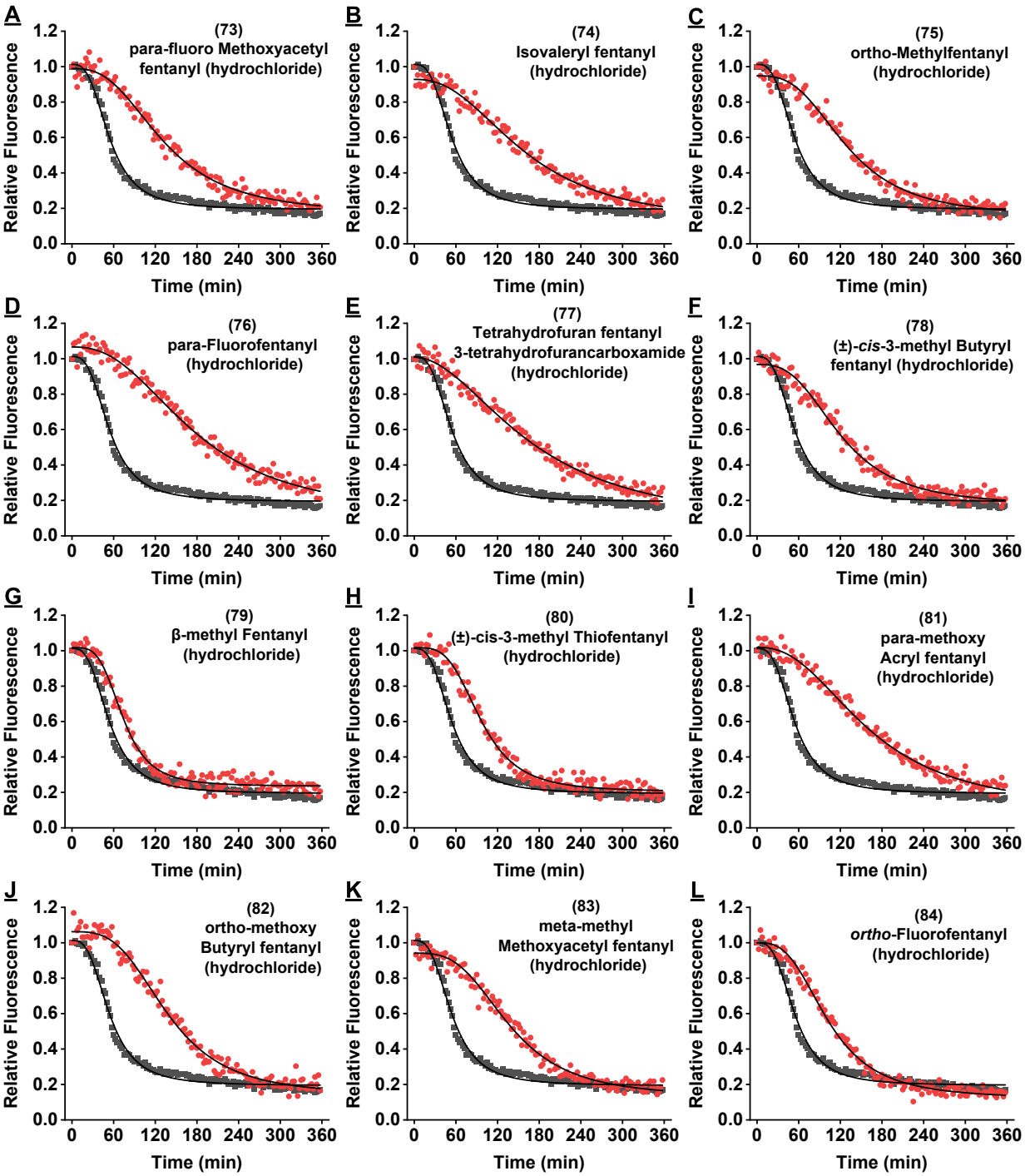

Figure S50. Fluorescence time-course data from the RT-Exo assay for F6-R91-4bp and fentanyl analog (**A**) 73, (**B**) 74, (**C**) 75, (**D**) 76, (**E**) 77, (**F**) 78, (**G**) 79, (**H**) 80, (**I**) 81, (**J**) 82, (**K**) 83, and (**L**) 84. The red and black datapoints respectively indicate data for samples with and without ligand.

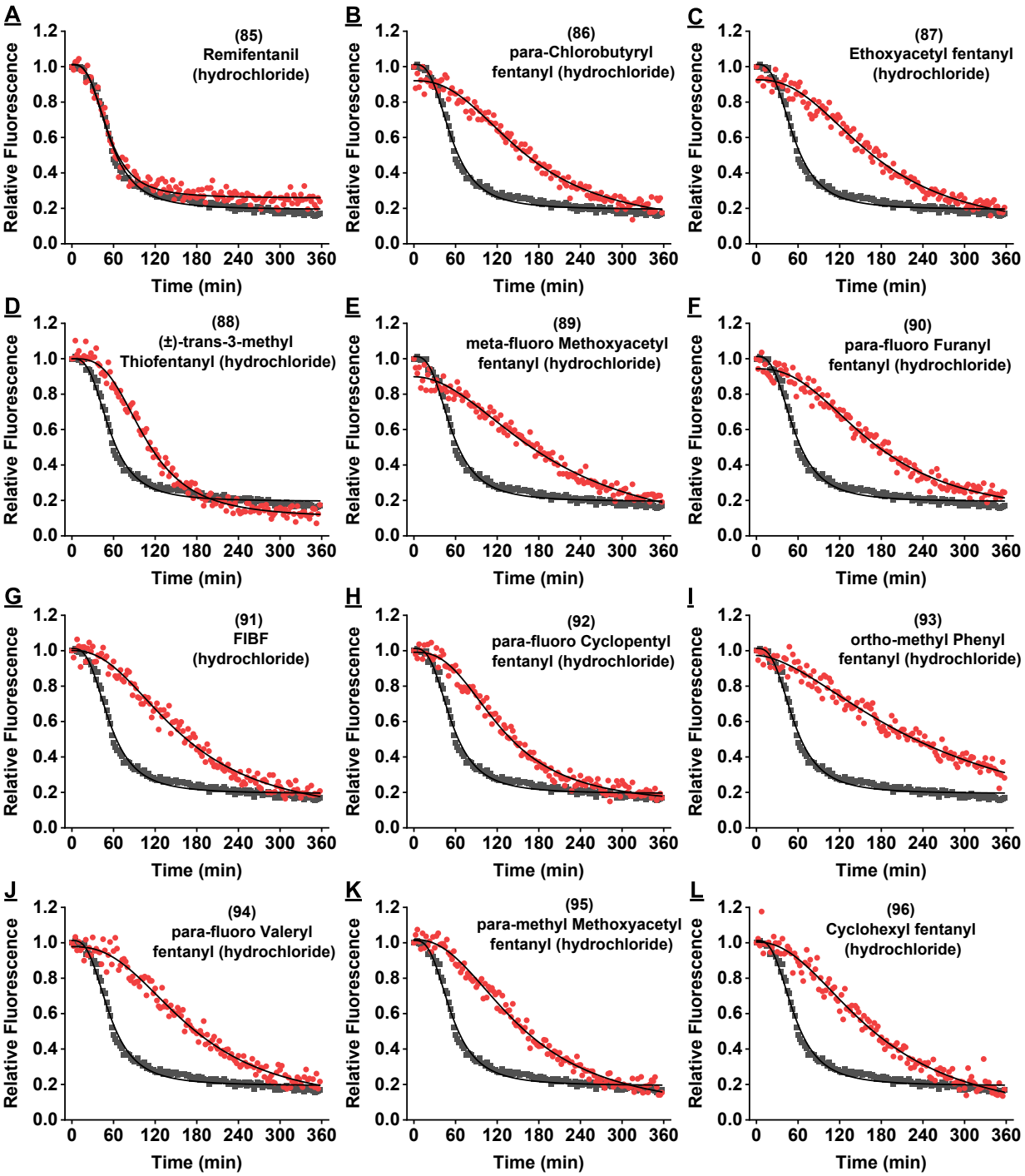

Figure S51. Fluorescence time-course data from the RT-Exo assay for F6-R91-4bp and fentanyl analog (**A**) 85, (**B**) 86, (**C**) 87, (**D**) 88, (**E**) 89, (**F**) 90, (**G**) 91, (**H**) 92, (**I**) 93, (**J**) 94, (**K**) 95, and (**L**) 96. The red and black datapoints respectively indicate data for samples with and without ligand.

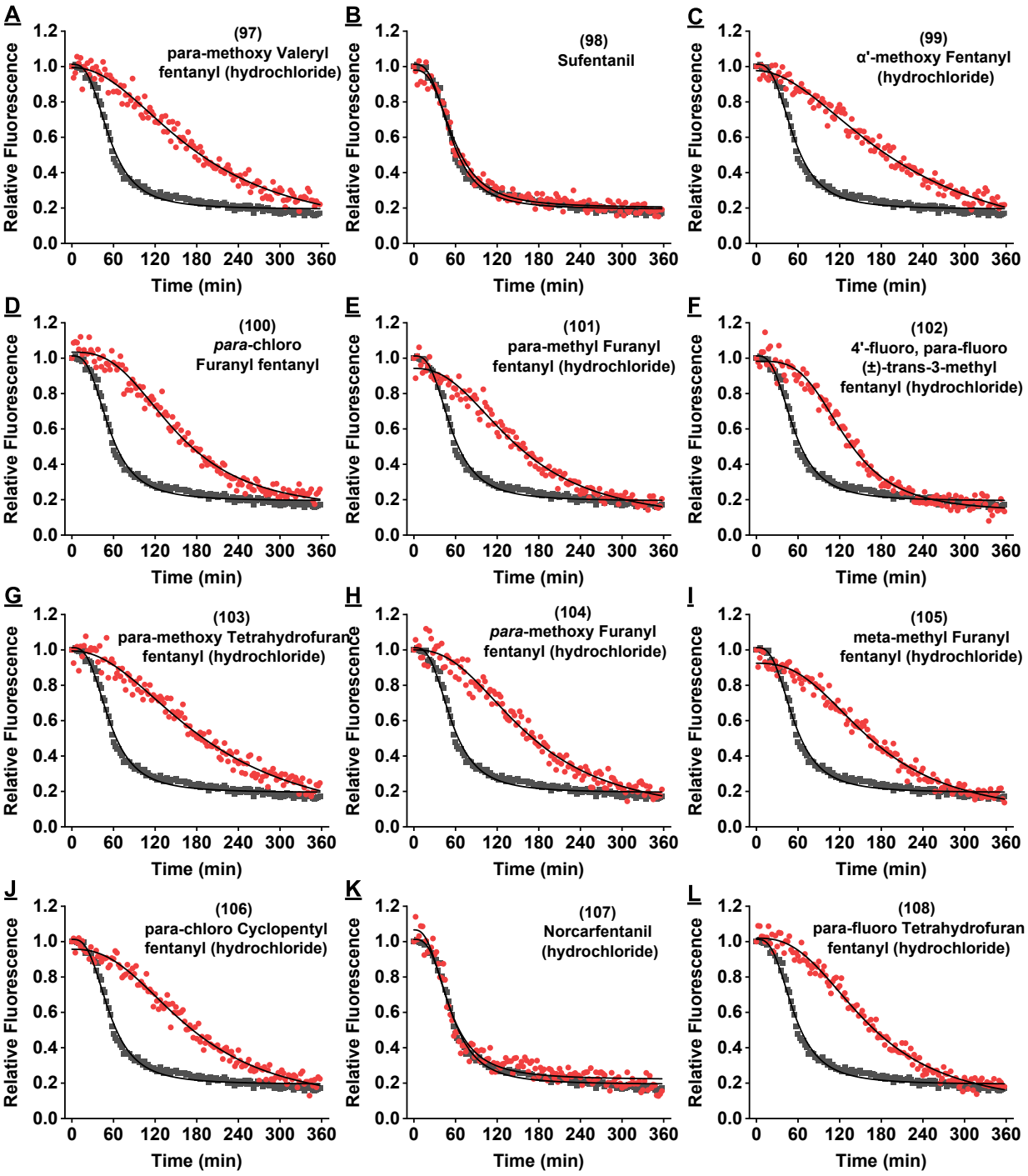

Figure S52. Fluorescence time-course data from the RT-Exo assay for F6-R91-4bp and fentanyl analog (**A**) 97, (**B**) 98, (**C**) 99, (**D**) 100, (**E**) 101, (**F**) 102, (**G**) 103, (**H**) 104, (**I**) 105, (**J**) 106, (**K**) 107, and (**L**) 108. The red and black datapoints respectively indicate data for samples with and without ligand.

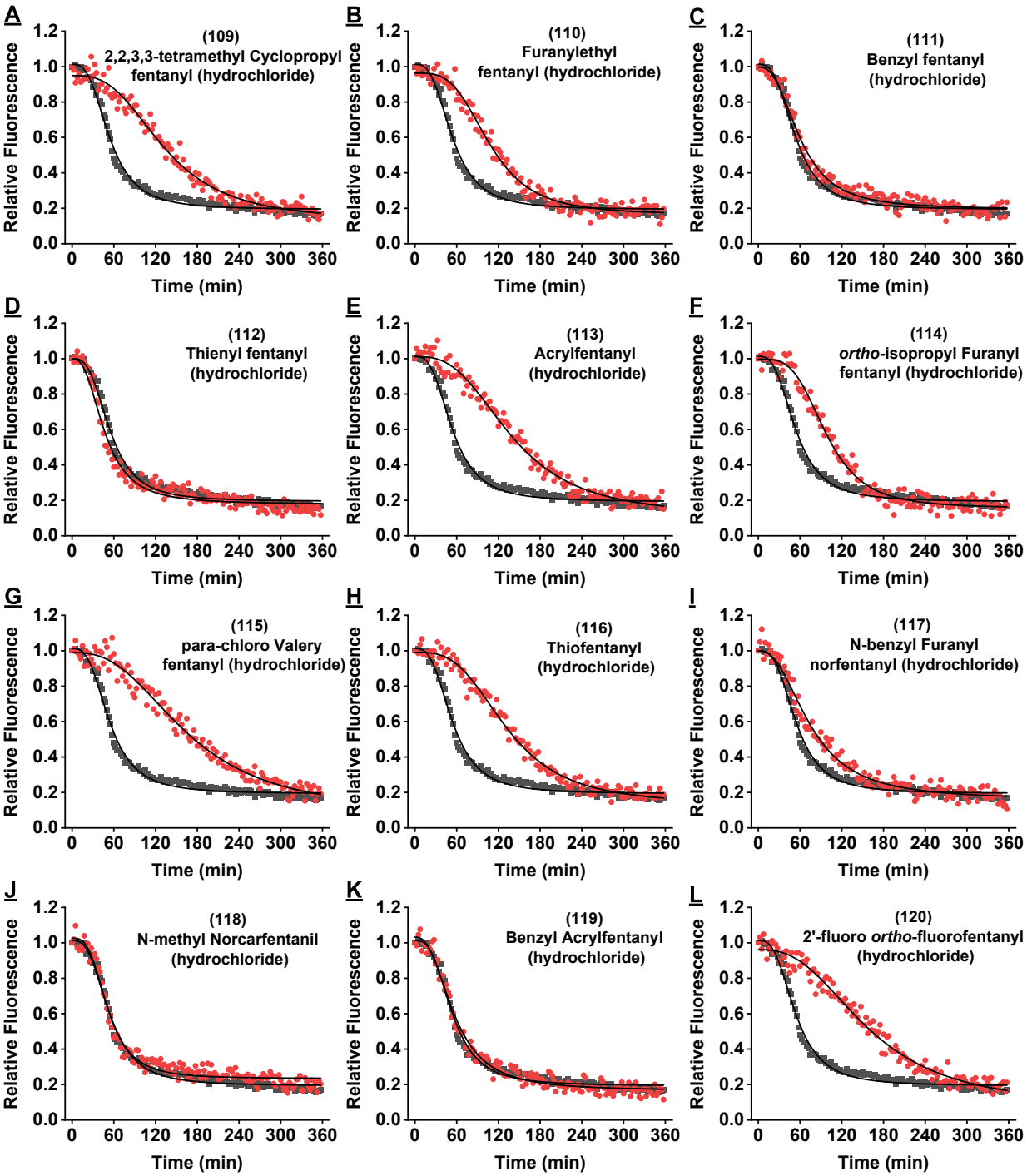

Figure S53. Fluorescence time-course data from the RT-Exo assay for F6-R91-4bp and fentanyl analog (**A**) 109, (**B**) 110, (**C**) 111, (**D**) 112, (**E**) 113, (**F**) 114, (**G**) 115, (**H**) 116, (**I**) 117, (**J**) 118, (**K**) 119, and (**L**) 120. The red and black datapoints respectively indicate data for samples with and without ligand.

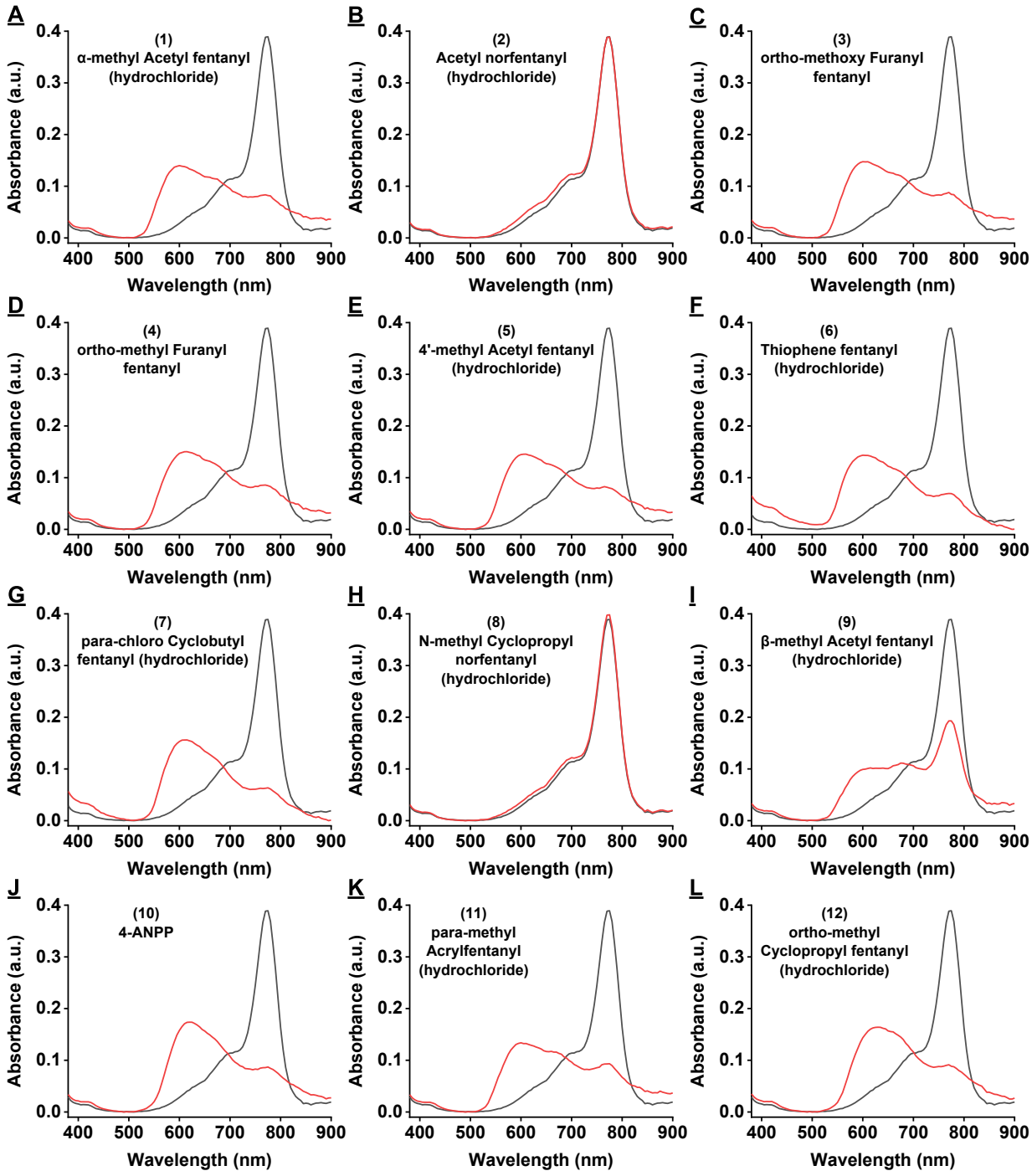

Figure S54. Absorbance spectra data from the Cy7 dye displacement for F6 and fentanyl analog (**A**) 1, (**B**) 2, (**C**) 3, (**D**) 4, (**E**) 5, (**F**) 6, (**G**) 7, (**H**) 8, (**I**) 9, (**J**) 10, (**K**) 11, and (**L**) 12. The red and black curves respectively indicate data for samples with and without ligand.

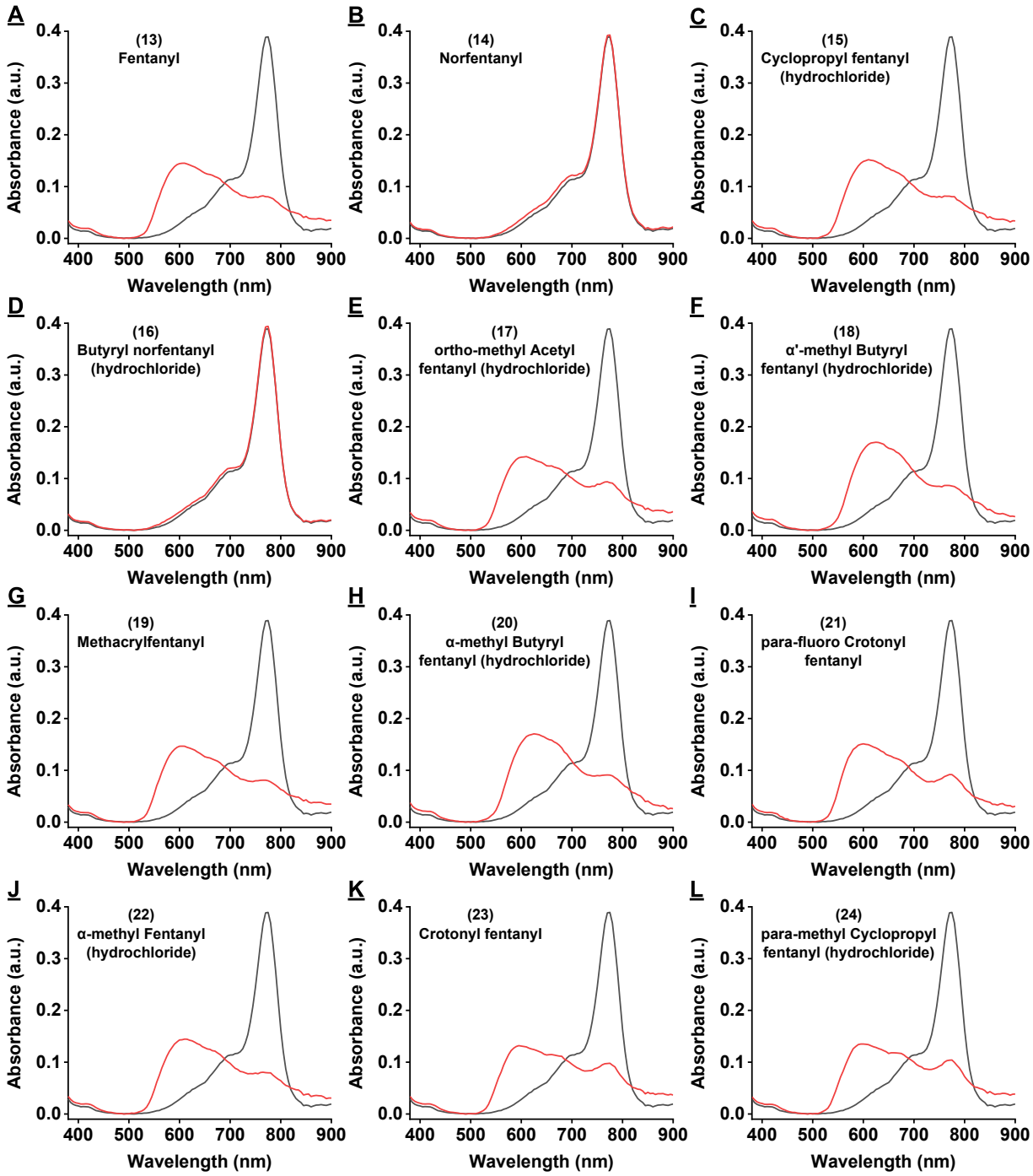

Figure S55. Absorbance spectra data from the Cy7 dye displacement for F6 and fentanyl analog (**A**) 13, (**B**) 14, (**C**) 15, (**D**) 16, (**E**) 17, (**F**) 18, (**G**) 19, (**H**) 20, (**I**) 21, (**J**) 22, (**K**) 23, and (**L**) 24. The red and black curves respectively indicate data for samples with and without ligand.

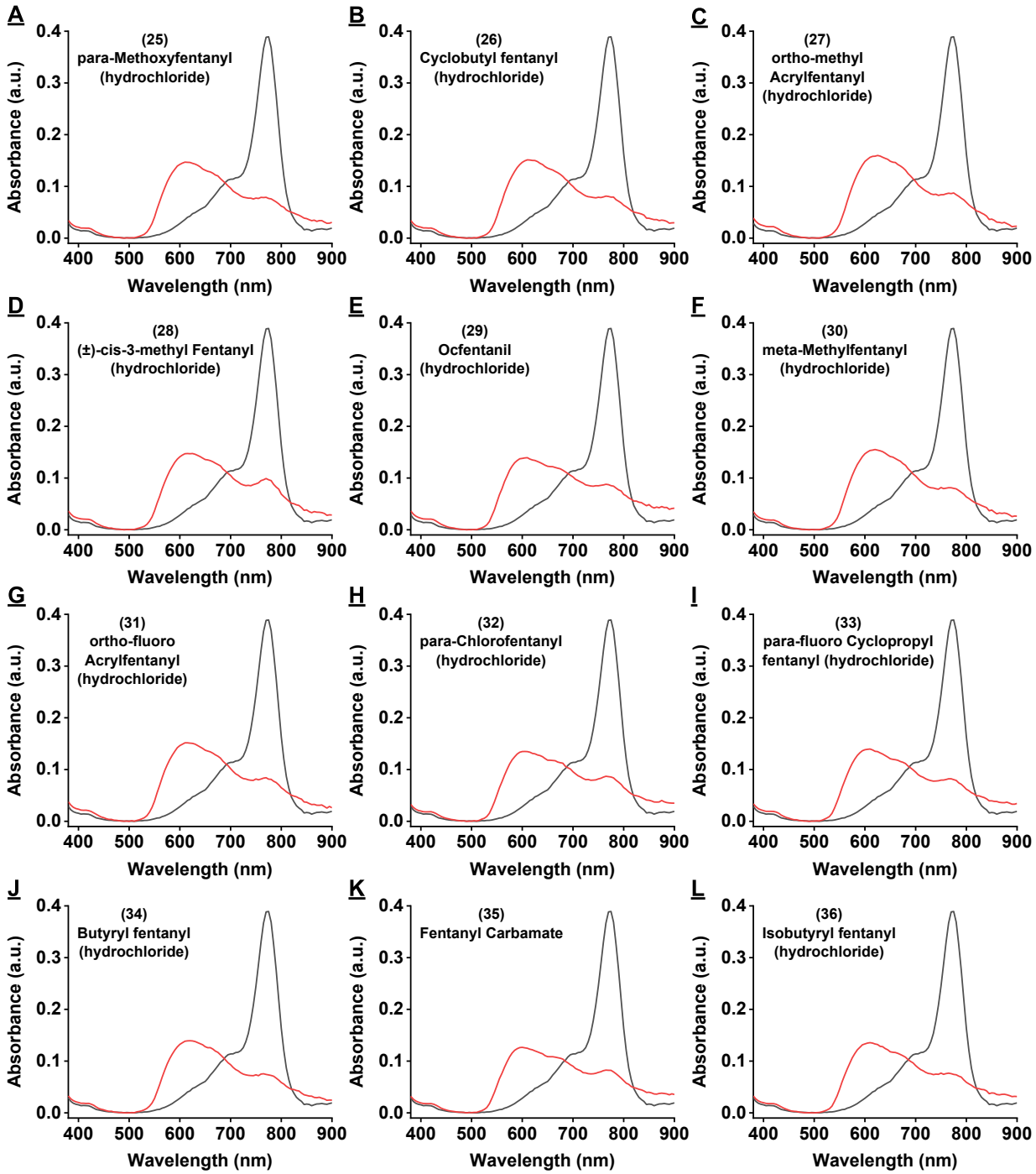

Figure S56. Absorbance spectra data from the Cy7 dye displacement for F6 and fentanyl analog (**A**) 25, (**B**) 26, (**C**) 27, (**D**) 28, (**E**) 29, (**F**) 30, (**G**) 31, (**H**) 32, (**I**) 33, (**J**) 34, (**K**) 35, and (**L**) 36. The red and black curves respectively indicate data for samples with and without ligand.

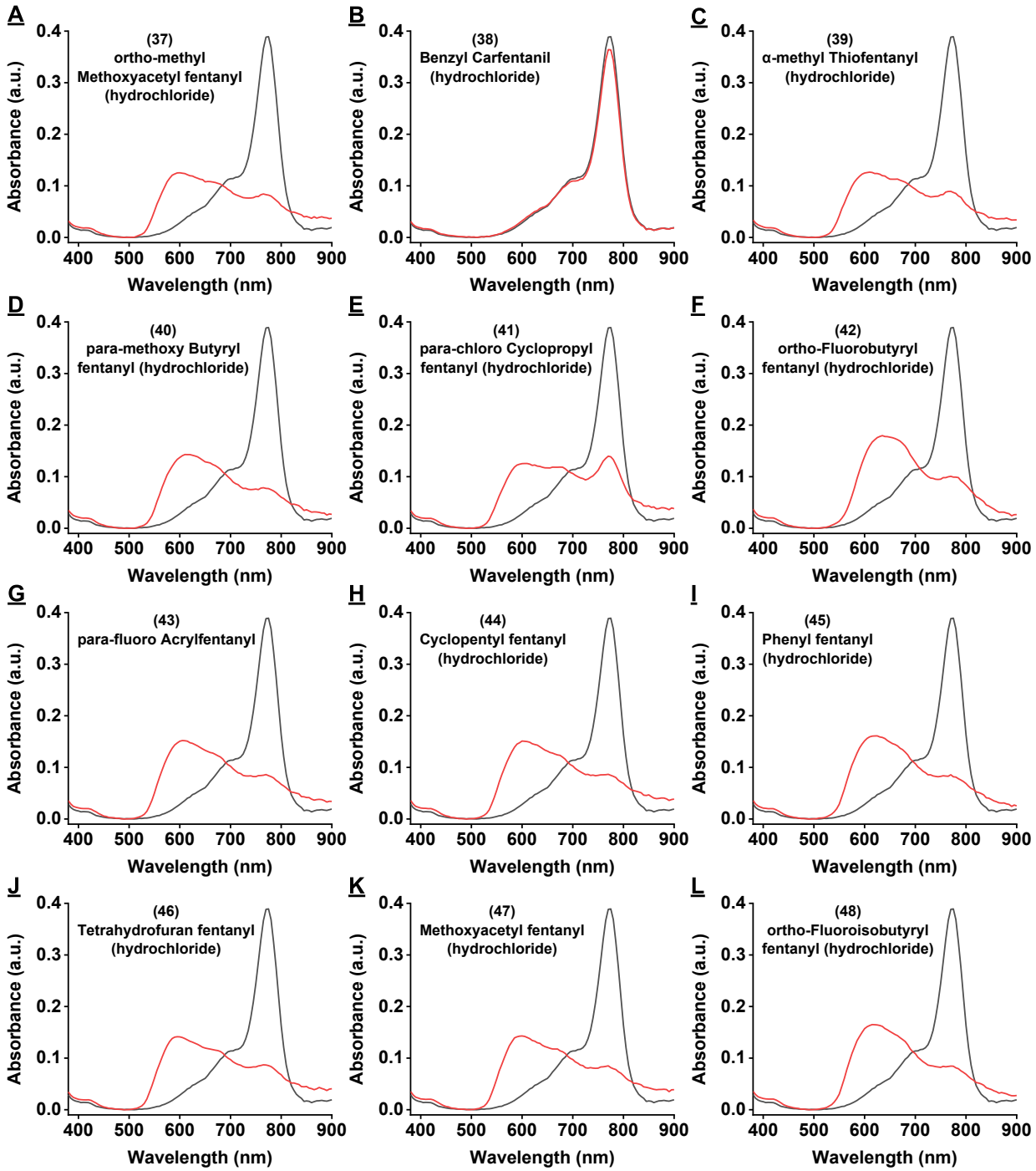

Figure S57. Absorbance spectra data from the Cy7 dye displacement for F6 and fentanyl analog (**A**) 37, (**B**) 38, (**C**) 39, (**D**) 40, (**E**) 41, (**F**) 42, (**G**) 43, (**H**) 44, (**I**) 45, (**J**) 46, (**K**) 47, and (**L**) 48. The red and black curves respectively indicate data for samples with and without ligand.

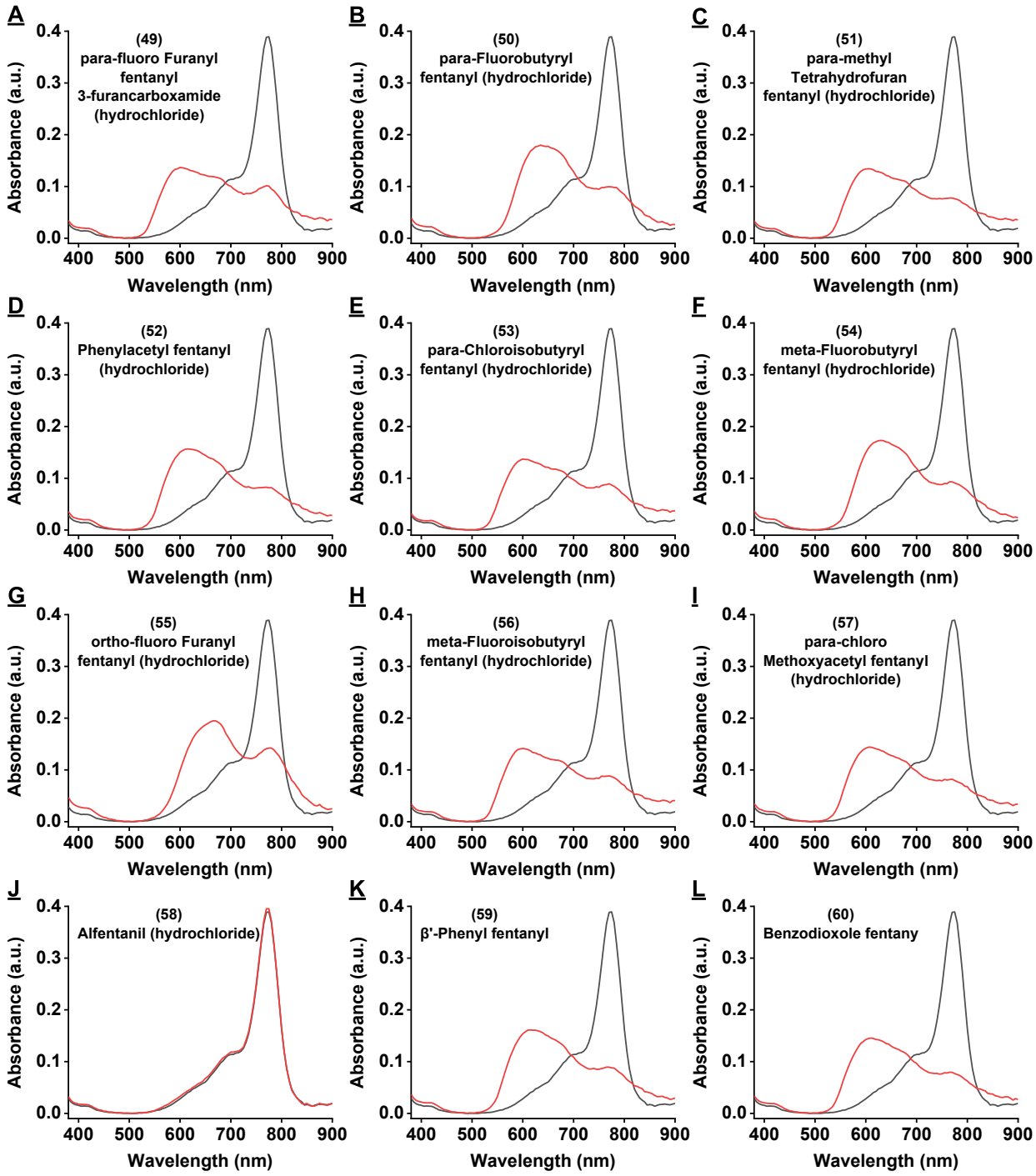

Figure S58. Absorbance spectra data from the Cy7 dye displacement for F6 and fentanyl analog (**A**) 49, (**B**) 50, (**C**) 51, (**D**) 52, (**E**) 53, (**F**) 54, (**G**) 55, (**H**) 56, (**I**) 57, (**J**) 58, (**K**) 59, and (**L**) 60. The red and black curves respectively indicate data for samples with and without ligand.

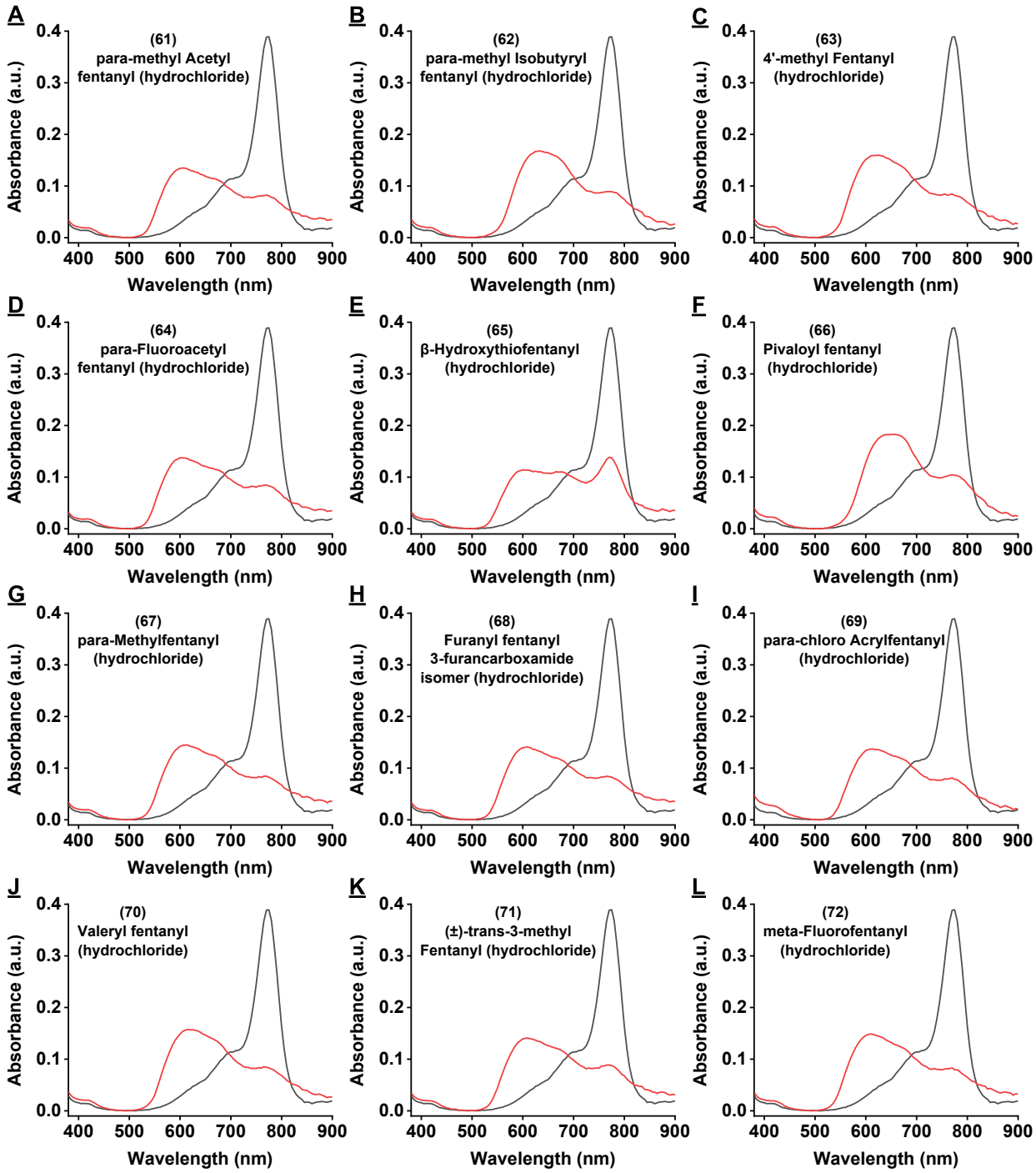

Figure S59. Absorbance spectra data from the Cy7 dye displacement for F6 and fentanyl analog (**A**) 61, (**B**) 62, (**C**) 63, (**D**) 64, (**E**) 65, (**F**) 66, (**G**) 67, (**H**) 68, (**I**) 69, (**J**) 70, (**K**) 71, and (**L**) 72. The red and black curves respectively indicate data for samples with and without ligand.

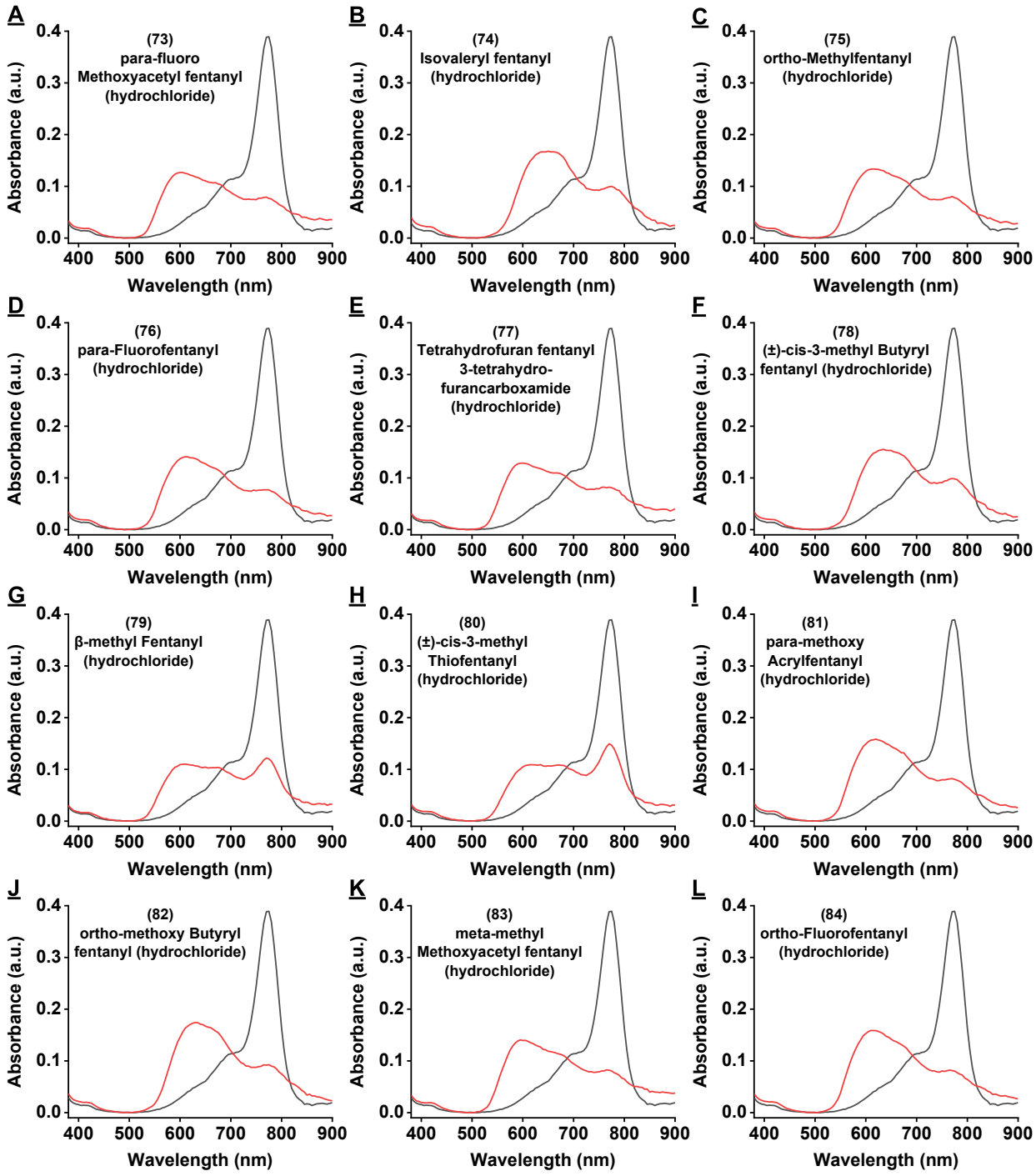

Figure S60. Absorbance spectra data from the Cy7 dye displacement for F6 and fentanyl analog (**A**) 73, (**B**) 74, (**C**) 75, (**D**) 76, (**E**) 77, (**F**) 78, (**G**) 79, (**H**) 80, (**I**) 81, (**J**) 82, (**K**) 83, and (**L**) 84. The red and black curves respectively indicate data for samples with and without ligand.

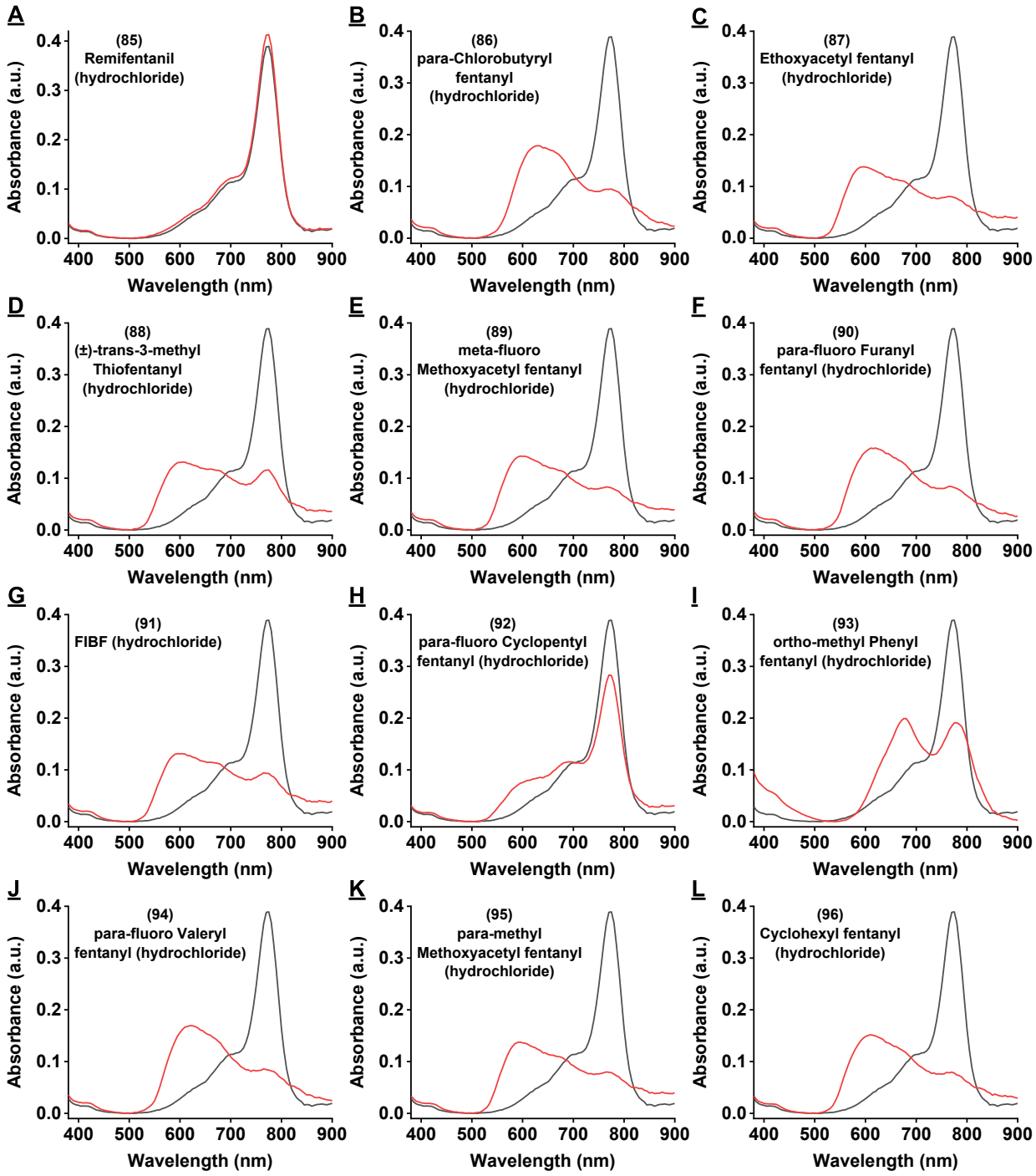

Figure S61. Absorbance spectra data from the Cy7 dye displacement for F6 and fentanyl analog (**A**) 85, (**B**) 86, (**C**) 87, (**D**) 88, (**E**) 89, (**F**) 90, (**G**) 91, (**H**) 92, (**I**) 93, (**J**) 94, (**K**) 95, and (**L**) 96. The red and black curves respectively indicate data for samples with and without ligand.

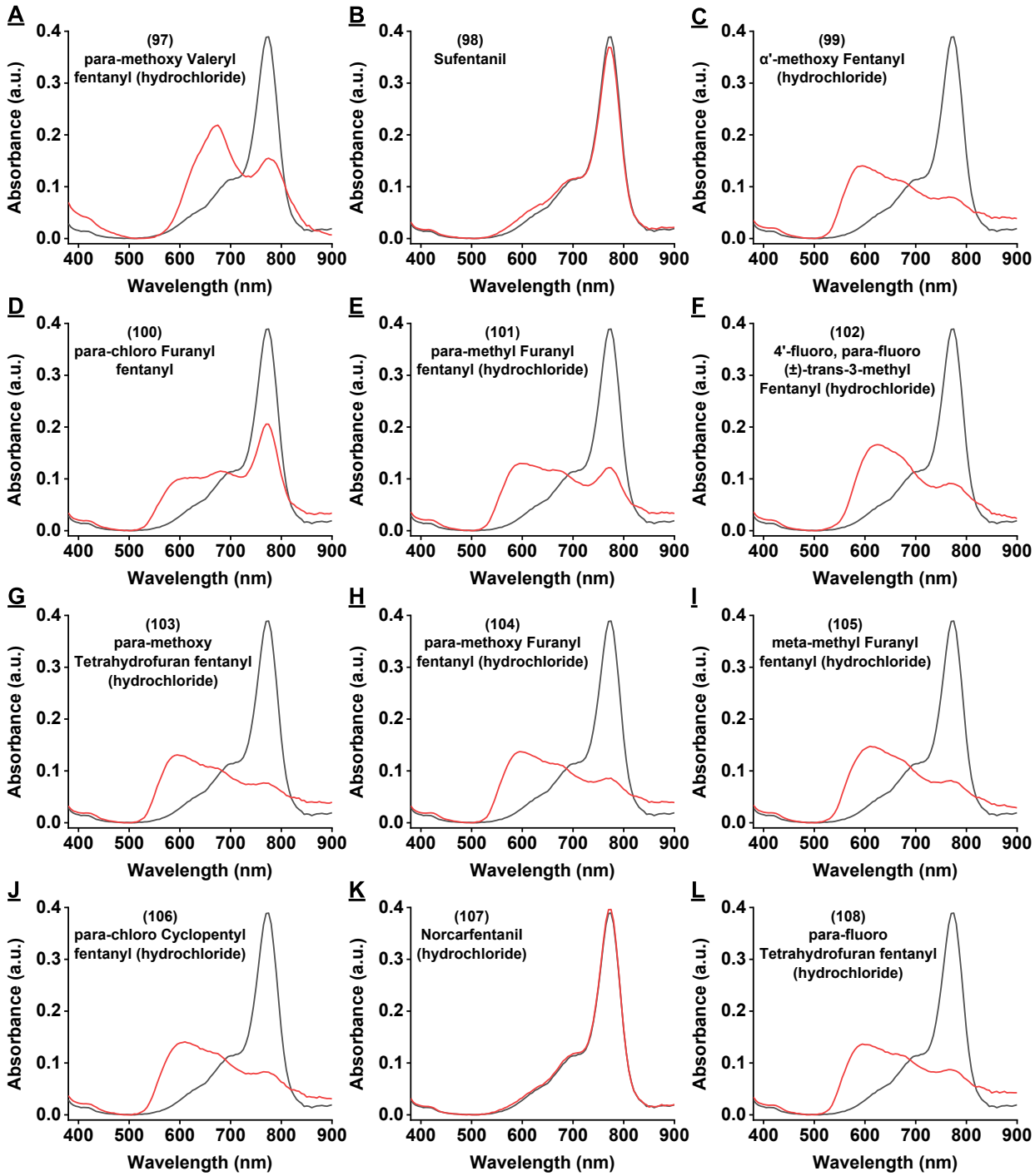

Figure S62. Absorbance spectra data from the Cy7 dye displacement for F6 and fentanyl analog (**A**) 97, (**B**) 98, (**C**) 99, (**D**) 100, (**E**) 101, (**F**) 102, (**G**) 103, (**H**) 104, (**I**) 105, (**J**) 106, (**K**) 107, and (**L**) 108. The red and black curves respectively indicate data for samples with and without ligand.

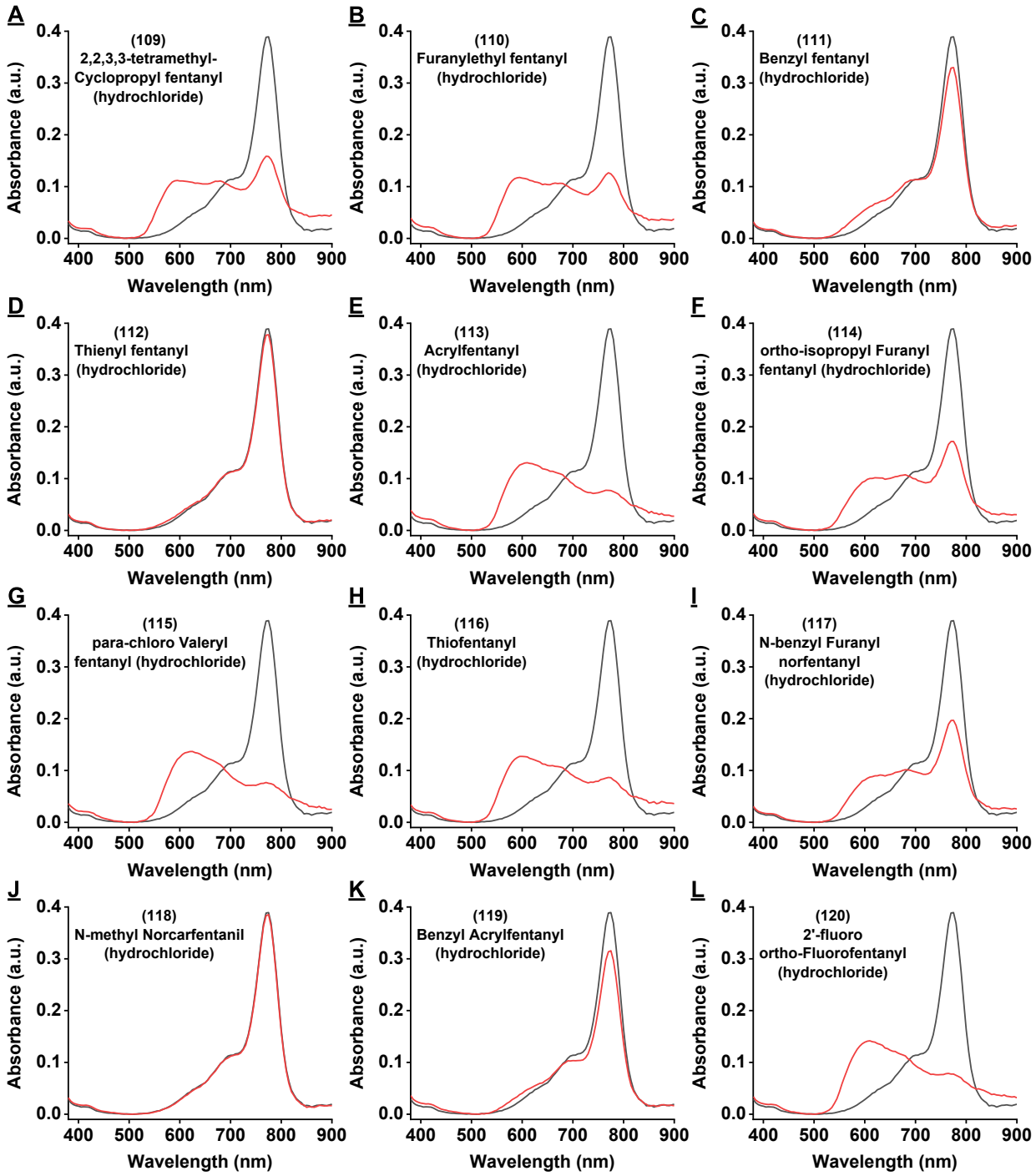

Figure S63. Absorbance spectra data from the Cy7 dye displacement for F6 and fentanyl analog (**A**) 109, (**B**) 110, (**C**) 111, (**D**) 112, (**E**) 113, (**F**) 114, (**G**) 115, (**H**) 116, (**I**) 117, (**J**) 118, (**K**) 119, and (**L**) 120. The red and black curves respectively indicate data for samples with and without ligand.

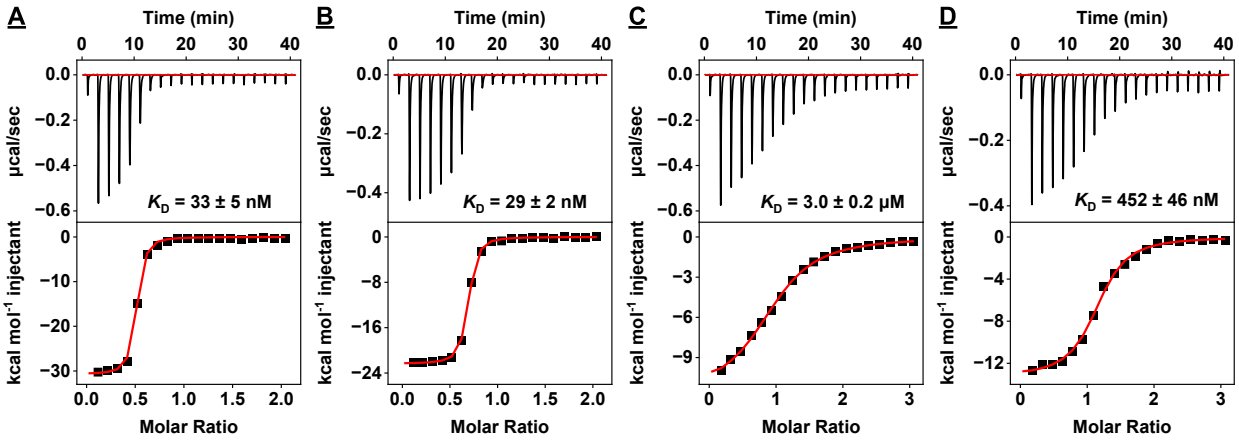

Figure S64. Determining the binding affinity of aptamer F6 to fentanyl and various analogs using ITC. Top panels display the heat generated from each titration of (**A**) fentanyl, (**B**) cyclopropyl fentanyl, (**C**) cis-3-methyl thiofentanyl, and (**D**) ortho-methyl phenyl fentanyl into F6. Bottom panels show integrated heat values per mole of injectant plotted as a function of the molar ratio of target to aptamer after correcting for the heat of dilution of the titrant. Data were fitted with a one-site binding model.

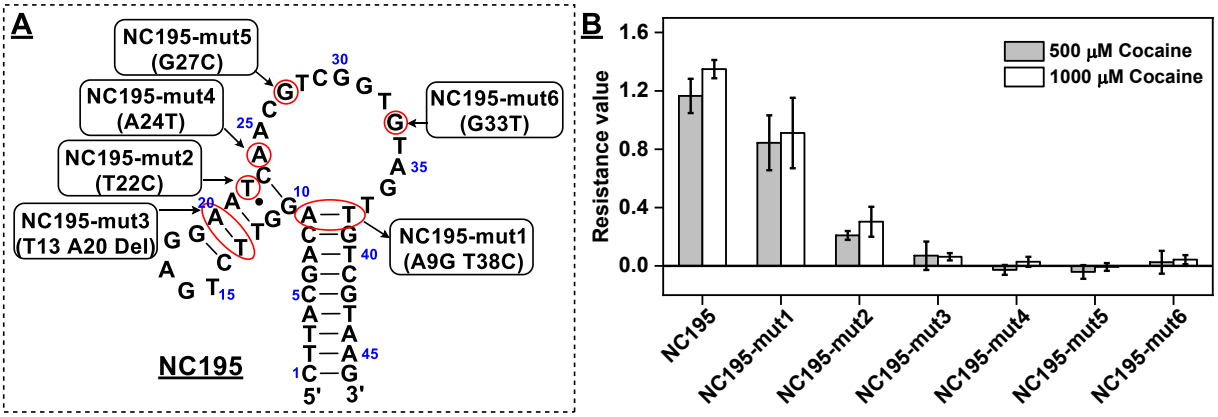

Figure S65. Structure-activity study conducted using the first-generation exonuclease digestion assay with cocaine aptamer NC195 and its mutants. (**A**) Predicted secondary structure of NC195; mutations tested in experiments are circled and labeled. (**B**) Results from the first-generation exonuclease assay to measure relative binding of NC195 and mutants to cocaine.

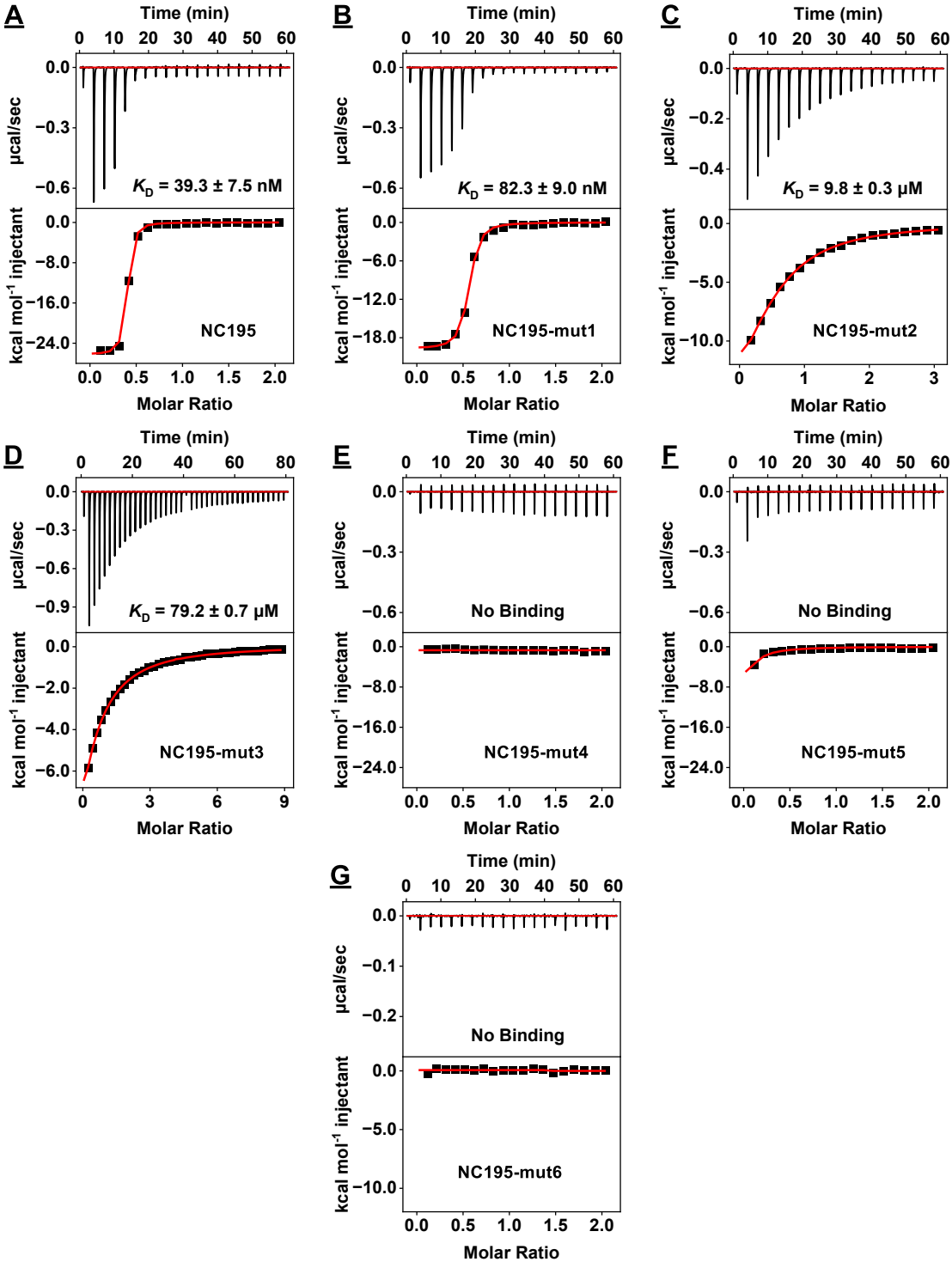

Figure S66. Binding affinity of NC195 and its six mutants to cocaine as measured by ITC. Top panels display the heat generated from each titration of cocaine into (**A**) NC195, (**B**) NC195-mut1, (**C**) NC195-mut2, (**D**) NC195-mut3, (**E**) NC195-mut4, (**F**) NC195-mut5, and (**G**) NC195-mut6. Bottom panels show integrated heat values per mole of injectant plotted as a function of the molar ratio of target to aptamer after correcting for the heat of dilution of the titrant. Data were fitted with a one-site binding model.

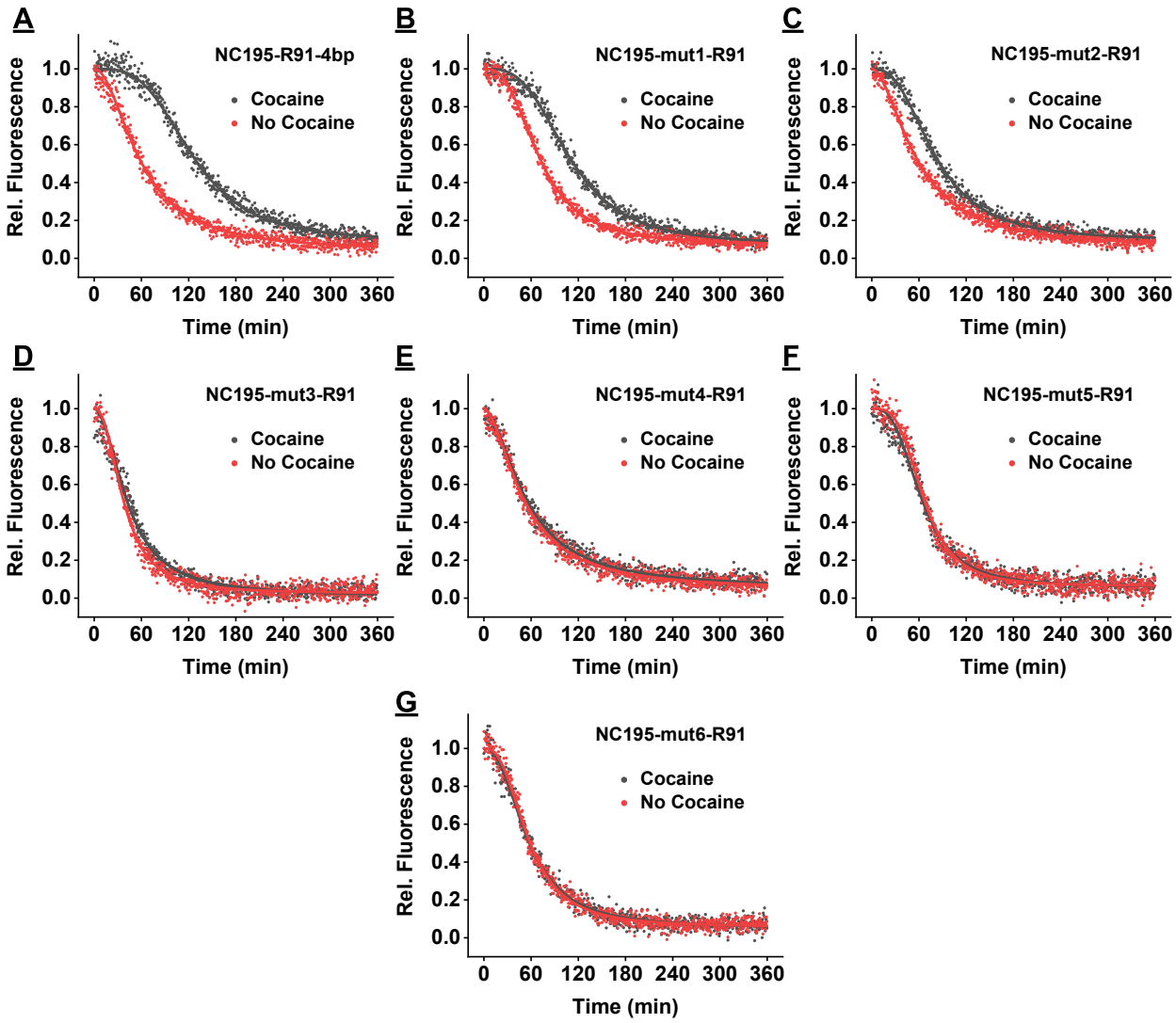

Figure S67. Fluorescence time-course data from the RT-Exo assay for the cocaine-binding aptamer NC195 and various mutants. (**A**) NC195-R91-4bp, (**B**) NC195-mut1-R91, (**C**) NC195-mut2-R91, (**D**) NC195-mut3-R91, (**E**) NC195-mut4-R91, (**F**) NC195-mut5-R91, and (**G**) NC195-mut6-R91.

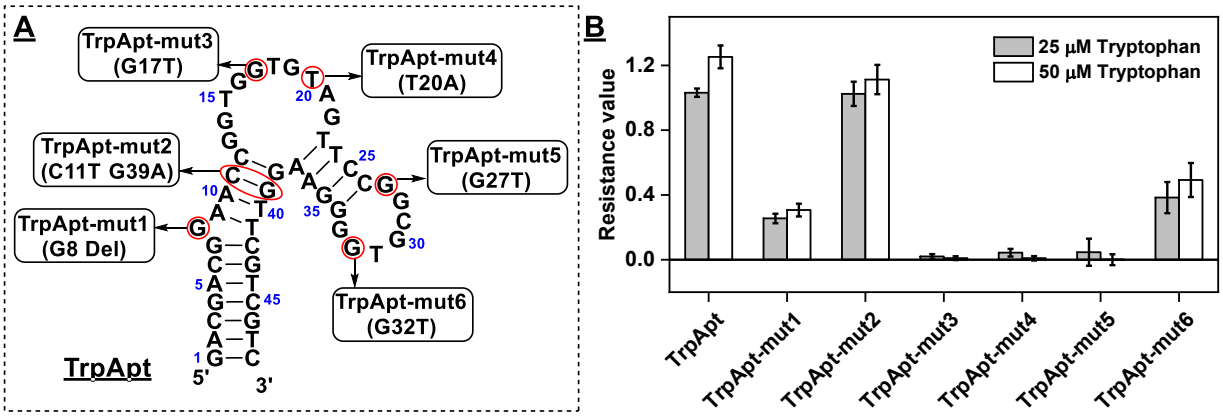

Figure S68. Structure-activity study conducted using the first-generation exonuclease digestion assay with the L-tryptophan aptamer TrpApt and its mutants. (**A**) Predicted secondary structure of TrpApt; mutations tested in subsequent experiments are circled and labeled. (**B**) Results from the first-generation exonuclease assay to measure relative binding of TrpApt and mutants to tryptophan.

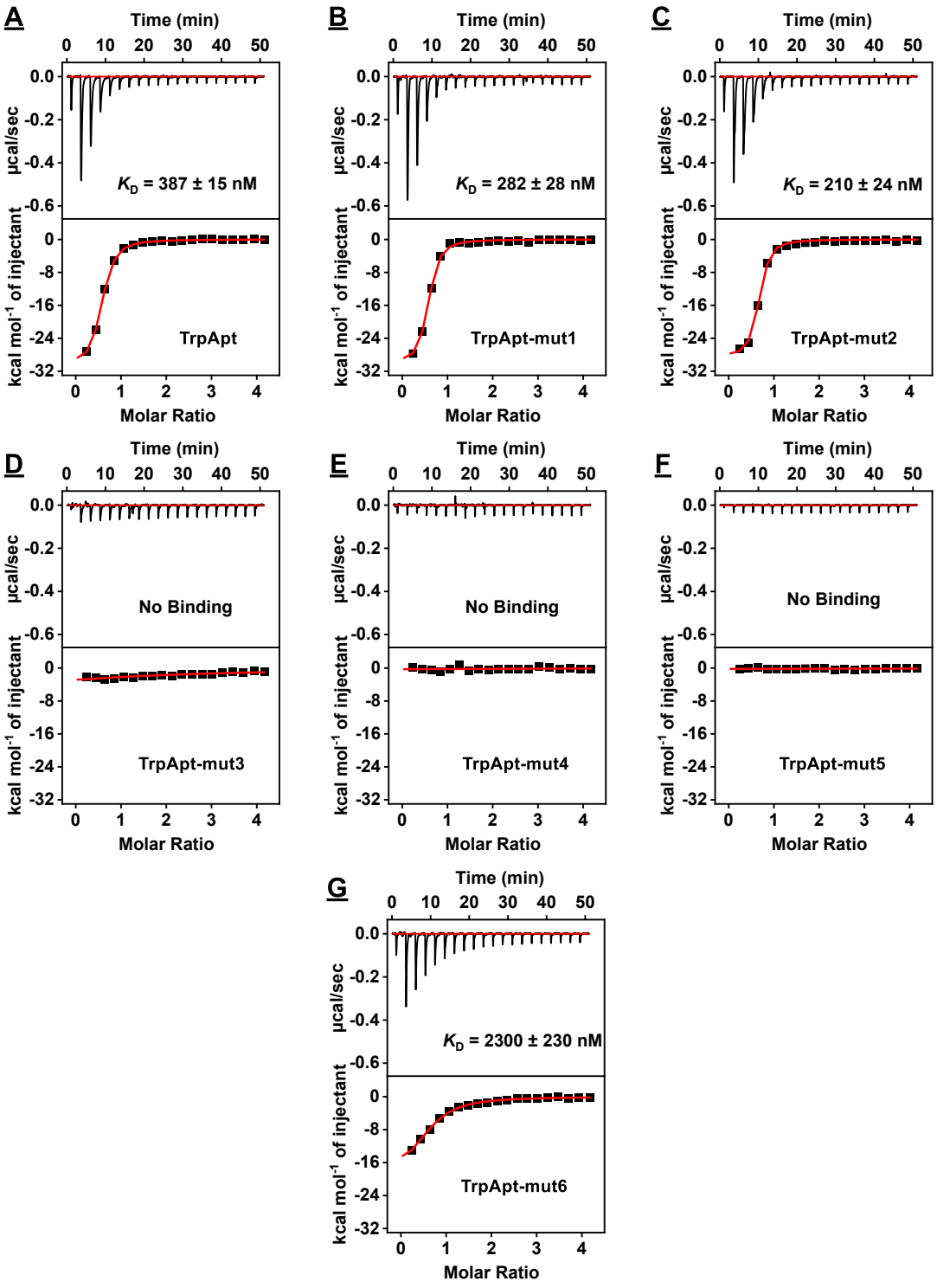

Figure S69. Binding of TrpApt and mutants to tryptophan as measured with ITC. Top panels display the heat generated from each titration of L-tryptophan into (**A**) TrpApt, (**B**) TrpApt-mut1, (**C**) TrpApt-mut2, (**D**) TrpApt-mut3, (**E**) TrpApt-mut4, (**F**) TrpApt-mut5, and (**G**) TrpApt-mut6. Bottom panels show integrated heat values per mole of injectant plotted as a function of the molar ratio of target to aptamer after correcting for the heat of dilution of the titrant. Data were fitted with a one-site binding model.

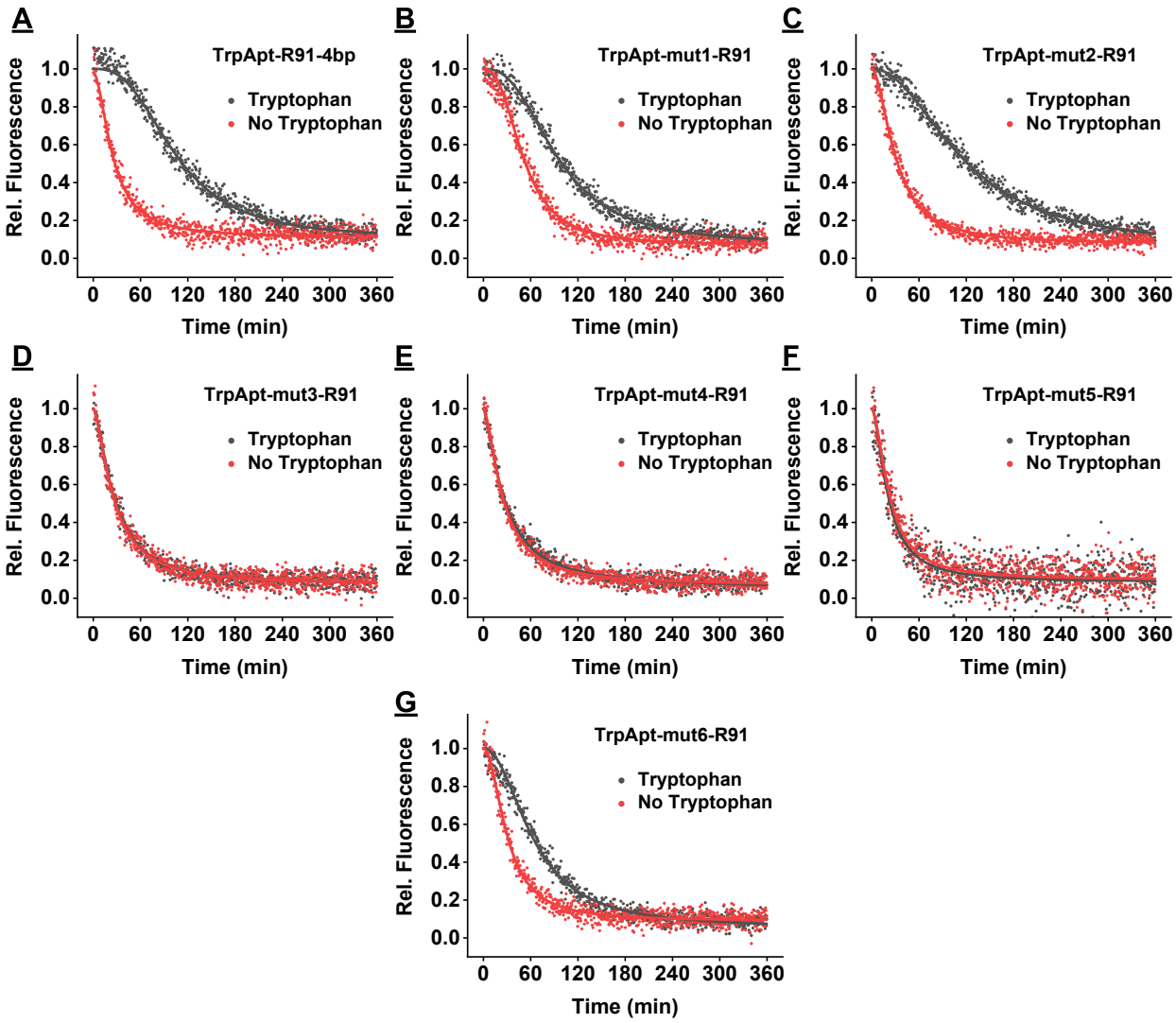

Figure S70. Fluorescence time-course data from the RT-Exo assay for TrpApt and its mutants. Data are shown for (**A**) TrpApt-R91-4bp, (**B**) TrpApt-mut1-R91, (**C**) TrpApt-mut2-R91, (**D**) TrpApt-mut3-R91, (**E**) TrpApt-mut4-R91, (**F**) TrpApt-mut5-R91, and (**G**) TrpApt-mut6-R91.